



Distance metric learning for image and webpage comparison

Marc Teva Law

► To cite this version:

Marc Teva Law. Distance metric learning for image and webpage comparison. Other [cs.OH]. Université Pierre et Marie Curie - Paris VI, 2015. English. NNT : 2015PA066019 . tel-01135698v2

HAL Id: tel-01135698

<https://theses.hal.science/tel-01135698v2>

Submitted on 18 Mar 2015

HAL is a multi-disciplinary open access archive for the deposit and dissemination of scientific research documents, whether they are published or not. The documents may come from teaching and research institutions in France or abroad, or from public or private research centers.

L'archive ouverte pluridisciplinaire **HAL**, est destinée au dépôt et à la diffusion de documents scientifiques de niveau recherche, publiés ou non, émanant des établissements d'enseignement et de recherche français ou étrangers, des laboratoires publics ou privés.



**THÈSE DE DOCTORAT DE
L'UNIVERSITÉ PIERRE ET MARIE CURIE**

Spécialité

Informatique

École Doctorale Informatique, Télécommunications et Électronique (Paris)

Présentée par

Marc Teva LAW

Pour obtenir le grade de

DOCTEUR de l'UNIVERSITÉ PIERRE ET MARIE CURIE

Sujet de la thèse :

Distance Metric Learning for Image and Webpage Comparison

Apprentissage de distance pour la comparaison d'images et de pages Web

soutenue le 20 janvier 2015 devant le jury composé de :

M. PATRICK PÉREZ	Technicolor	Rapporteur
M. ALAIN RAKOTOMAMONJY	Université de Rouen	Rapporteur
M. FRANCIS BACH	Inria - École Normale Supérieure	Examinateur
M. PATRICK GALLINARI	Université Pierre et Marie Curie	Examinateur
M. JEAN PONCE	École Normale Supérieure	Examinateur
M. FRÉDÉRIC PRÉCIOSO	Polytech'Nice-Sophia	Examinateur
M. MATTHIEU CORD	Université Pierre et Marie Curie	Directeur de thèse
M. STÉPHANE GANÇARSKI	Université Pierre et Marie Curie	Co-directeur de thèse
M. NICOLAS THOME	Université Pierre et Marie Curie	Invité

Contents

Introduction	1
1 Big (Visual) Data	1
2 Motivation	1
3 Contributions	4
1 Background	5
1.1 Image Representations for Classification	5
1.1.1 Visual Bag-of-Words	5
1.1.2 Deep representations	8
1.2 Metric Learning for Computer Vision	10
1.3 Supervised Distance Metric Learning	13
1.3.1 Notations	13
1.3.2 Distance and similarity metrics	13
1.3.3 Learning scheme	15
1.3.4 Review of popular metric learning approaches	17
1.4 Training Information in Metric Learning	23
1.4.1 Binary similarity labels	23
1.4.2 Richer provided information	23
1.4.3 Quadruplet-wise approaches	23
1.5 Regularization in Metric Learning	25
1.5.1 Representative regularization terms	25
1.5.2 Other regularization methods in Computer Vision	26
1.6 Summary	28
2 Quadruplet-wise Distance Metric Learning	29
2.1 Motivation	29
2.2 Quadruplet-wise Similarity Learning Framework	30
2.2.1 Quadruplet-wise Constraints	30
2.2.2 Full matrix Mahalanobis distance metric learning	32
2.2.3 Simplification of the model by optimizing over vectors	34
2.3 Quadruplet-wise (Qwise) Optimization	35
2.3.1 Full matrix metric optimization	35
2.3.2 Vector metric optimization	36

2.3.3	Implementation details	37
2.4	Experimental Validation on Relative Attributes	38
2.4.1	Integrating quadruplet-wise constraints	39
2.4.2	Classification experiments	40
2.5	Experimental Validation on Hierarchical Information	44
2.5.1	Formulation of our metric and constraints	44
2.5.2	Experiments	44
2.6	Conclusion	47
3	Fantope Regularization	49
3.1	Introduction	49
3.2	Regularization Scheme	50
3.2.1	Regularization term linearization	51
3.2.2	Optimization scheme	51
3.3	Theoretical Analysis	53
3.3.1	Concavity analysis	53
3.3.2	(Super-)Gradient of the regularizer	54
3.4	Experimental Validation	55
3.4.1	Synthetic example	55
3.4.2	Real-world experiments	57
3.5	Discussion	61
3.6	Conclusion	63
4	Discovering Important Semantic Regions in Webpages	65
4.1	Introduction	65
4.2	Constraint Formalization	67
4.2.1	Automatic generation of constraints	67
4.2.2	Similarity information provided by human users	68
4.2.3	Distance metric formulation	70
4.3	Visual and Structural Comparisons of Webpages	70
4.3.1	Regular grid segmentation	70
4.3.2	Structural segmentation	71
4.3.3	Integration of structural distance metrics	71
4.4	Experimental Results	71
4.4.1	Dataset	72
4.4.2	Setup parameter	72
4.4.3	Evaluation protocol	72
4.4.4	Learning results without human supervision	74
4.4.5	Supervised learning results	78
4.4.6	Structural segmentation maps	79
4.4.7	Summary	80
4.5	Conclusion	80

Conclusion	81
A Positive Semidefinite Cone	83
A.1 Definitions	83
A.2 Rank of a Matrix	85
A.3 Projection onto the PSD Cone	85
B Solver for the Vector Optimization Problem	87
B.1 Primal Form of the Optimization Problem	87
B.2 Loss Functions	88
B.3 Gradient and Hessian Matrices	89
Bibliography	91

Introduction

1 Big (Visual) Data

With the explosion of information shared on the World Wide Web, the amount of accessible text and visual data has significantly increased over time. This is a result of the accelerated expansion of social networks, combined with user-friendly file-sharing tools and improved high-tech products, such as readily available high-quality image capturing devices. Some illustrative examples of the omnipresence of information on the Internet are: 1 billion websites¹ and 14.3 trillion active webpages² on the Internet, 50 billion webpages indexed by Google.Inc.², 350 million photos uploaded each day to the social network website Facebook.³, 6 billion hours of video watched each month on YouTube, with 400 years of video uploaded every day.⁴ In order to exploit and enjoy that immense collection of data, people need tools to retrieve information. A first solution to that problem is manual annotation, for which a significant example is human-edited web directories such as *DMOZ*⁵ and *Yahoo! Directory*⁶. These are websites specialized in linking to other websites and categorizing those links. Many human-edited directories, including DMOZ, are edited by volunteers who are often experts in particular categories. These directories are sometimes criticized due to long delays in approving submissions. Indeed, manual annotation is a tedious task that can cover only a tiny part of the available information due to the exponential growth of data on the Web.

We then need methods to automatically store the information so that it is easy to retrieve, compare and exploit in a user-oriented and semantically meaningful way. For this reason, the problem of automatic information categorization has attracted lots of research effort over decades. Automatic image understanding is a domain in full expansion, in which great improvements have been proposed in the last decade.

2 Motivation

In the context of visual data understanding, the challenge is that the low-level image representation (i.e., the pixels) provides no or little clue about its semantic aspect. This absence of relationship is called *semantic gap* [Smeulders et al., 2000]. In order to fill the gap, a first critical step is the extraction of appropriate features from images, which are used to create an adequate representation of the visual content. These “appropriate” features and “adequate” image representations greatly depend on the application task. In classification, various computer vision models were developed by exploiting the popular Support Vector Machine (SVM) [Cortes and Vapnik, 1995] model. The SVM is usually combined with one particular image representation model, the Bag-of-Words model [Ma and Manjunath, 1997, Sivic and Zisserman, 2003] which has emerged to achieve good image classification performances for many challenging datasets. The

¹<http://www.internetlivestats.com/total-number-of-websites/>

²<http://www.factshunt.com/2014/01/total-number-of-websites-size-of.html>

³<http://www.businessinsider.com/facebook-350-million-photos-each-day-2013-9>

⁴<https://www.youtube.com/yt/press/statistics.html>

⁵<http://www.dmoz.org/>

⁶<https://dir.yahoo.com/>

model maps from the pixel-level to the semantic-level through a series of data transformation steps, namely: 1) feature extraction, 2) feature coding, 3) pooling and 4) classification with SVM. *Deep learning* has recently attracted a lot of attention by reaching state-of-the-state performance on many computer vision tasks, particularly in classification [Krizhevsky et al., 2012]. While the bag-of-words model uses data transformation to map from images to vector mid-level representations, deep connectionist models learn a mapping from input data to output classes via several successions of linear and non-linear operations.

Many machine learning methods, such as SVMs and clustering, are based on a notion of similarity. Their generalization performance then greatly depends on the choice of the metric. For some problems, experts can determine an appropriate metric. However, when no prior knowledge is available, standard metrics such as the Euclidean distance are often chosen. Unfortunately, most of them ignore any statistical regularities that might be estimated from a large training set of examples. For this reason, a number of researchers have demonstrated that learning an appropriate distance metric greatly improves the generalization performance for the problem at hand [Xing et al., 2002, Goldberger et al., 2004]. This is the so-called problem of *distance metric learning*, which is the focus of this dissertation.

Different types of data have been successfully exploited with metric learning. For instance, in contexts where datasets are large-scale and dynamic (i.e., new images and new classes can be added and the semantics of existing classes might evolve), classifier approaches that learn a global distance metric [Mensink et al., 2013] enable the addition of new classes and new images to existing classes at (near) zero cost. This approach is in contrast with discriminative models, such as SVM and deep neural networks, that have to be relearned at a relatively high computational cost each time a new category is added. In contexts where classes are described by high-level attributes (i.e., human-nameable descriptions), metric learning approaches [Parikh and Grauman, 2011] have also been successfully applied to increase the similarity of an image to the representation of its class in a high-level latent space. New classes, represented by a high-level description, can therefore be introduced in the latent space to perform “zero-shot” transfer learning [Lampert et al., 2009], where one trains a classifier for an unseen category simply by specifying which attributes it has. In contexts where the goal is to determine whether two images represent the same object or not [Xing et al., 2002], the learning problem usually infers a model that returns small distances for similar pairs of samples, and large distances for dissimilar pairs of samples. The metric has to be able to compare two samples whose respective labels were not necessarily in the training dataset. An illustrative case of application is face verification [Chopra et al., 2005, Guillaumin et al., 2009] where the goal is to determine whether two face images represent the same person or not. For this type of problem different from predicting the label of an image, an appropriate similarity metric which is robust to possible variations in appearance (e.g., scale, pose, lighting, background, expression, hairstyle, glasses, age) has to be chosen. Metric learning approaches outperform the recognition obtained with standard metrics in this task.

Distance metric learning rises many important questions. The first one concerns the type of information provided about training data. When no label is available, the goal is usually to learn a representation of data in a low-dimensional space such that the distances between observed data points are preserved [Tenenbaum et al., 2000, Borg and Groenen, 2005]. This is particularly useful for visualization purpose. On the other hand, when category or similarity information on training data is provided, a distance metric can be learned in a supervised way [Xing et al., 2002, Weinberger and Saul, 2009] to make prediction. The learning framework depends on the kind of information available on training data.

Another crucial question concerns the formulation of the learned (dis)similarity model. Some approaches [Frome et al., 2007] consider their metric as a linear combination of a set of local distances between images (e.g., patch-to-patch or patch-to-image distances), some others [Chechik et al., 2009] consider their similarity metric as a bilinear form between vector image representations. The most widely used model in metric learning is the Mahalanobis distance metric which learns a linear transformation of the input space. It is inferred so that the Euclidean distance in the transformed space can improve prediction. When the linear transformation is low-rank, it allows a compact representation of the data and cheap distance computations. Thanks to these nice properties, this model has attracted a lot of attention.

The examples of applications given above illustrate our interest of understanding images by learning a meaningful distance metric. In this dissertation, supervised distance metric learning for image comparison is considered for two specific aspects: exploiting rich information on training data, and learning a *simple* metric model. We particularly focus on three challenging contexts that exploit metric learning to compare visual information:

Image classification Recognizing categories of objects is a fundamental and natural human ability. Indeed, psychologists have postulated that humans can recognize visually about 30 thousand visual object categories [Biederman, 1987]. Moreover, humans can learn new classes in a very fast, effortless way which requires minimal supervision and a small quantity of examples. Despite the relative simplicity of the task for a human, this is a very challenging task in computer vision. Several works [Goldberger et al., 2004, Weinberger et al., 2005, Mensink et al., 2013] have proposed to learn a distance metric so that images from the same category are closer to each other than to images from other categories.

Face verification Face verification or authentication means deciding whether two face images show the same person or not. This is a difficult problem due to possible variations in appearance (e.g., scale, pose). This task is related to image classification since it involves face recognition and can be seen as a binary classification problem over pairs of images (i.e., an image pair is either similar or dissimilar). It generally involves being able to estimate an appropriate distance [Chopra et al., 2005, Guillaumin et al., 2009, Mignon and Jurie, 2012] between two face images explicitly. This distance is then thresholded to determine whether the faces are similar or dissimilar. Face recognition is particularly useful in biometrics since it is a non-intrusive process that can be done without the cooperation, or even the knowledge, of the respective subject.

Web archiving Due to the growing importance of the World Wide Web, many national libraries and organizations such as *Internet Archive*⁷ consider the Web as a cultural artifact and work to prevent the Internet - a new medium with major historical significance - and other *born-digital* materials from disappearing into the past. Archiving organizations have the mission of storing portions of the Web to prevent useful content from disappearing. The major challenge of such organizations is to collect, preserve and enable (possibly far) future accesses to a rich part of the Internet content from around the world. Web archiving is typically performed using web crawlers (robots) which periodically harvest the Web and update the archive with fresh versions. Crawlers cannot frequently visit all pages to archive them due to the huge number of pages on the Web. Nevertheless, Web crawling strategies can be optimized to capture the largest number of pages that have changed, and thus limit the loss of global useful information.. For this purpose, a robot regularly visits webpages and measures their quantity of (semantical) change over time. A page that changes frequently should be visited more often than a page that rarely changes.

To illustrate the importance of Web archiving, *Internet Archive* reports to store 450 billion webpages saved over time, 2 million videos, 7 million digital books, 2 million audio recordings, 14 million historic images⁸. In this thesis, we want to automatically quantify semantic changes and detect when a change occurred between successive versions of the same webpage. In this way, the change frequency of pages can be discovered, and optimized crawling strategies can be adopted to limit the loss of useful information on the Internet.

⁷<http://www.archive.org>

⁸<https://blog.archive.org/2014/08/29/millions-of-historic-images-posted-to-flickr/>

3 Contributions

The main contributions of this dissertation concern the development of novel techniques in supervised metric learning for visual data. Supervised metric learning has been vastly investigated, particularly Mahalanobis(-like) distance metric learning to compare feature vectors. Mahalanobis distance metric learning essentially infers a linear transformation of the data into a new space wherein the Euclidean distance in the transformed space satisfies similarity information better than in the original input space.

We pointed out two issues in supervised metric learning methods that have motivated our PhD work:

First, metric learning algorithms generally exploit only binary similarity labels (i.e., two images are similar or dissimilar). In the context of classification, these binary labels correspond to the class membership information: two images are similar if they are in the same class, they are dissimilar otherwise. Nonetheless, in some contexts, information richer than basic class membership is available. This is for instance the case when categories are part of an underlying semantic taxonomy (e.g., owl and pigeon categories both belong to the bird family), and the corresponding taxonomy structure for the categories is known. Some approaches [Weinberger and Chapelle, 2008, Verma et al., 2012] have considered this type of context. One may then want to exploit rich information in order to learn a metric that reflects the underlying relations between data. We propose in Chapter 2 a novel way to exploit rich information and learn a metric that better reflects the relations between data. For this purpose, we introduce constraints that involve quadruplets of images. The proposed constraints are generalizations of the constraints widely used in popular metric learning approaches, and can express relations that are not possible with classical metric learning constraints.

Second, many metric learning algorithms do not control the complexity of their learned model, and are thus prone to overfitting. As already mentioned, Mahalanobis distance metric learning infers a linear transformation of the data. The number of independent parameters of the model is then proportional to both the dimensionality of the input space and the rank of the learned linear transformation. In order to avoid overfitting, it may be preferable to control the rank of the learned linear transformation. Many approaches [McFee and Lanckriet, 2010, Shen et al., 2009, Lim et al., 2013] use specific regularization methods for this purpose. We propose in Chapter 3 a new regularization method to explicitly control the rank of the learned distance metric model. Our proposed approach minimizes the sum of the k smallest singular values of the learned matrix. We provide a theoretical justification for our method and experimentally demonstrate its effectiveness on synthetic and real-world datasets.

We validate our approaches on different types of recent and popular applications, namely the contexts of relative attributes, hierarchical image classification, face verification and webpage comparison for archiving. Furthermore, another major contribution of this thesis, presented in Chapter 4, is a novel method that exploits temporal relations in order to learn a distance metric that automatically focuses on meaningful regions in webpages. The learned metric is used for webpage change detection purpose.

Chapter 1

Background

In this chapter, we briefly present image representations and machine learning techniques in order to compare images and solve popular computer vision tasks such as image classification. We then provide the necessary background on supervised metric learning used in the subsequent chapters.

1.1 Image Representations for Classification

How to properly represent images for challenging tasks such as classification or retrieval, and hence fill the semantic gap, remains a major issue in computer vision. One of the most popular tasks in computer vision is image classification which refers to the ability to predict a semantic concept based on the visual content of the image. In this context, the problem of image representation has been extensively studied in the last decades due to its large number of applications. Different methodologies have been explored to fulfill this goal. Biologically inspired models [Serre et al., 2007, Theriault et al., 2013] try to mimic the mammalian visual system, and show interesting performances for classification and detection. Recently, deep learning has regained a lot of attention due to the large success of deep convolutional networks in the ImageNet Large Scale Visual Recognition Challenge 2012 (ILSVRC2012)⁹. Using pixels as input, the network automatically learns useful image representations for the classification task. The results [Krizhevsky et al., 2012] reveal that deep learning significantly outperforms state-of-the-art computer vision representation competitors. In contexts where fewer training images are available for training, the visual Bag-of-Words (BoW) model [Ma and Manjunath, 1997, Sivic and Zisserman, 2003] proved to be the leading strategy in the last decade and remains a very competitive representation model. We present in the following two popular image representation models used for image classification: the visual Bag-of-Words and deep representations.

1.1.1 Visual Bag-of-Words

In the popular classification task, many approaches in the last decade have exploited the same classification framework [Lazebnik et al., 2006, Yang et al., 2009, Liu et al., 2011], the only difference between them is how they fine-tuned the low-level and mid-level feature extraction process to gain in recognition performance.

To better understand this rush for performance, we describe the popular visual Bag-of-Words image representation model that is illustrated in Fig. 1.1 and inspired from the Bag-of-Words used in text information retrieval. The text Bag-of-Words model represents a document by a histogram, it assigns to each term in a document a *weight* for that term that depends on the number of occurrences of the term

⁹<http://www.image-net.org/challenges/LSVRC/2012/>

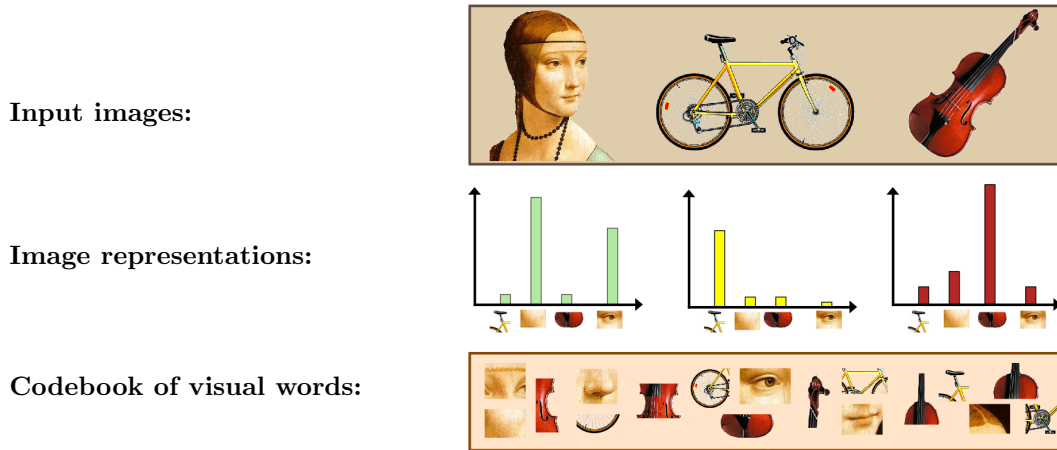


Figure 1.1: An illustration of the visual Bag-of-Words (BoW) representation for three input images: the presence of visual words from a codebook (bottom row) in input images (top row) is quantified in a histogram. The histogram of “word counts” (middle row) is used to represent the image. Image courtesy of Li Fei-Fei.

in the document. In the visual BoW model, images are first decomposed as a set of local features, usually obtained by regular grid-based sampling (i.e., images are segmented as patches that are regularly spaced). Converting the set of local descriptors of an image into the final image representation is performed by a succession of two steps: coding and pooling. In the original BoW model, coding consists in assigning each local descriptor to the closest visual word, while pooling averages the local descriptor projections. The final BoW vector, which is the representation of the image, can thus be regarded as a histogram counting the occurrences of each visual word in the image. Since the notion of “word” is not as easily interpretable for image classification as for text retrieval, many efforts have been devoted to improve coding and pooling.

Fig. 1.2 illustrates the whole classification pipeline of the visual Bag-of-Words model for image classification. Local features are first extracted from the input image, and encoded into an off-line trained dictionary. The codes are then pooled to generate the image signature. This mid-level representation is subsequently normalized before training the classifier, which is usually a Support Vector Machine (SVM) [Cortes and Vapnik, 1995] model. Each block of the figure is detailed in the following.

A pioneer work using the visual BoW framework is probably Netra [Ma and Manjunath, 1997] which exploits color feature dictionary learning.

1.1.1.1 Low-level feature extraction

The first step of the BoW framework corresponds to local feature extraction. To extract local descriptors, one first issue is to detect relevant image regions. Many attempts have been done to achieve that goal, generally based on a geometric criterion, using Harris affine region detector [Harris and Stephens, 1988] or its multi-scale version [Mikolajczyk and Schmid, 2004], SIFT detector [Lowe, 2004], *etc.* However, for classification tasks, most evaluations reveal that a regular grid-based sampling strategy leads to optimal performances [Fei-Fei and Perona, 2005]. In each region of the image, SIFT descriptors [Lowe, 2004] are computed because of their excellent performances attested in various datasets.

1.1.1.2 Mid-level coding and pooling scheme

We explain here how to compute the mid-level representation of images in order to obtain their BoW representations.

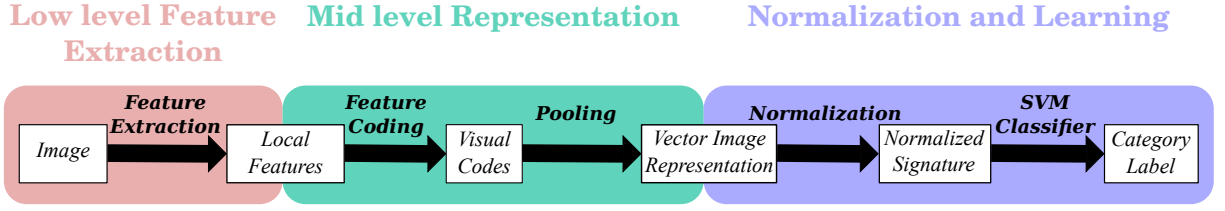


Figure 1.2: BoW pipeline for classification

Let $\mathbf{X} = (\mathbf{x}_1, \dots, \mathbf{x}_j, \dots, \mathbf{x}_N)$ be the set of local descriptors in an image, where N is the number of local descriptors in the image. In the BoW model, the mid-level signature generation first requires a set of visual words (also called codewords) $\{\mathbf{b}_i \in \mathbb{R}^d\}_{i=1}^M$ (where d is the local descriptor's dimensionality, and M is the number of visual words). This set of visual words is called visual codebook or dictionary, we denote it \mathbf{B} .

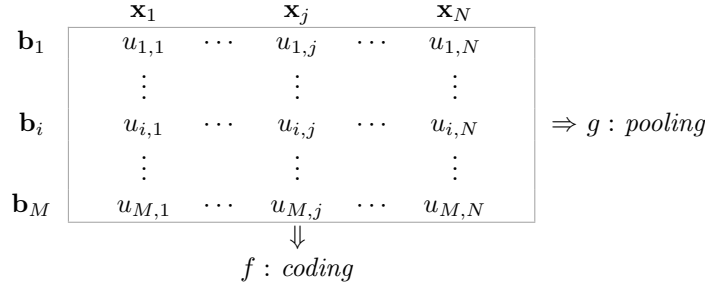
Table 1.1 gives a matrix illustration of the mid-level representation extraction in the BoW pipeline, for scalar coding and pooling schemes. The set of local descriptors \mathbf{X} is represented in columns, while the set of dictionary elements \mathbf{B} occupies the rows. One column of the matrix thus represents the encoding of a given local descriptor \mathbf{x}_j into the codebook, that we denote as $f(\mathbf{x}_j) = \mathbf{u}_j = (u_{1,j}, u_{2,j}, \dots, u_{M,j}) \in \mathbb{R}^M$. In each row, aggregating the codes for a given dictionary element \mathbf{b}_i results in the pooling operation, denoted as $g(\mathbf{X}, f)$.

Codebook Different strategies to compute the codebook exist. The codebook can be determined with a *static* clustering, e.g., Smith and Chang [Smith and Chang, 1997] use a codebook of 166 regular colors defined a priori. These techniques are generally far from optimal, except in very specific applications. Usually, the codebook is learned using an unsupervised clustering algorithm applied on local descriptors randomly selected from an image dataset, providing a set of M clusters with centers \mathbf{b}_i . K -means is widely used in the BoW pipeline. Other approaches [Boureau et al., 2010, Goh et al., 2012] try to include supervision to improve the dictionary learning. However, Coates and Ng [Coates and Ng, 2011] report that dictionary elements learned with “naive” unsupervised methods (e.g., k -means or even random sampling) are sufficient to reach high performances on different image datasets. They also claim [Coates and Ng, 2011] that the recognition performance mostly depends on the choice of architecture. Specifically a good encoding function (i.e., sparse or soft) is required.

Coding The coding step has attracted a lot of attention in the computer vision community, different coding methods have thus been proposed. In the original BoW model, the value of $u_{i,j}$ is 1 if \mathbf{b}_i is the nearest visual word of \mathbf{x}_j and 0 otherwise. This method is called hard assignment or hard coding. In other methods, such as the Local Soft Coding (LSC) algorithm [Liu et al., 2011], the value of $u_{i,j}$ is between 0 and 1 and grows with the relative proximity between \mathbf{x}_j and the codeword \mathbf{b}_i .

Note that some representation models, such as Fisher vector [Perronnin and Dance, 2007] or VLAD [Jégou et al., 2010] descriptors, use a vector representation of $u_{i,j} \in \mathbb{R}^P$, which results in vectors \mathbf{u}_j in \mathbb{R}^{PM} . For instance, the Fisher Vector model [Perronnin et al., 2010] extends the BoW by encoding the average first- and second-order differences between the descriptors and codewords.

Pooling The pooling step aggregates the resulting codes $u_{i,j}$ in order to compute the final vector image representation $\mathbf{z} = \{z_i\}_{i=1}^n$ of the image. The two most popular pooling methods are the sum and the max poolings. Sum pooling counts the number of occurrences of each codeword in the image (i.e., $z_i = \sum_{j=1}^N u_{i,j}$). Max pooling detects for each codeword its maximum score among all the patches of the image (i.e., $z_i = \max_{j \in \{1, \dots, N\}} u_{i,j}$). Sum pooling is particularly useful when hard coding is applied since max pooling would return binary values of z_i in this context. In the context of soft coding, where codes are usually real values between 0 and 1, the max pooling plays the role of a codeword detector. Other

Table 1.1: Coding and pooling strategies. The functions f and g are explicited below

pooling methods have been proposed. For instance, the BossaNova representation [Avila et al., 2013] keeps more information than the BoW during the pooling step by estimating the distribution of the descriptors around each codeword.

1.1.1.3 Normalization and learning

Once the signatures of the different images in the dataset are computed, the classic approach is to learn a statistical machine learning model, usually an SVM learned using a one-against-all strategy. Some authors normalize the image representations before learning the classifiers [Perronnin et al., 2010, Avila et al., 2013]. The choice of normalization also depends on the chosen representation model and classifier model (e.g., linear or non-linear SVM).

1.1.1.4 Beyond Bag-of-Words

The pipeline described in Fig. 1.2 has been exploited in the last decade by many approaches on various datasets [Lazebnik et al., 2006, Yang et al., 2009, Perronnin et al., 2010, Liu et al., 2011]. In particular, many attempts for improving the coding and pooling steps have been done. Fig. 1.3 illustrates the performance evaluations of different state-of-the-art methods on the Caltech-101 [Fei-Fei et al., 2007] dataset. Most of them are extensions of the Bag-of-Words model which improve its mid-level representation.

The improvement of the mid-level step since 2006 significantly boosted performances: for example, using 30 training examples, there is a substantial gain of about 20 points from the baseline work of Lazebnik et al. [Lazebnik et al., 2006] ($\sim 64\%$ in 2006) to the pooling learning method of Feng et al. [Feng et al., 2011] ($\sim 83\%$ in 2011). This work on the BoW model over years demonstrates in this particular application task that the performance of machine learning methods is heavily dependent on the choice of data representations. Especially, as a preliminary of this thesis, we performed a thorough study of the different low-level and mid-level parameters of this pipeline that have an impact on classification performance. This study led to the following publications [Law et al., 2012a, Law et al., 2014a].

While the methods mentioned above are interested in manually tuning the extraction process to generate a useful image representation, other methods are concerned with questions surrounding how we can best learn meaningful and useful representations of data. The latter approach is known as *representation learning* and includes *distance metric learning*.

1.1.2 Deep representations

In the last decade, datasets of labeled images for computer vision tasks (e.g., image classification or detection) have grown considerably. Recently, the handcrafted extensions of the BoW pipeline have been substantially outperformed by the latest generation of *Convolutional Neural Networks* (CNNs)

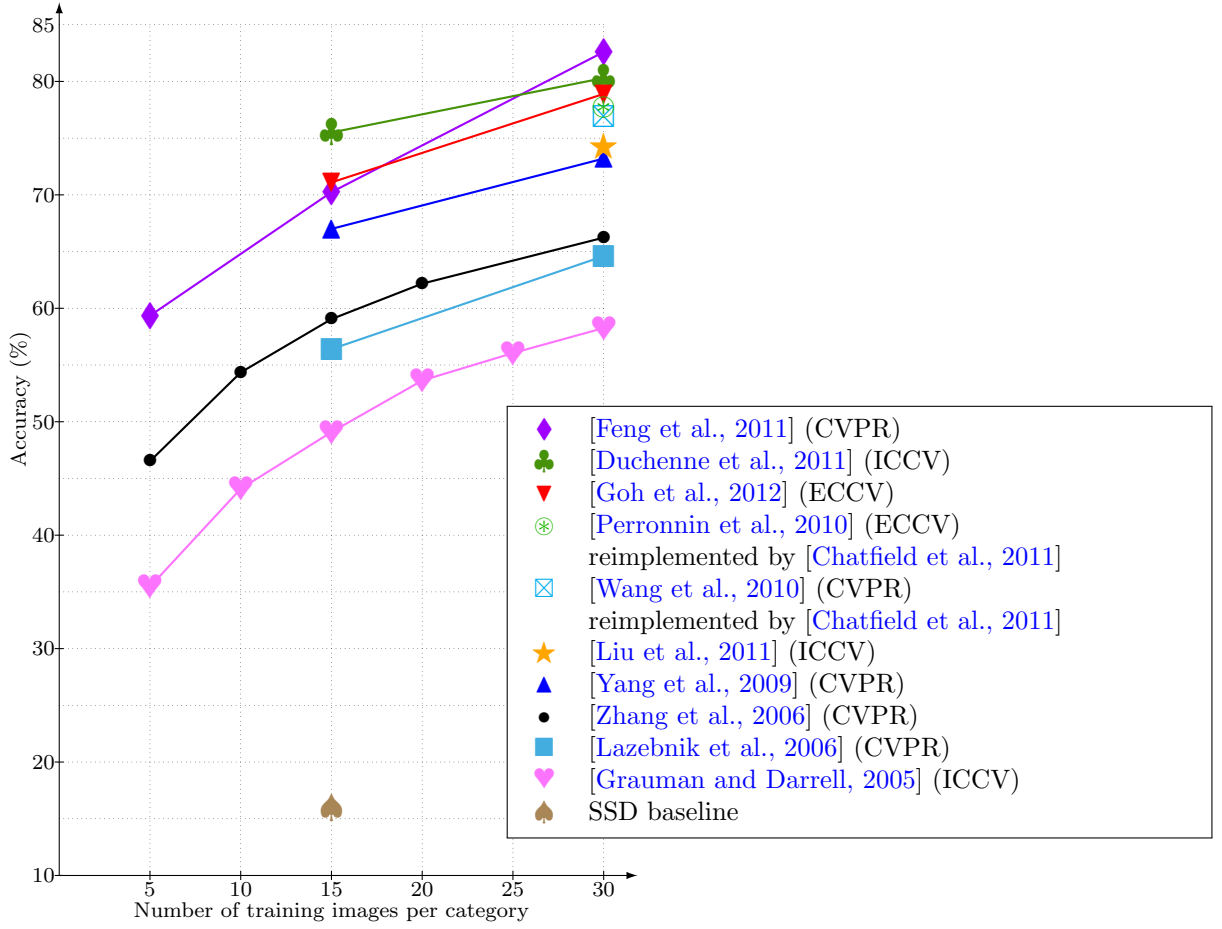


Figure 1.3: State-of-the-art results since 2006 on the Caltech 101 dataset for BoW pipeline methods in mono-feature setup.

[LeCun et al., 1989] to many tasks that involve very large datasets, particularly in classification and detection [Krizhevsky et al., 2012, Szegedy et al., 2013]. The general idea of deep representations is to learn a hierarchy of representations from a dataset of images. CNNs have a substantially more sophisticated structure than standard (shallow) representations such as BoWs. They comprise several layers of non-linear feature extractors, and are therefore said to be *deep*. The representation at each level is composed of lower-level ones. Since they involve a very large number of parameters to learn, they benefit from large scale datasets of images to limit overfitting¹⁰. Note that an architecture with at least four layers is considered to be a deep representation [Hinton et al., 2006, Bengio et al., 2007].

The architecture of CNNs takes raw input data at the lowest level (i.e., pixels) and processes them via a sequence of basic computational units until the data is transformed to a suitable representation in the higher layers to perform classification. Deep connectionist models learn a mapping from input data to output classes by attempting to untangle the manifold of the highly nonlinear input space [LeCun et al., 1989]. The strength of these models is that they are learned entirely in a supervised way from the pixel level to the class level.

Furthermore, recent work observed the relevance of deep models for transfer learning. Features learned on the ImageNet dataset may be used successfully in action recognition on a different benchmark dataset

¹⁰CNNs also benefit from other improvements, such as GPU computation and data augmentation (also known as virtual sampling or data jittering).

[Oquab et al., 2014]. Recently, the enthusiasm of computer vision researchers for CNNs has reached the same level as the enthusiasm they had for BoWs some years ago. Many recent works try to extend CNNs to increase performance in the same way as they extended BoW. For instance, at the ImageNet Large-Scale Visual Recognition Challenge (ILSVRC) 2014¹¹, the first and second places in the localisation and classification tracks respectively, were achieved by a very deep architecture that has more than 15 weight layers [Simonyan and Zisserman, 2014]. By contrast, the winner of the ILSVRC-2012 challenge had 8 layers.

The interested reader on deep learning of representations can refer to [Bengio, 2013].

Conclusion The choice of an appropriate image representation model remains a challenging task for the good performance of recognition methods in many computer vision contexts. For instance, deep learning which learns how to represent images directly from pixels, obtains state-of-the results in the context of image classification when the model is trained on very large datasets. From this observation, learning representations seems a promising paradigm to investigate for computer vision tasks such as image classification. In this thesis, we focus on a special case of representation learning which consists in learning an appropriate distance metric to compare images. For instance, we want to be able to determine whether two images represent the same object or not. For this purpose, we take some given image representation (e.g., BoW or deep features) as input of our model and infer a metric whose goal is to compare two (possibly never seen) images. Our task actually learns a new transformation of the input data such that the Euclidean distance in the transformed space satisfies most of the desired properties. We present in the next section some interesting representation learning contexts where an appropriate metric is learned.

1.2 Metric Learning for Computer Vision

Metrics play an important role for comparing images in many machine learning and computer vision problems. In this section, we briefly present contexts where learning an appropriate metric may be useful. Some successful examples of applications that greatly depend on the choice of metric are: **k -Nearest Neighbors (k -NN)** classification [Cover and Hart, 1967] where an object is classified by a majority vote of its nearest neighbors: the object is assigned to the class most common among its k nearest neighbors. The nearest neighbors are determined based on a given metric (usually the Euclidean distance in the input space). Notably, a recent work [Mensink et al., 2013] has shown that a metric learned for k -NN reaches state-of-the-art performance when new images or classes are integrated in the dataset. **K -Means clustering** [Steinhaus, 1956, MacQueen et al., 1967] aims at partitioning the training set into K clusters in which each sample belongs to the cluster with the nearest mean. Test samples are assigned to the nearest cluster by distance. **Information/Image retrieval** [Salton, 1975, Goodrum, 2000] returns (the most) similar samples to a given query. **Kernel methods** [Scholkopf and Smola, 2001] exploit kernel functions, a special case of similarity metrics. The most popular example of kernel methods is the Support Vector Machines (SVM) model [Cortes and Vapnik, 1995] for which the choice of the kernel, which is critical to the success of the method, is typically left to the user. Moreover, when the data is multimodal (i.e., heterogeneous), multiple kernel learning (MKL) methods [Bach et al., 2004, Rakotomamonjy et al., 2008] allow to integrate data into a single, unified space and compare them.

Contexts that transform the input data into another space (usually with lower dimensionality) to make it interpretable are considered as metric learning approaches. Some examples are:

Manifold learning Humans often have difficulty comprehending data in many dimensions (more than 3). Thus, reducing data to a small number of dimensions is useful for visualization purposes. Moreover, reducing data into fewer dimensions often makes analysis algorithms more efficient, and can help machine learning algorithms make more accurate predictions. One approach to simplification is to assume that

¹¹<http://www.image-net.org/challenges/LSVRC/2014/>



Figure 1.4: High-level attributes describe categories of objects (here animals) with information that is understandable by humans. Images from the *Animals with Attributes* dataset [Lampert et al., 2009].

the data of interest lies on an embedded non-linear manifold within the higher-dimensional space. If the manifold is of low enough dimensionality, the data can be visualised in the low-dimensional space. The key idea of *manifold learning* is to learn an underlying low-dimensional manifold preserving the distances between observed data points. Some good representatives of *manifold learning* are Multidimensional Scaling (MDS) [Borg and Groenen, 2005] and Isomap [Tenenbaum et al., 2000]. Since manifold learning methods do not consider labels of data to learn the low-dimensional space, they are considered as unsupervised metric learning approaches.

Eigenvector methods Eigenvector methods such as Linear Discriminant Analysis (LDA) [Fisher, 1938] or Principal Component Analysis (PCA) [Galton, 1889, Pearson, 1901, Hotelling, 1933] have been widely used to discover informative linear transformations of the input space. They learn a linear transformation $\mathbf{x} \mapsto \mathbf{Lx}$ that projects the training inputs in another space that satisfies some criterion. For instance, PCA projects training inputs into a variance-maximizing subspace while LDA maximizes the amount of between-class variance relative to the amount of within-class variance. PCA can be viewed as a simple linear form of linear *manifold learning*, i.e., characterizing a lower-dimensional region in input space near which the data density is peaked [Bengio et al., 2013].

Visual high-level attributes While traditional visual recognition approaches map low-level image features directly to object category labels, some recent works have proposed to focus on visual attributes [Farhadi et al., 2009, Lampert et al., 2009]. Visual attributes are high-level descriptions of concepts in images. Generally, they have human-designated names (e.g., striped, four-legged, see Fig. 1.4) and are valuable tools to give a semantic meaning to objects or classes in various problems. They are also easy to interpret and manipulate. Visual attributes have shown their benefit in face verification [Kumar et al., 2009] and object classification [Lampert et al., 2009, Akata et al., 2013], particularly in the context of zero-shot learning for which the goal is to learn a classifier that must predict novel categories that were omitted from the training set. It is particularly useful for contexts where datasets are large and dynamic (i.e., new images and new classes can be added and the semantics of existing classes might evolve). Indeed, when images of new labels are introduced in the dataset, discriminative models, such as SVM, have to be relearned at a relatively high computational cost in large scale settings (i.e., when the dataset contains more than 10 million images and 10,000 categories). Methods that learn

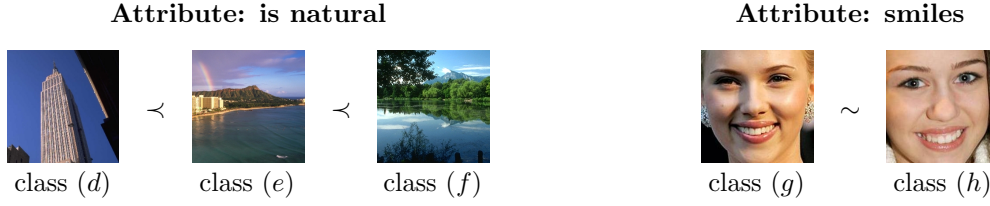


Figure 1.5: Relative attributes: high-level descriptions of classes are given as a function of other classes. While it is difficult to determine whether the image of class (e) is natural or not, it is easier to say that it is more natural than class (d) and less natural than class (f). Scarlett Johansson (class (g)) smiles as much as Miley Cyrus (class (h)).

an appropriate metric [Akata et al., 2013, Mensink et al., 2013] have shown promising results in these contexts since the learned metric can be generalized to new images.

In many attribute problems [Parikh and Grauman, 2011, Yu et al., 2013, Akata et al., 2013], a (linear) transformation is learned so that *low-level* representations of images are projected into a high-level semantic space. Such a space is usually constructed so that each dimension describes the degree of presence of an attribute in a given image. In other words, an image is described by a vector, and each element of the vector is the degree of presence of a given attribute in the image. In the high-level space, images can be semantically compared to one another.

One of the most popular contexts that compare images with attributes is the relative attribute problem [Parikh and Grauman, 2011]. In this problem, the representations of images in the high-level semantic space are learned relatively to the learned representations of other images. The original relative attribute problem considers relations between pairs of classes:

- inequality constraints: i.e., $(e) \prec (f)$: the presence of an attribute is stronger in class (f) than in class (e)
- and equivalence constraints: i.e., $(g) \sim (h)$: the presence of an attribute is equivalent in class (g) and class (h).

This type of relationship is particularly useful when a boolean score for the presence an attribute is difficult to annotate for a class or an image (see Fig. 1.5). Relative attributes have also been used in image retrieval [Kovashka et al., 2012] to find objects that match semantic queries (e.g., an example query would be “Find a red shoe that is shinier than some given image of shoe”).

Conclusion Similarity metrics are key ingredients of many applications, such as image retrieval. The choice of metric is a difficult task and is determined by the problem at hand. An appropriate metric can be picked by experts in some problems, but it can also be learned to improve performance. In this dissertation, we are interested in supervised distance metric learning that we present in the following.

1.3 Supervised Distance Metric Learning

1.3.1 Notations

Throughout this thesis, \mathbb{S}^d , \mathbb{S}_+^d and \mathbb{S}_{++}^d denote the sets of $d \times d$ real-valued symmetric, symmetric positive semidefinite (PSD) matrices and symmetric positive definite matrices, respectively. The set of considered images is $\mathcal{P} = \{\mathcal{I}_i\}_{i=1}^I$, each image \mathcal{I}_i is represented by a feature vector $\mathbf{x}_i \in \mathbb{R}^d$. For matrices $\mathbf{A} \in \mathbb{R}^{b \times c}$ and $\mathbf{B} \in \mathbb{R}^{b \times c}$, denote the Frobenius inner product by $\langle \mathbf{A}, \mathbf{B} \rangle = \text{tr}(\mathbf{A}^\top \mathbf{B})$ where tr denotes the trace of a matrix. $\Pi_{\mathcal{C}}(\mathbf{x})$ is the Euclidean projection of the vector or matrix \mathbf{x} on the convex set \mathcal{C} (see Chapter 8.1 in [Boyd and Vandenberghe, 2004]). For a given vector $\mathbf{a} = (a_1, \dots, a_d)^\top \in \mathbb{R}^d$, $\text{Diag}(\mathbf{a}) = \mathbf{A} \in \mathbb{S}^d$ corresponds to a square diagonal matrix such that $\forall i, A_{ii} = a_i$ where $\mathbf{A} = [A_{ij}]$. For a given square matrix $\mathbf{A} \in \mathbb{R}^{d \times d}$, $\text{Diag}(\mathbf{A}) = \mathbf{a} \in \mathbb{R}^d$ corresponds to the diagonal elements of \mathbf{A} set in a vector: i.e., $a_i = A_{ii}$. $\lambda(\mathbf{A})$ is the vector of eigenvalues of matrix \mathbf{A} arranged in non-increasing order. $\lambda(\mathbf{A})_i$ is the i -th largest eigenvalue of \mathbf{A} . Finally, for $x \in \mathbb{R}$, let $[x]_+ = \max(0, x)$.

1.3.2 Distance and similarity metrics

The choice of an appropriate metric is crucial in many machine learning and computer vision problems. For some problems, the selected metric and its parameters are fine-tuned by experts, but its choice remains a difficult task in general. Extensive work has been done to learn relevant metrics from labeled or unlabeled data. The most useful property of metrics in this thesis is that they can be used to compare two never seen samples, i.e., that were not present in the training dataset.

We present here widely used metrics in computer vision, especially the Mahalanobis distance metric which is the focus of this thesis.

Minkowski distances The Minkowski distance is a metric on Euclidean space which can be considered as a generalization of both the Euclidean distance and the Manhattan distance. The Minkowski distance of order $p \geq 1$ between two points $\mathbf{x} = (x_1, x_2, \dots, x_d) \in \mathbb{R}^d$ and $\mathbf{z} = (z_1, z_2, \dots, z_d) \in \mathbb{R}^d$ is defined as:

$$\left(\sum_{i=1}^d |x_i - z_i|^p \right)^{1/p} = \|\mathbf{x} - \mathbf{z}\|_p$$

The most widely used Minkowski distance in Computer Vision is the Euclidean distance, which corresponds to $p = 2$. Note that for $p < 1$, the triangle inequality is violated.

Histogram distances In some contexts, the data is sampled from a probability simplex defined as $\mathbb{P}^d = \{\mathbf{x} \in \mathbb{R}^d | \mathbf{x} \geq \mathbf{0}, \mathbf{x}^\top \mathbf{1} = 1\}$ where $\mathbf{1} \in \mathbb{R}^d$ denotes the vector of all-ones. Each input $\mathbf{x} \in \mathbb{P}^d$ can be interpreted as a histogram over d buckets. Examples of applications that use this type of data are ubiquitous in computer vision (e.g., distributions over visual codebooks [Tuytelaars and Mikolajczyk, 2008] or histograms of colors [Stricker and Orengo, 1995]). Different distance metrics have been proposed to compare such histograms: e.g., quadratic-form distance [Globerson and Roweis, 2007], Earth Mover's distance [Rubner et al., 2000]. One of the most popular distance metrics is the χ^2 histogram distance whose origin is the χ^2 statistical hypothesis test [Mood, 1950]. It is formulated as:

$$D_{\chi^2}(\mathbf{x}, \mathbf{z}) = \frac{1}{2} \sum_{i=1}^d \frac{(x_i - z_i)^2}{x_i + z_i}$$

and has been successfully applied in many computer vision domains. Some successful examples are [Cula and Dana, 2004, Tuytelaars and Mikolajczyk, 2008, Varma and Zisserman, 2009].

Mahalanobis(-like) distance metric We present here Mahalanobis distance metrics that are the focus of this thesis and the most popular type of learned distance metrics in the machine learning and computer vision communities.

The Mahalanobis distance [Mahalanobis, 1936] is originally a measure of the distance between an observation \mathbf{x} and from a group of observations with mean $\boldsymbol{\mu}$ and covariance matrix $\boldsymbol{\Sigma}$:

$$D_{\boldsymbol{\Sigma}^{-1}}^2(\mathbf{x}) = (\mathbf{x} - \boldsymbol{\mu})^\top \boldsymbol{\Sigma}^{-1} (\mathbf{x} - \boldsymbol{\mu}) \quad (1.1)$$

It can also be defined as a dissimilarity measure between two random vectors \mathbf{x} and \mathbf{x}' of the same distribution with the covariance matrix $\boldsymbol{\Sigma}$:

$$D_{\boldsymbol{\Sigma}^{-1}}^2(\mathbf{x}, \mathbf{x}') = (\mathbf{x} - \mathbf{x}')^\top \boldsymbol{\Sigma}^{-1} (\mathbf{x} - \mathbf{x}')$$

In this thesis, we consider that a Mahalanobis distance metric is any dissimilarity function parameterized by a symmetric positive semidefinite (PSD) matrix \mathbf{M} . It is written in this form:

$$D_{\mathbf{M}}^2(\mathcal{I}_i, \mathcal{I}_j) = (\mathbf{x}_i - \mathbf{x}_j)^\top \mathbf{M} (\mathbf{x}_i - \mathbf{x}_j) = \langle \mathbf{M}, (\mathbf{x}_i - \mathbf{x}_j)(\mathbf{x}_i - \mathbf{x}_j)^\top \rangle \text{ s.t. } \mathbf{M} \in \mathbb{S}_+^d$$

where \mathbb{S}_+^d is the set of symmetric positive semidefinite matrices. This formulation guarantees that $D_{\mathbf{M}}^2$ is a pseudo-metric (i.e., it is symmetric, its value is nonnegative and it satisfies the triangle inequality). In this thesis, we will often refer to pseudo-metrics as metrics to simplify the discussion.

The mere fact that the learned model has to be in \mathbb{S}_+^d , which is a proper cone (see Definition A.1.3), makes the learning framework more complex than classic optimization problems for which the domain (i.e., search space) is the whole input space. We give the definition of positive semidefiniteness for matrices:

Definition 1.3.1. (Positive semidefinite matrix) A matrix $\mathbf{A} \in \mathbb{R}^{d \times d}$ is positive semidefinite (PSD) iff it satisfies:

$$\forall \mathbf{x} \in \mathbb{R}^d, \mathbf{x}^\top \mathbf{A} \mathbf{x} \geq 0$$

PSD matrices can be nonsymmetric (see [Dattorro, 2005], Appendix A). However, we are only interested in symmetric PSD matrices in this thesis. When we define a PSD matrix, we implicitly consider that it is symmetric.

The set \mathbb{S}_+^d is fundamental in Mahalanobis distance metric learning approaches, the interested reader can refer to Appendix A for details on \mathbb{S}_+^d and its properties. The main property to know is that a matrix \mathbf{M} is in \mathbb{S}_+^d iff it can be rewritten as $\mathbf{M} = \mathbf{L}^\top \mathbf{L}$ where $\mathbf{L} \in \mathbb{R}^{e \times d}$ and $e \geq \text{rank}(\mathbf{M})$. From this property, the (squared) Mahalanobis distance metric $D_{\mathbf{M}}$ can be rewritten equivalently:

$$\begin{aligned} D_{\mathbf{M}}^2(\mathcal{I}_i, \mathcal{I}_j) &= (\mathbf{x}_i - \mathbf{x}_j)^\top \mathbf{M} (\mathbf{x}_i - \mathbf{x}_j) \\ &= (\mathbf{x}_i - \mathbf{x}_j)^\top \mathbf{L}^\top \mathbf{L} (\mathbf{x}_i - \mathbf{x}_j) \\ &= \|\mathbf{L}(\mathbf{x}_i - \mathbf{x}_j)\|_2^2 = \|\mathbf{L}\mathbf{x}_i - \mathbf{L}\mathbf{x}_j\|_2^2 \end{aligned}$$

A Mahalanobis distance metric parameterized by the matrix $\mathbf{M} = \mathbf{L}^\top \mathbf{L}$ can then be seen as calculating the Euclidean distance in the space induced by the linear transformation parameterized by \mathbf{L} . Actually, since Mahalanobis distance metrics can be induced from linear transformations and vice versa, any method that returns a linear transformation can be considered as a metric learning method. For this reason, methods such as Principal component analysis (PCA) and Linear discriminant analysis (LDA) can be seen as metric learning approaches.

Some approaches [Shalev-Shwartz et al., 2004, Globerson and Roweis, 2006, Mignon and Jurie, 2012] have extended Mahalanobis distance metric so that a non-linear mapping is learned. Instead of considering the linear transformation $\mathbf{x} \mapsto \mathbf{L}\mathbf{x}$, they consider the transformation $\mathbf{x} \mapsto \mathbf{L}(\phi(\mathbf{x}))$ where ϕ is a mapping

from the input space (denoted \mathcal{X}) to a reproducing kernel Hilbert space (RKHS) \mathcal{H} . The data is then mapped to \mathbb{R}^N by a linear transformation $\mathbf{L} : \mathcal{H} \rightarrow \mathbb{R}^N$. Since ϕ can be non-linear, this allows to learn a non-linear metric $D_{\mathbf{M}}^2(\mathcal{I}_i, \mathcal{I}_j) = \|\mathbf{L}(\phi(\mathbf{x}_i)) - \mathbf{L}(\phi(\mathbf{x}_j))\|_2^2$.

By exploiting the generalized representer theorem [Schölkopf et al., 2001], the operator \mathbf{L} can be expressed as the matrix product $\mathbf{L} = \mathbf{P}\Phi^\top$ where Φ is a matrix representation of \mathcal{X} in \mathcal{H} (i.e., the i -th column of Φ is $\phi(\mathbf{x}_i)$ for $i = \{1, \dots, N\}$) and for some real-valued matrix $\mathbf{P} \in \mathbb{R}^{e \times N}$ (with the parameter $e > 0$ manually chosen). By denoting $\mathbf{K} \in \mathbb{S}_+^N$ the kernel matrix:

$$\mathbf{K} = \Phi^\top \Phi = [K_{ij}] \text{ with } K_{ij} = \langle \phi(\mathbf{x}_i), \phi(\mathbf{x}_j) \rangle = k(\mathbf{x}_i, \mathbf{x}_j)$$

the non-linear mapping can be written:

$$\mathbf{L}(\phi(\mathbf{x})) = \mathbf{P}\Phi^\top(\phi(\mathbf{x})) = \mathbf{P}(\langle \phi(\mathbf{x}_i), \phi(\mathbf{x}) \rangle)_{i=1}^N = \mathbf{P}(k(\mathbf{x}_i, \mathbf{x}))_{i=1}^N$$

where $(\cdot)_{p=1}^N$ denotes concatenation in a N -dimensional vector. The main limitation of this approach is that the resulting computational complexity, which depends on the size of the dataset, is generally increased for a relatively small gain in recognition performance. Since the number of independent parameters can be very large when N is large, the risk of overfitting is high. For computational reasons and to avoid overfitting, a simple linear mapping is generally used for Mahalanobis distance metrics.

Bilinear Similarity An approach very similar to Mahalanobis distance metric is the bilinear similarity. The bilinear similarity between two vectors $\mathbf{x} \in \mathbb{R}^d$ and $\mathbf{z} \in \mathbb{R}^e$ is formulated as:

$$S_{\mathbf{M}}(\mathbf{x}, \mathbf{z}) = \mathbf{x}^\top \mathbf{M} \mathbf{z}$$

where the matrix $\mathbf{M} \in \mathbb{R}^{d \times e}$ is not required to be PSD nor square. When $d = e$ and \mathbf{M} is in \mathbb{S}_+^d , this corresponds to the similarity function $S_{\mathbf{M}}(\mathbf{x}, \mathbf{z}) = \langle \mathbf{L}\mathbf{x}, \mathbf{L}\mathbf{z} \rangle$ where $\mathbf{M} = \mathbf{L}^\top \mathbf{L}$.

This type of similarity has been used for image classification [Chechik et al., 2009] and retrieval [Chechik et al., 2009, Deng et al., 2011]. It has two main advantages: when the vectors \mathbf{x} and \mathbf{z} are sparse and have k_x and k_z nonzero elements, $S_{\mathbf{M}}(\mathbf{x}, \mathbf{z})$ can be computed in $O(k_x k_z)$ time. Moreover, it can be used to compare objects of different types: for instance, in [Akata et al., 2013], images and attributes (high-level descriptions of concepts) are embedded and compared in a single space.

1.3.3 Learning scheme

The goal of supervised distance metric learning is to infer a (linear) transformation that is optimized for a specific prediction task, such as ranking or nearest-neighbor classification. The transformation induces a distance metric that is generally learned so that distances between similar (resp. dissimilar) samples are small (resp. large) or to preserve orders of distances between training samples. Metric Learning has been applied to compare different types of data representations such as vectors, character strings or trees (see [Bellet et al., 2013] for details). In this thesis, we focus on learning distance metrics to compare vector representations of images (or webpages).

Distance metric learning is an area of machine learning and, as such, the formulation of its problems is similar to many (supervised) machine learning problems. In this section, we present the general formulation of machine learning problems, and particularly focus on metric learning problems.

1.3.3.1 Optimization problem

A metric learning algorithm aims at determining the matrix $\mathbf{M} \in \mathbb{R}^{d \times d}$ such that the metric parameterized by \mathbf{M} satisfies most of the constraints defined by the training information. The training information is usually either:

- Similar/Dissimilar pairs: the training set is composed of a set \mathcal{S} of similar pairs of samples, and a set \mathcal{D} of dissimilar pairs of samples.
- Ordered relations of distances: the training set is composed of a set $\mathcal{T} = \{(\mathcal{I}_i, \mathcal{I}_i^+, \mathcal{I}_i^-)\}_i$ of triplets of samples. The goal is to learn a distance metric such that the distance between \mathcal{I}_i and \mathcal{I}_i^+ is smaller than the distance between \mathcal{I}_i and \mathcal{I}_i^- .

The way the training information is provided and exploited will be discussed in Section 1.4. For simplicity, we consider that all the sets \mathcal{S} , \mathcal{D} and \mathcal{T} are subsets of the training set \mathcal{N} . Metric learning problems are generally formulated as an optimization problem of the form:

$$\min_{\mathbf{M}} \mu R(\mathbf{M}) + \ell(\mathbf{M}, \mathcal{N}) \text{ s.t. } \mathbf{M} \in \mathcal{C} \quad (1.2)$$

where \mathcal{C} an arbitrary convex domain (e.g., \mathbb{S}^d or \mathbb{S}_+^d), $\ell(\mathbf{M}, \mathcal{N})$ is a loss function that penalizes constraints that are not satisfied by the model induced by \mathbf{M} , $R(\mathbf{M})$ is a regularization term on the parameter \mathbf{M} , and $\mu \geq 0$ is the regularization parameter. The loss function $\ell(\mathbf{M}, \mathcal{N})$ measures the ability of the matrix \mathbf{M} to satisfy some distance constraints provided by the training set \mathcal{N} . The details on the design of the set \mathcal{N} and the loss $\ell(\mathbf{M}, \mathcal{N})$ are specified in the following.

In this thesis, we only consider the case where the learned model is a Mahalanobis(-like) distance metric (i.e., $\mathcal{C} = \mathbb{S}_+^d$, and the model is the metric $D_{\mathbf{M}}^2(\mathcal{I}_i, \mathcal{I}_j) = (\mathbf{x}_i - \mathbf{x}_j)^\top \mathbf{M}(\mathbf{x}_i - \mathbf{x}_j)$).

1.3.3.2 Loss and surrogate functions

Choosing an appropriate loss function is not an easy task and strongly depends on the problem at hand. In order to explain surrogate functions, we first need to introduce how training data is provided and exploited in supervised machine learning problems. We use the binary-class classification setting as a reference problem for explanation. We are given a set of n training samples $\{(\mathbf{x}_1, y_1), (\mathbf{x}_2, y_2), \dots, (\mathbf{x}_n, y_n)\}$ where each \mathbf{x}_i belongs to some input space \mathcal{X} , usually \mathbb{R}^d , and $y_i \in \{-1, 1\}$ is the class label of \mathbf{x}_i . The goal of classification machine learning algorithms is to find a model that maximizes the number of correct labels predicted for a given set of test samples.

For this purpose, we are given a loss function $L : \{-1, 1\} \times \{-1, 1\} \rightarrow \mathbb{R}$ that measures the error of a given prediction. The loss function L takes as argument an arbitrary point (\hat{y}, y) , and its value is interpreted as the cost incurred by predicting the label \hat{y} when the true label is y . In the classification context, this loss function L is usually the zero-one (0/1) loss, i.e., $L(\hat{y}, y) = 0$ if $y = \hat{y}$, and $L(\hat{y}, y) = 1$ otherwise. The goal is then to find a classifier, represented by the function $h : \mathcal{X} \rightarrow \{-1, 1\}$, with the smallest expected loss on a new sample. However, the probability distribution of the variables is usually unknown to the learning algorithm, and computing the exact expected value is not possible. That is why it is approximated by averaging the loss function on the training set (i.e., averaging the number of wrongly classified examples in the training set):

$$\mathcal{R}_{emp}(h) = \frac{1}{n} \sum_{i=1}^n L(h(\mathbf{x}_i), y_i)$$

which is called the empirical risk. Empirical risk minimization states that the learning algorithm should choose a hypothesis \hat{h} which minimizes the empirical risk $\hat{h} = \operatorname{argmin}_{h \in \mathcal{F}} \mathcal{R}_{emp}(h)$ where \mathcal{F} is a fixed class of functions.

Another issue is that the problem of finding the function \hat{h} that maximizes the number of correctly classified training examples is NP-hard. The 0/1 loss is therefore generally replaced by a proxy to the loss, called a surrogate loss function, which is usually convex and hence has better convergence properties. The interested reader can refer to [Bartlett et al., 2006, Tewari and Bartlett, 2007]. For classification, the most commonly used surrogate loss functions (with $y \in \{-1, 1\}$ and $h(\mathbf{x}) \in \mathbb{R}$) are:

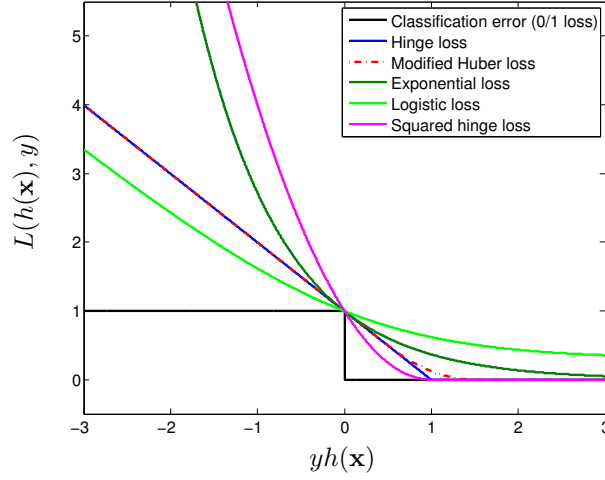


Figure 1.6: Examples of surrogate loss functions for the zero-one loss.

- the hinge loss $\ell_{\text{hinge}}(h(\mathbf{x}), y) = [1 - yh(\mathbf{x})]_+ = \max(0, 1 - yh(\mathbf{x}))$ used in the support vector machine (SVM) [Cortes and Vapnik, 1995] (note that slack variables used in SVMs are equivalent to the hinge loss function: the non-negative ξ that minimizes the constraint $t \geq 1 - \xi$ is $\max(0, 1 - t)$).
- the squared hinge loss $\ell_{\text{hinge}}^2(h(\mathbf{x}), y) = [1 - yh(\mathbf{x})]_+^2 = \max(0, 1 - yh(\mathbf{x}))^2$ used for relative attributes [Parikh and Grauman, 2011].
- The modified Huber loss [Chapelle, 2007], a differentiable approximation of the hinge loss:

$$L_{\text{hub}}^\gamma(h(\mathbf{x}), y) = \begin{cases} 0 & \text{if } yh(\mathbf{x}) > 1 + \gamma \quad (\text{zero loss}) \\ \frac{(1 + \gamma - yh(\mathbf{x}))^2}{4\gamma} & \text{if } |1 - yh(\mathbf{x})| \leq \gamma \quad (\text{quadratic part}) \\ 1 - yh(\mathbf{x}) & \text{if } yh(\mathbf{x}) < 1 - \gamma \quad (\text{linear part}) \end{cases}$$

where γ is typically a value in $[0.01, 0.5]$.

- the exponential loss: $\ell_{\text{exp}}(h(\mathbf{x}), y) = e^{-yh(\mathbf{x})}$ used in Adaboost [Freund and Schapire, 1995].
- the logistic loss: $\ell_{\text{log}}^\beta(h(\mathbf{x}), y) = \frac{1}{\beta} \ln(1 + e^{-y\beta h(\mathbf{x})})$ used in Logitboost [Friedman et al., 2000] and PCCA [Mignon and Jurie, 2012].

Fig. 1.6 illustrates these loss functions¹² along with the nonconvex 0/1 loss.

Since multiple surrogate loss functions exist to replace the 0/1 loss, a natural question is “which one should be chosen?”. The answer strongly depends on the application task and the training data. In the context of classification, Rosasco et al. [Rosasco et al., 2004] concluded that the hinge loss has better convergence rate than the logistic loss. Chapelle [Chapelle, 2007] proposed to use the squared hinge loss or the modified Huber loss functions that have better convergence rate than the hinge loss by using Newton’s method. The interested reader can refer to [Mahdavi, 2014].

1.3.4 Review of popular metric learning approaches

We present some of the most popular approaches in metric learning. We particularly focus on Mahalanobis distance metric learning where the goal is to learn a distance metric parameterized by a matrix $\mathbf{M} \in \mathbb{S}_+^d$ such that the learned metric can be formulated: $D_{\mathbf{M}}^2(\mathcal{I}_i, \mathcal{I}_j) = \Phi(\mathcal{I}_i, \mathcal{I}_j)^\top \mathbf{M} \Phi(\mathcal{I}_i, \mathcal{I}_j) = \langle \mathbf{M}, \mathbf{C}_{ij} \rangle$ where $\mathbf{C}_{ij} = \Phi(\mathcal{I}_i, \mathcal{I}_j) \Phi(\mathcal{I}_i, \mathcal{I}_j)^\top$ and $\Phi(\mathcal{I}_i, \mathcal{I}_j)$ is usually $(\mathbf{x}_i - \mathbf{x}_j)$. For an exhaustive list of metric learning algorithms, the interested reader can read the recent surveys of [Kulis, 2012, Bellet et al., 2013].

¹²For the logistic loss, we actually plot $\ell_{\text{log}2}(h(\mathbf{x}), y) = \log(1 + e^{-yh(\mathbf{x})}) - \log(2) + 1$.

1.3.4.1 MMC (Xing et al.)

The work of [Xing et al., 2002] is the first Mahalanobis distance metric learning problem. It relies on a convex Semi-Definite Programming (SDP) formulation which aims at minimizing the distances of similar samples while maintaining the sum of the dissimilar samples beyond a given threshold (here 1)¹³:

$$\min_{\mathbf{M} \in \mathbb{S}_+^d} \sum_{(\mathcal{I}_i, \mathcal{I}_j) \in \mathcal{S}} D_{\mathbf{M}}^2(\mathcal{I}_i, \mathcal{I}_j) \quad s.t. \quad \sum_{(\mathcal{I}_i, \mathcal{I}_j) \in \mathcal{D}} \sqrt{D_{\mathbf{M}}^2(\mathcal{I}_i, \mathcal{I}_j)} \geq 1 \quad (1.3)$$

The term $\sum_{(\mathcal{I}_i, \mathcal{I}_j) \in \mathcal{S}} D_{\mathbf{M}}^2(\mathcal{I}_i, \mathcal{I}_j)$ can be seen as a regularization term [Kulis, 2012] as will be explained in Section 1.5.1.

The main drawback of the method is the basic SDP solver proposed by [Xing et al., 2002] which makes it unscalable. Moreover, there is no regularization term to control the rank of the solution, this can lead to high-rank solutions that are prone to overfitting.

1.3.4.2 Schultz & Joachims' method

Schultz and Joachims [Schultz and Joachims, 2004] propose to write the PSD matrix $\mathbf{M} = \mathbf{A}\mathbf{W}\mathbf{A}$ where \mathbf{A} is a fixed matrix, and the matrix \mathbf{W} is diagonal. Instead of working on similar/dissimilar pairs as in [Xing et al., 2002], they work on triplets $(\mathcal{I}_i, \mathcal{I}_i^+, \mathcal{I}_i^-) \in \mathcal{T}$ and want the distance $D_{\mathbf{M}}^2(\mathcal{I}_i, \mathcal{I}_i^+)$ to be smaller than $D_{\mathbf{M}}^2(\mathcal{I}_i, \mathcal{I}_i^-)$. For this purpose, they write their problem as:

$$\begin{aligned} \min_{\mathbf{M} \in \mathbb{S}_+^d} \quad & \|\mathbf{M}\|_F^2 + \sum_{(\mathcal{I}_i, \mathcal{I}_i^+, \mathcal{I}_i^-) \in \mathcal{T}} \xi_i \\ \text{s.t.} \quad & \forall (\mathcal{I}_i, \mathcal{I}_i^+, \mathcal{I}_i^-) \in \mathcal{T}, \quad D_{\mathbf{M}}^2(\mathcal{I}_i, \mathcal{I}_i^-) \geq 1 + D_{\mathbf{M}}^2(\mathcal{I}_i, \mathcal{I}_i^+) - \xi_i \\ & \xi_i \geq 0, \quad \mathbf{M} = \mathbf{A}\mathbf{W}\mathbf{A}, \quad \mathbf{A} \text{ fixed}, \quad \mathbf{W} \text{ diagonal} \end{aligned} \quad (1.4)$$

where $\|\mathbf{M}\|_F^2$ is the squared Frobenius norm of \mathbf{M} . Slack variables ξ_i are introduced to allow penalized constraints. The problem in Eq. (1.4) is convex and actually an extension of RankSVM [Joachims, 2002], it can thus be solved efficiently. The main drawback of the method is that the learned matrix \mathbf{W} is diagonal, which limits the domain of the solution but greatly reduces the number of learned parameters (from $\frac{d(d+1)}{2}$ to d) and thus limits overfitting. Moreover, the matrix \mathbf{A} has to be chosen carefully.

1.3.4.3 Neighbourhood Component Analysis (NCA)

Neighbourhood Component Analysis (NCA) [Goldberger et al., 2004] is the first approach that learns a Mahalanobis distance metric for k -NN classification. They consider the multi-class classification problem and want to find a distance metric that maximizes the performance of nearest neighbor classification. Ideally, they would like to optimize performance on future test data, but since they do not know the true data distribution, they instead attempt to optimize leave-one-out (LOO) performance on the training data. For this purpose, they consider the decomposition $\mathbf{M} = \mathbf{L}^\top \mathbf{L}$. They introduce a differentiable cost function based on stochastic neighbor assignments in the space induced by \mathbf{L} . Each point \mathcal{I}_i selects another point \mathcal{I}_j as its neighbor with some probability p_{ij} , and inherits its class label from the point it selects. They define the p_{ij} using a softmax over Euclidean distances in the space induced by \mathbf{L} :

$$p_{ij} = \frac{\exp(-\|\mathbf{L}\mathbf{x}_i - \mathbf{L}\mathbf{x}_j\|_2^2)}{\sum_{k \neq i} \exp(-\|\mathbf{L}\mathbf{x}_i - \mathbf{L}\mathbf{x}_k\|_2^2)} = \frac{\exp(-D_{\mathbf{M}}^2(\mathcal{I}_i, \mathcal{I}_j))}{\sum_{k \neq i} \exp(-D_{\mathbf{M}}^2(\mathcal{I}_i, \mathcal{I}_k))} \quad p_{ii} = 0$$

¹³The authors use the constraint $\sum_{(\mathcal{I}_i, \mathcal{I}_j) \in \mathcal{D}} \sqrt{D_{\mathbf{M}}^2(\mathcal{I}_i, \mathcal{I}_j)}$ instead of the usual squared Mahalanobis distance to avoid learning a matrix \mathbf{M} that is rank 1.

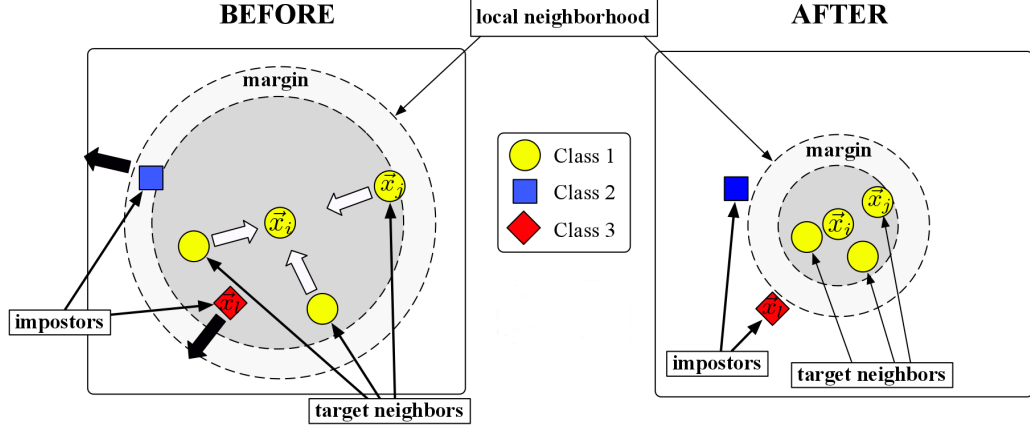


Figure 1.7: LMNN: schematic illustration of one input's neighborhood before training (left) versus after training (right). The learned distance metric is optimized so that the $k = 3$ target neighbors of the input image are its nearest neighbors. Image courtesy of Kilian Weinberger [Weinberger and Saul, 2009].

Let y_i be the class label of \mathcal{I}_i , and denote $C_i = \{\mathcal{I}_j \mid y_i = y_j\}$ the set of images in the same class as \mathcal{I}_i . Their objective problem then tries to maximize:

$$\max_{\mathbf{L}} \sum_i \sum_{j \in C_i} p_{ij}$$

This problem is nonconvex and the optimization scheme is thus subject to local maxima.

1.3.4.4 Large Margin Nearest Neighbors (LMNN)

LMNN [Weinberger et al., 2005, Weinberger and Saul, 2009] is the most popular nearest neighbor metric learning algorithm. For each sample \mathcal{I}_i , LMNN tries to satisfy the condition that members of a pre-defined set of k target neighbors (of the same class y_i) are closer than samples from other classes. In [Weinberger and Saul, 2009], those target neighbors are chosen using the ℓ_2 -distance in the input space. Formally, the constraints are defined in the following way:

$$\begin{aligned} \mathcal{S} &= \{(\mathcal{I}_i, \mathcal{I}_j) \mid y_i = y_j \text{ and } \mathcal{I}_j \text{ is one of the } k \text{ target neighbors of } \mathcal{I}_i\} \\ \mathcal{T} &= \{(\mathcal{I}_i, \mathcal{I}_j, \mathcal{I}_k) \mid (\mathcal{I}_i, \mathcal{I}_j) \in \mathcal{S}, y_i = y_j \neq y_k\} \end{aligned}$$

Their optimization problem is formulated as:

$$\begin{aligned} \min_{\mathbf{M} \in \mathbb{S}_+^d} \quad & \sum_{(\mathcal{I}_i, \mathcal{I}_i^+) \in \mathcal{S}} D_{\mathbf{M}}^2(\mathcal{I}_i, \mathcal{I}_i^+) + \sum_{(\mathcal{I}_i, \mathcal{I}_i^+, \mathcal{I}_i^-) \in \mathcal{T}} \xi_i \\ \text{s.t.} \quad & \forall (\mathcal{I}_i, \mathcal{I}_i^+, \mathcal{I}_i^-) \in \mathcal{T}, D_{\mathbf{M}}^2(\mathcal{I}_i, \mathcal{I}_i^-) \geq 1 + D_{\mathbf{M}}^2(\mathcal{I}_i, \mathcal{I}_i^+) - \xi_i \\ & \xi_i \geq 0 \end{aligned} \tag{1.5}$$

It is convex in \mathbf{M} when the target neighbors remain fixed.¹⁴ Note that the regularization term (i.e., the sum of distances between similar samples $\sum_{(\mathcal{I}_i, \mathcal{I}_i^+) \in \mathcal{S}} D_{\mathbf{M}}^2(\mathcal{I}_i, \mathcal{I}_i^+)$) is the same as in [Xing et al., 2002]. The authors developed an efficient method based on projected subgradient method to optimize this problem with billions of constraints. This method obtains in practice excellent recognition performance,

¹⁴However, it would be nonconvex if the nearest neighbors were updated for each value of \mathbf{M} .

although it is prone to overfitting [Chechik et al., 2010] when the input space dimensionality is large. Indeed, it usually returns high-rank solutions due to the lack of regularizer that controls its complexity.

1.3.4.5 Information-Theoretical Metric Learning (ITML)

ITML [Davis et al., 2007] introduces the LogDet divergence regularization. The LogDet divergence between the learned matrix $\mathbf{M} \in \mathbb{S}_+^d$ and the fixed matrix $\mathbf{M}_0 \in \mathbb{S}_+^d$ is defined as:

$$D_{\ell d}(\mathbf{M}, \mathbf{M}_0) = \text{tr}(\mathbf{M}\mathbf{M}_0^{-1}) - \log \det(\mathbf{M}\mathbf{M}_0^{-1}) - d \quad (1.6)$$

where d is the dimensionality of the input space. It represents a measure of “closeness” between \mathbf{M} and \mathbf{M}_0 via an information-theoretic approach, which will be explained in Section 1.5.1.3.

The matrix \mathbf{M} is learned so that it remains as “close” as possible to the fixed matrix \mathbf{M}_0 . In practice, the matrix \mathbf{M}_0 is usually the identity matrix, i.e., the learned metric is learned to be similar to the Euclidean distance that works well in practice. The advantage of this regularizer is that the value $D_{\ell d}(\mathbf{M}, \mathbf{M}_0)$ is finite if and only if \mathbf{M} is in \mathbb{S}_{++}^d (a subset of \mathbb{S}_+^d), which provides a cheap way to ensure that we learn a Mahalanobis distance metric. However, the LogDet regularizer of ITML constrains \mathbf{M} to be (strictly) positive definite, which means that it returns a full rank matrix and is thus prone to overfitting.

They consider the binary-class classification of pairs (with pairs either in \mathcal{S} or \mathcal{D}) and want the distance of similar pairs to be smaller than a given threshold $u > 0$, and the distance of dissimilar pairs to be greater than the threshold l (with $u < l$):

- $\forall (\mathcal{I}_i, \mathcal{I}_j) \in \mathcal{S}, D_{\mathbf{M}}^2(\mathcal{I}_i, \mathcal{I}_j) \leq u$
- $\forall (\mathcal{I}_i, \mathcal{I}_j) \in \mathcal{D}, l \leq D_{\mathbf{M}}^2(\mathcal{I}_i, \mathcal{I}_j)$

Let $c(i, j)$ denote the index of the (i, j) -th constraint, and let $\boldsymbol{\xi}$ be a vector of slack variables initialized to $\boldsymbol{\xi}_0$ (whose components equal u for similarity constraints and l for dissimilarity constraints). They pose the following problem¹⁵:

$$\begin{aligned} \min_{\mathbf{M} \in \mathbb{S}_+^d, \boldsymbol{\xi}} \quad & D_{\ell d}(\mathbf{M}, \mathbf{M}_0) + \gamma D_{\ell d}(\text{Diag}(\boldsymbol{\xi}), \text{Diag}(\boldsymbol{\xi}_0)) \\ \text{s.t.} \quad & \forall (\mathcal{I}_i, \mathcal{I}_j) \in \mathcal{S}, D_{\mathbf{M}}^2(\mathcal{I}_i, \mathcal{I}_j) \leq \xi_{c(i,j)} \\ & \forall (\mathcal{I}_i, \mathcal{I}_j) \in \mathcal{D}, \xi_{c(i,j)} \leq D_{\mathbf{M}}^2(\mathcal{I}_i, \mathcal{I}_j) \end{aligned}$$

The optimization method, based on a succession of Bregman projections, is efficient and works well in practice. However, it returns full rank solutions and the matrix \mathbf{M}_0 has to be chosen carefully.

1.3.4.6 Logistic Discriminant-based Metric Learning (LDML)

In the context of binary-class classification of pairs, LDML [Guillaumin et al., 2009] defines the probability p_{ij} that the pair $(\mathcal{I}_i, \mathcal{I}_j)$ is positive/similar:

$$p_{ij} = p((\mathcal{I}_i, \mathcal{I}_j) \in \mathcal{S} | \mathbf{M}, b) = S(b - D_{\mathbf{M}}^2(\mathcal{I}_i, \mathcal{I}_j))$$

where $S(t) = \frac{1}{1+e^{-t}}$ is the sigmoid function, and $b > 0$ is a bias term that works as a threshold value to know whether $(\mathcal{I}_i, \mathcal{I}_j)$ is in \mathcal{S} or \mathcal{D} . The probability that $(\mathcal{I}_i, \mathcal{I}_j)$ is negative/dissimilar is $(1 - p_{ij})$. Their optimization problem is formulated as a maximization of the log-likelihood:

$$\mathcal{L} = \sum_{(\mathcal{I}_i, \mathcal{I}_j) \in \mathcal{S}} \ln(p_{ij}) + \sum_{(\mathcal{I}_i, \mathcal{I}_j) \in \mathcal{D}} \ln(1 - p_{ij})$$

¹⁵Note that the term $D_{\ell d}(\text{Diag}(\boldsymbol{\xi}), \text{Diag}(\boldsymbol{\xi}_0))$ implicitly constraints all the components of $\boldsymbol{\xi}$ to be positive.

which is known to be smooth and concave. They optimize it using gradient ascent and claim that their method is faster than ITML and LMNN since they remove the constraint $\mathbf{M} \in \mathbb{S}_+^d$. If needed, the constraint $\mathbf{M} \in \mathbb{S}_+^d$ can be added and the problem is solved using the projected gradient method.

The main limitations of the method are that LDML does not guarantee \mathbf{M} to be PSD, and it does not use any regularization term to control the rank of \mathbf{M} , which can lead to overfitting when the input space is high-dimensional.

1.3.4.7 Pairwise Constrained Component Analysis (PCCA)

In order to deal with high-dimensional input spaces, PCCA [Mignon and Jurie, 2012] controls the rank of $\mathbf{M} \in \mathbb{S}_+^d$ by directly optimizing over the transformation matrix $\mathbf{L} \in \mathbb{R}^{d \times e}$ where $e < d$ and $\mathbf{M} = \mathbf{L}^\top \mathbf{L}$ (in the same way as NCA). Optimizing over \mathbf{L} ensures that the rank of \mathbf{M} is low since $e \geq \text{rank}(\mathbf{L}) = \text{rank}(\mathbf{M})$. Their constraints are similar to the ones used in ITML, i.e., $\forall (\mathcal{I}_i, \mathcal{I}_j) \in \mathcal{S}, D_{\mathbf{M}^2}(\mathcal{I}_i, \mathcal{I}_j) < 1$, and $\forall (\mathcal{I}_i, \mathcal{I}_j) \in \mathcal{D}, D_{\mathbf{M}^2}(\mathcal{I}_i, \mathcal{I}_j) > 1$. Instead of using a hinge loss (or its equivalent formulation with slack variables) to optimize the problem, they use another surrogate to the 0/1 loss, which is the logistic loss function (see Section 1.3.3.2): $\ell_{\log}^\beta(x) = \frac{1}{\beta} \ln(1 + e^{-\beta x})$. It is a smooth and differentiable approximation of the hinge loss function. Their problem is formulated as

$$\min_{\mathbf{M}} \sum_{(\mathcal{I}_i, \mathcal{I}_j) \in \{\mathcal{S} \cup \mathcal{D}\}} \ell_{\log}^\beta(y_{ij} (D_{\mathbf{M}^2}(\mathcal{I}_i, \mathcal{I}_j) - 1))$$

where $y_{ij} = 1$ if $(\mathcal{I}_i, \mathcal{I}_j) \in \mathcal{D}$ and $y_{ij} = -1$ otherwise.

The advantage of their method is that it is fast to optimize, and their method returns a low rank PSD matrix. However, the problem is nonconvex in \mathbf{L} , and they do not use an explicit regularization term (although they control the rank of \mathbf{M} by optimizing over \mathbf{L}). They then use *early stopping* to avoid overfitting.

Structural metric learning Another family of metric learning approaches [McFee and Lanckriet, 2010, Lim et al., 2013] are inspired from structural SVM [Tschantz et al., 2005] which predicts a structure output.

Structural SVM can be viewed as a generalization of multi-class SVM [Crammer and Singer, 2002] for which the set of predicted outputs contains structures (instead of labels for the classic SVM). The output of the structural SVM can be a parse tree, permutation, ranking, sequence alignment etc. The multiclass SVM [Crammer and Singer, 2002] learns a different model $\mathbf{w}_y \in \mathcal{X}$ for each class $y \in \{1, \dots, K\}$ where K is the number of classes in the training set. For each training example (\mathbf{x}, y^*) , the models are learned so that the prediction score for the true class y^* is greater (by a margin of 1) than the prediction scores for the other classes:

$$\forall y \neq y^*, \mathbf{w}_{y^*}^\top \mathbf{x} \geq \mathbf{w}_y^\top \mathbf{x} + 1$$

In a similar manner, structural SVM enforces the prediction score of the *true* structure y^* to be greater than the score of other structures y in the set of outputs \mathcal{Y} (by a margin of $\Delta(y^*, y) \geq 0$ which quantifies the loss associated with a prediction y if the true structure is y^*):

$$\forall y \in \mathcal{Y} \setminus \{y^*\}, \mathbf{w}^\top \psi(\mathbf{x}, y^*) \geq \mathbf{w}^\top \psi(\mathbf{x}, y) + \Delta(y^*, y) \quad (1.7)$$

where $\psi(\mathbf{x}, y^*)$ is a vector-valued joint feature map which characterizes the relationship between an input \mathbf{x} and an output structure y . Structural predictions for a test example $\hat{\mathbf{x}}$ are made by finding the structure y in \mathcal{Y} which maximizes $\mathbf{w}^\top \psi(\hat{\mathbf{x}}, y)$.

Since the set \mathcal{Y} of possible output structures is generally very large, enforcing all margin constraints in Eq. (1.7) may not be feasible in practice. Therefore, cutting plane methods have been proposed [Tschantz et al., 2005], the idea is to find a small working set $\mathcal{W} \subset \mathcal{Y}$ that is a subset of all possible predictions. These methods work with very small active sets and are sufficient to optimize \mathbf{w} within some

Method	Optimum	Regularization	Rank control	Constraints
MMC	Global	$\sum_{(\mathcal{I}_i, \mathcal{I}_j) \in \mathcal{S}} D_{\mathbf{M}}^2(\mathcal{I}_i, \mathcal{I}_j)$	No	Pairwise
Schultz & Joachims	Global	Frobenius norm	No	Triplet-wise
NCA	Local	Optimization over \mathbf{L}	Yes	For k -NN
LMNN	Global	$\sum_{(\mathcal{I}_i, \mathcal{I}_j) \in \mathcal{S}} D_{\mathbf{M}}^2(\mathcal{I}_i, \mathcal{I}_j)$	No	Triplet-wise for k -NN
ITML	Global	LogDet divergence	No	Pairwise
LDML	Global	None	No	Pairwise
PCCA	Local	optimization over \mathbf{L}	Yes	Pairwise

Table 1.2: Popular metric learning approaches.

prescribed tolerance. At each iteration of the cutting plane method, a vector \mathbf{w} is first optimized for a given small active set $\mathcal{W} \subset \mathcal{Y}$, and the output \hat{y} in \mathcal{Y} that maximizes:

$$\hat{y} \leftarrow \underset{y \in \mathcal{Y}}{\operatorname{argmax}} \mathbf{w}^\top \psi(\hat{\mathbf{x}}, y) + \Delta(y^*, y) \quad (1.8)$$

is added to the active set \mathcal{W} . Efficient algorithms [Joachims, 2005, Yue et al., 2007] have been proposed to compute Eq. (1.8) accurately or approximately depending on the context.

Structural SVM has shown promising results to learn a model optimized for information retrieval evaluation metrics such as Average Precision [Yue et al., 2007], it was then naturally adapted to metric learning for image retrieval [McFee and Lanckriet, 2010]. For each image, a ranking is learned so that similar images to the given image are ranked better than dissimilar images. Moreover, the 1-slack cutting plane method [Joachims et al., 2009], that shares a single slack variable ξ across all constraint batches, allows to optimize the problem more efficiently than classic cutting plane methods.

Recently, structural metric learning has been extended [Lajugie et al., 2014] to predict a partition for a given dataset. It has been successfully applied to image and video segmentation, and bioinformatics application.

Conclusion We have presented popular metric learning approaches summarized in Table 1.2. Two important aspects can be highlighted from them. First, we note that all these methods exploit binary similarity information to generate their constraints. For instance in LMNN, they exploit the class membership information $(\mathcal{I}_i, \mathcal{I}_i^+) \in \mathcal{S}$ and $(\mathcal{I}_i, \mathcal{I}_i^-) \in \mathcal{D}$ to generate their constraints $D_{\mathbf{M}}^2(\mathcal{I}_i, \mathcal{I}_i^+) < D_{\mathbf{M}}^2(\mathcal{I}_i, \mathcal{I}_i^-)$. However, in some contexts that we will present in the following, this binary similarity information can be unknown. Moreover, we remark that large margin metric learning approaches are the most widely used metric learning approaches nowadays. Second, we remark that most of the popular approaches do not control the complexity of their learned model and are thus prone to overfitting. We investigate these two aspects in the following.

1.4 Training Information in Metric Learning

In this section, we study the way information and/or knowledge are exploited to create training constraints and learn a distance metric.

1.4.1 Binary similarity labels

A first remark is that all the approaches presented in Section 1.3 exploit binary similarity labels to generate pairwise or triplet-wise constraints¹⁶. Depending on the application, different criteria generate these binary similarity labels:

- two images represent the same object/face or not. [Guillaumin et al., 2009, Mignon and Jurie, 2012].
- two images belong to the same class or not. [Goldberger et al., 2004, Weinberger and Saul, 2009].
- an image/document is relevant to a given query or not. [Frome et al., 2007, Chechik et al., 2010, McFee and Lanckriet, 2010].

In pairwise approaches [Xing et al., 2002, Davis et al., 2007, Mignon and Jurie, 2012], the problem is formulated as learning the PSD matrix $\mathbf{M} \in \mathbb{S}_+^d$ such that the distance metric $D_{\mathbf{M}}$ allows to separate the set \mathcal{S} of pairs of similar samples from the set \mathcal{D} of pairs of dissimilar samples.

Triplet-wise approaches [Weinberger and Saul, 2009, Frome et al., 2007, Chechik et al., 2010] also exploit binary similarity labels: for a given image \mathcal{I}_i , similar images \mathcal{I}_i^+ and dissimilar images \mathcal{I}_i^- are provided. Since the goal in k -NN classification and retrieval is to find the closest images rather than determining whether images are similar or not, a learning to rank approach is adopted. From the pairs $(\mathcal{I}_i, \mathcal{I}_i^+) \in \mathcal{S}$ and $(\mathcal{I}_i, \mathcal{I}_i^-) \in \mathcal{D}$, they generate the triplet $(\mathcal{I}_i, \mathcal{I}_i^+, \mathcal{I}_i^-) \in \mathcal{T}$ and want $D_{\mathbf{M}}^2(\mathcal{I}_i, \mathcal{I}_i^+)$ to be smaller than $D_{\mathbf{M}}^2(\mathcal{I}_i, \mathcal{I}_i^-)$.

1.4.2 Richer provided information

In order to learn a metric that reflects more accurately relations between data, some approaches exploit information different from binary similarity labels. For instance, in [Weinberger and Chapelle, 2008], a class taxonomy is used in order to get elements of related classes, close to each other. Verma et al. [Verma et al., 2012] extend this work by learning a local Mahalanobis distance metric for each category in a hierarchy. Shaw et al. [Shaw et al., 2011] learn a distance metric from a network such that the learned distances are tied to the inherent connectivity structure of the network. Hwang et al. [Hwang et al., 2011] learn discriminative visual representations while exploiting external semantic knowledge about object category relationships. Parikh and Grauman [Parikh and Grauman, 2011] use semantic comparisons between classes over different criteria, called attributes. They consider totally ordered sets of classes that describe relations among classes. Based on these rich relations, they learn image representations by exploiting only pairwise class relations.

In this thesis, we propose to explore this type of data knowledge in metric learning for image comparison. Particularly, from these contexts where rich information is provided, we will exploit meaningful constraints between quadruplets of images that are not possible in the contexts handled by the methods presented in Section 1.3.

1.4.3 Quadruplet-wise approaches

Approaches that exploit relative distances between quadruplets of objects have been proposed in the context of embedding problems. Embedding problems consist in assigning Euclidean coordinates to a set of objects such that a given set of dissimilarity, similarity or ordinal relations between the points are satisfied. Unlike metric learning approaches, classic embedding methods do not extend to new samples,

¹⁶Even the softmax formulation of NCA can be seen as an aggregation of triplet-wise constraints.

a new embedding has to be learned each time a (new) test sample is added. Shepard [Shepard, 1962a, Shepard, 1962b] considered in 1962 the following problem that involves quadruplets of samples:

Problem: Given a symmetric zero diagonal matrix of distances $\Delta = [d_{ij}] \in \mathbb{S}^n$ between samples i and j , find the Euclidean coordinates $\mathbf{X} = [\mathbf{x}_i] \in \mathbb{R}^{d \times n}$ such that:

$$\forall i, j, k, l \quad \|\mathbf{x}_i - \mathbf{x}_j\|_2^2 < \|\mathbf{x}_k - \mathbf{x}_l\|_2^2 \iff d_{ij} < d_{kl} \quad (1.9)$$

In 1964, Kruskal posed the problem as an optimization problem and introduced an algorithm to solve it [Kruskal, 1964]. He formulated the distance matrix Δ as an exhaustive table of distances where all the values of d_{ij} are given as input. The goal is then to find an Euclidean embedding such that each distance $\|\mathbf{x}_i - \mathbf{x}_j\|^2$ is close enough to d_{ij} . This leads to the problem of minimizing the stress-1 functional:

$$\sigma_1(\mathbf{X}) = \min_{\theta} \frac{\sum_{ij} (\|\mathbf{x}_i - \mathbf{x}_j\|^2 - \theta(d_{ij}))^2}{\sum_{ij} \|\mathbf{x}_i - \mathbf{x}_j\|^2} \quad (1.10)$$

where θ is an arbitrary monotonic function. The problem in Eq. (1.10) consists in minimizing the distance between the scalar input value $\theta(d_{ij})$ and the distance between the samples i and j in the underlying low-dimensional space. The underlying idea is that if $\sigma_1(\mathbf{X})$ is minimized, then (most of) the constraints in Eq. (1.9) are satisfied.

Noticing that the problem formulated by Kruskal requires the magnitudes of all the distances d_{ij} as input, and not the relative orderings of distances as in Eq. (1.9), Agarwal et al. [Agarwal et al., 2007] propose to consider only ordinal information as input to learn a generalized non-metric multidimensional scaling. This work is extended to kernels in [McFee and Lanckriet, 2009]. Hwang et al. [Hwang et al., 2013] exploit analogy preserving constraints that involve four different classes (e.g., “a canine is to a dog as a cat is to feline” or “a fish is to water as a bird is to sky”). However, they are only interested in equivalence constraints.

The idea of comparing pairs of distances (between quadruplets of images) seemed interesting to us to adapt in the context of supervised distance metric learning.

Conclusion We have shown in this section that popular metric learning methods exploit basic similarity information in order to generate their constraints and solve generic metric learning problems. Nonetheless, some metric learning approaches [Weinberger and Chapelle, 2008, Verma et al., 2012] have considered specific problems where rich information (in this case class taxonomy) is exploited to generate appropriate training constraints.

In this thesis, we will investigate such contexts where the training information is not simply binary similarity information. In particular, we will propose a general distance metric learning framework that exploits meaningful relations between quadruplets of images in specific problems. Our motivation to exploit constraints between quadruplets of images will be detailed in Chapter 2.

1.5 Regularization in Metric Learning

The goal of regularization in machine learning is to prevent overfitting. The choice of regularization has a significant impact on the learned model, both theoretically and algorithmically. The most popular regularization methods in machine learning are the inclusion of a regularization term in the objective function or stopping the learning process before convergence by using a validation set. In this section, we present popular regularization methods applied in Mahalanobis distance metric learning where the learned model is a vector or PSD matrix.

1.5.1 Representative regularization terms

This subsection presents popular regularization terms used in metric learning.

1.5.1.1 Frobenius norm regularization

One of the most popular regularization techniques is based on the squared Frobenius norm:

$$R(\mathbf{M}) = \frac{1}{2} \|\mathbf{M}\|_F^2 = \frac{1}{2} \langle \mathbf{M}, \mathbf{M} \rangle$$

which can be viewed as the matrix analog of the standard- ℓ_2 regularizer used in SVMs or ridge regression. Since the Frobenius norm does not promote low rank solution, using it as a regularizer can lead to a learned matrix $\mathbf{M} \in \mathbb{S}^d$ with $d(d+1)/2$ independent parameters, which is prone to overfitting when d is large.

When the learned matrix $\mathbf{M} = \text{Diag}(\mathbf{w}) \in \mathbb{S}^d$ is constrained to be diagonal (as for instance in [Schultz and Joachims, 2004]), the advantage of the method is that the number of parameters grows linearly (instead of quadratically in the general case) in the input space dimensionality and is therefore more scalable and more robust. Moreover, the optimization over the diagonal $\mathbf{w} \in \mathbb{R}^d$ becomes similar to the SVM with the exception that the constraint $\mathbf{M} \in \mathbb{R}_+^d$ implies $\mathbf{w} \in \mathbb{R}_+^d$ since the diagonal elements of a symmetric matrix are its eigenvalues.

1.5.1.2 Linear regularization

We now consider two cases where the regularization term can be written as:

$$R(\mathbf{M}) = \text{tr}(\mathbf{M}\mathbf{C}) = \langle \mathbf{M}, \mathbf{C} \rangle \text{ where } \mathbf{C} \in \mathbb{S}_+^d$$

Sum of distances between similar samples The sum of the distances between similar samples is used in popular metric learning approaches [Xing et al., 2002, Weinberger and Saul, 2009]. It is formulated $\sum_{(\mathcal{I}_i, \mathcal{I}_j) \in \mathcal{S}} D_{\mathbf{M}}^2(\mathcal{I}_i, \mathcal{I}_j) = \langle \mathbf{M}, \mathbf{C} \rangle$ where $\mathbf{C} = \sum_{(\mathcal{I}_i, \mathcal{I}_j) \in \mathcal{S}} \Phi(\mathcal{I}_i, \mathcal{I}_j) \Phi(\mathcal{I}_i, \mathcal{I}_j)^\top$.

The advantage of this regularizer is that it does not only focus on separating similar and dissimilar samples, it also promotes small distances for similar samples, which is the natural goal of a learned metric. Let b be the bias term that works as a threshold value to know whether a given pair $(\mathcal{I}_i, \mathcal{I}_j)$ is in \mathcal{S} or \mathcal{D} , this regularizer implicitly promotes small values of b . The main problem of this regularizer is that it does not promote a low-rank solution and is then prone to overfitting when d is large.

Nuclear norm/Trace-norm regularization : $\mathbf{C} = \mathbf{I}_d$

The two previously presented regularizers are prone to overfitting when the dimensionality d of the input space is large since they can lead to matrix solutions with $d(d+1)/2$ independent parameters. Two standard ways to limit the number of independent parameters are promoting (1) sparsity (small number of nonzero elements) or (2) low-rank solutions (since a matrix in \mathbb{S}_+^d of rank e has $O(e \times d)$

independent parameters). Low-rank solutions are usually preferred because they allow to better exploit correlations between data. However, minimizing a convex function subject to a rank constraint is NP-hard [Natarajan, 1995]. A standard way to promote low-rank solutions is then to use the nuclear norm $\|\mathbf{X}\|_*$ as a regularization term as it is the convex envelope¹⁷ of $\text{rank}(\mathbf{X})$ on the set $\{\mathbf{X} \in \mathbb{R}^{m \times n} : \|\mathbf{X}\| \leq 1\}$ [Fazel, 2002]. The nuclear norm can also be thought of as a convex relaxation of the number of non-zero singular values (i.e., the rank). In the case of PSD matrices, the nuclear norm (i.e., the sum of singular values of a matrix) corresponds to the trace (i.e., the sum of eigenvalues) since the singular values of a symmetric PSD matrix are also its eigenvalues (see Proposition A.1.5): $\forall \mathbf{M} \in \mathbb{S}_+^d, \|\mathbf{M}\|_* = \text{tr}(\mathbf{M}) = \langle \mathbf{M}, \mathbf{I}_d \rangle$ where $\mathbf{I}_d \in \mathbb{S}_+^d$ is the identity matrix.

This formulation of the nuclear norm for PSD matrices allows nice methods to optimize it.

1.5.1.3 LogDet divergence regularization

The regularization term considered in ITML [Davis et al., 2007] is:

$$R(\mathbf{M}) = \text{tr}(\mathbf{M}) - \log \det(\mathbf{M})$$

which is a special case of the *LogDet divergence*:

$$D_{\ell d}(\mathbf{M}, \mathbf{M}_0) = \text{tr}(\mathbf{M}\mathbf{M}_0^{-1}) - \log \det(\mathbf{M}\mathbf{M}_0^{-1}) - d$$

where d is the dimensionality of the input data (and hence, a constant value). Minimizing $R(\mathbf{M})$ is then equivalent to minimizing $D_{\ell d}(\mathbf{M}, \mathbf{I}_d)$ where \mathbf{I}_d is the identity matrix. We also have the following equivalence: $D_{\ell d}(\mathbf{M}, \mathbf{M}_0) = R(\mathbf{M}_0^{-1/2}\mathbf{M}\mathbf{M}_0^{-1/2})$.

The *LogDet divergence* has some nice properties that are useful for metric learning:

- Its value is finite (and can thus be minimized) only if \mathbf{M} is in \mathbb{S}_{++}^d . This ensures that the learned matrix satisfies the constraint $\mathbf{M} \in \mathbb{S}_+^d$ (since $\mathbb{S}_{++}^d \subset \mathbb{S}_+^d$) without performing projections onto \mathbb{S}_+^d .
- Scale invariance: it satisfies $D_{\ell d}(\mathbf{M}, \mathbf{M}_0) = D_{\ell d}(\alpha\mathbf{M}, \alpha\mathbf{M}_0)$ for all $\alpha > 0$.
- Translation invariance: for any invertible \mathbf{S} , it satisfies $D_{\ell d}(\mathbf{M}, \mathbf{M}_0) = D_{\ell d}(\mathbf{S}^\top \mathbf{M} \mathbf{S}, \mathbf{S}^\top \mathbf{M}_0 \mathbf{S})$.
- Connection to multivariate Gaussians: let us consider the multivariate Gaussian parameterized by mean $\boldsymbol{\mu}$ and precision matrix \mathbf{M} : $p(\mathbf{x}; \boldsymbol{\mu}, \mathbf{M}) = \frac{1}{Z} \exp(-D_{\mathbf{M}}^2(\mathbf{x}, \boldsymbol{\mu}))$. We have the following property between the Kullback-Leibler divergence (KL) between two multivariate Gaussians of the same mean:

$$\text{KL}(p(\mathbf{x}; \boldsymbol{\mu}, \mathbf{M}_0) \| p(\mathbf{x}; \boldsymbol{\mu}, \mathbf{M})) = \frac{1}{2} D_{\ell d}(\mathbf{M}, \mathbf{M}_0)$$

The last property exhibits the connection between this regularization term and information theory.

The main limitation of this method is that it returns a solution matrix in \mathbb{S}_{++}^d , which is full rank and thus prone to overfitting when the input space is high-dimensional.

1.5.2 Other regularization methods in Computer Vision

Other regularization methods that do not include a regularization term in the objective function are used in metric learning, particularly in the computer vision community.

¹⁷The convex envelope of a function $f : \mathcal{C} \rightarrow \mathbb{R}$ is the largest convex function g such that $g \leq f$ on convex domain $\mathcal{C} \subseteq \mathbb{R}^n$.

Name	Formula	Pros	Cons
ℓ_0 -norm $\ \mathbf{M}\ _0$	Number of nonzero elements	sparsity	nonconvex, nonsmooth
ℓ_1 -norm $\ \mathbf{M}\ _1$	$\sum_{ij} M_{ij} $	convex, sparsity	nonsmooth
Nuclear norm $\ \mathbf{M}\ _*$	Sum of singular values	convex, low-rank	nonsmooth
Sq. Frobenius norm $\ \mathbf{M}\ _F^2$	$\sum_{ij} M_{ij}^2$	convex, smooth	no rank control
Sum of similar distances	$\sum_{(\mathcal{I}_i, \mathcal{I}_j) \in \mathcal{S}} D_{\mathbf{M}}^2(\mathcal{I}_i, \mathcal{I}_j)$	convex	nonsmooth ¹⁸ , no rank control
LogDet Divergence	$\text{tr}(\mathbf{M}) - \log \det(\mathbf{M})$	convex, smooth	full-rank

Table 1.3: Common regularizers for PSD matrices in metric learning.

1.5.2.1 Optimizing a metric over a transformation matrix

Since every matrix $\mathbf{M} \in \mathbb{S}_+^d$ can be decomposed $\mathbf{M} = \mathbf{L}^\top \mathbf{L}$ where $\mathbf{L} \in \mathbb{R}^{e \times d}$ and $e \geq \text{rank}(\mathbf{M})$, some methods [Mignon and Jurie, 2012, Mensink et al., 2013] directly write their optimization problem as a function of \mathbf{L} , and optimize over \mathbf{L} . This type of regularization has some nice properties:

- The induced matrix $\mathbf{L}^\top \mathbf{L} = \mathbf{M}$ is guaranteed to be PSD.
- The rank of the induced matrix \mathbf{M} is upperbounded by e , which guarantees a low-rank solution and limits overfitting if e is small.

However, the problem is generally nonconvex in \mathbf{L} and can lead to degenerate solutions. Indeed, the gradient $\nabla_{\mathbf{L}}$ of the optimization problem w.r.t. \mathbf{L} is generally written $\nabla_{\mathbf{L}} = 2\mathbf{L}\nabla_{\mathbf{M}}$ where $\nabla_{\mathbf{M}}$ is the gradient of the optimization problem w.r.t. \mathbf{M} . This implies that two linearly dependent rows of \mathbf{L} will remain linearly dependent after the next gradient descent iteration. The rank of \mathbf{L} is then nonincreasing as a function of the number of gradient descent iterations. If $\mathbf{L} = \mathbf{0}$ at some iteration, it will remain $\mathbf{0}$.

1.5.2.2 Early stopping

The last popular regularization method presented in this thesis and used in metric learning is *early stopping*. Most machine learning methods are iterative algorithms that try to minimize an objective function. However, the real goal of these methods is not to learn an algorithm that minimizes the objective function, it is to minimize prediction error on a test set. Models with a large number of parameters to learn compared to the size of the training dataset are prone to overfitting. To avoid a model that overfits training data, *early stopping* stops the training process before the iterative algorithm converges. For this purpose, a validation set is generally exploited and the training process stops when the average prediction error on the validation set increases. Early stopping has been widely used and studied for neural networks [Prechelt, 1998], and has been reported to be superior to regularization methods in many cases [Geman et al., 1992]. Its simplicity to understand and implement has made it easy to adapt to various machine learning methods.

In distance metric learning, *early stopping* is exploited by methods that do not use an explicit regularization term [Mignon and Jurie, 2012, Mensink et al., 2013] and thus have to stop the learning process before the model overfits training data. It is particularly problematic in the main application of [Mignon and Jurie, 2012] where they learn a model that has more than 100,000 independent parameters, and exploit only $\sim 5,000$ training constraints. Their performance accuracy on the test dataset drops from 82.2% with *early stopping* to 63.2% when their training algorithm converges.

¹⁸It is nonsmooth because it is not differentiable at points $\mathbf{M} \in \mathbb{S}_+^d$ for which there exists a pair $(\mathcal{I}_i, \mathcal{I}_j) \in \mathcal{S}$ such that $D_{\mathbf{M}}^2(\mathcal{I}_i, \mathcal{I}_j) = 0$. Indeed, both $\mathbf{0}$ and $\Phi(\mathcal{I}_i, \mathcal{I}_j)\Phi(\mathcal{I}_i, \mathcal{I}_j)^\top$ are subgradients of $D_{\mathbf{M}}^2(\mathcal{I}_i, \mathcal{I}_j)$ when the domain is \mathbb{S}_+^d and $D_{\mathbf{M}}^2(\mathcal{I}_i, \mathcal{I}_j) = 0$.

Conclusion Regularization terms are summarized in Table 1.3 along with the ℓ_0 and ℓ_1 -norms. Most of them do not control the complexity of the learned model although it is a crucial task in machine learning to avoid overfitting. In Mahalanobis distance metric learning, promoting low-rank solutions is the most popular way to control the number of independent parameters of the model. The two most popular approaches for this purpose are (1) optimizing over the matrix $\mathbf{L} \in \mathbb{R}^{e \times d}$ (where $\mathbf{L}^\top \mathbf{L} = \mathbf{M}$) which leads to nonconvex problems and prevents solutions with rank greater than e or (2) using trace-norm regularization that minimizes all the singular values and can also lead to solutions whose rank is too small.

We propose an alternative regularization method that minimizes the sum of the k smallest singular values of the learned matrix. Such a regularizer has been proposed in the Computer Vision community (e.g., for image inpainting [Criminisi et al., 2004]) to learn any type of real-valued matrix (i.e., which does not have to be a square matrix, nor PSD), it is called the truncated nuclear norm [Hu et al., 2013]. However, we exploit special properties of the cone \mathbb{S}_+^d to propose efficient algorithms.

1.6 Summary

We have presented an overview of metric learning techniques for computer vision. This allowed us to highlight two fundamental points in metric learning schemes, namely: the generation of constraints from training information, and the control of the complexity of the learned metric through regularization.

One of the main contributions of this thesis is the proposal of a metric learning framework to incorporate rich knowledge between data. We investigate in Chapter 2 how constraints which involve quadruplets of images can be useful in some contexts such as relative attributes and hierarchical image classification.

Another contribution is the introduction of a novel regularization method in metric learning to explicitly control the rank of the learned Mahalanobis distance metric. Specifically, a regularization term that minimizes the sum of the k smallest singular values of the learned PSD matrix is proposed in Chapter 3 to limit overfitting.

We also propose in Chapter 4 a novel metric learning application that exploits a type of learning information different from classic metric learning approaches. In particular, we use temporal relationships between successive versions of a same webpage to automatically discover meaningful regions in webpages. We will investigate how the proposed method can be useful in the context of Web archiving and allows to compare only meaningful regions in webpages to detect semantic changes.

Chapter 2

Quadruplet-wise Distance Metric Learning

Chapter Abstract This chapter is concerned with the problem of learning a distance metric by considering meaningful and discriminative distance constraints in some contexts where rich information between data is provided.

Classic metric learning approaches focus on constraints that involve pairs or triplets of images. We first present the limitations of such constraints in some contexts, and the necessity for more general constraints (Section 2.1). We then propose a general Mahalanobis distance metric learning framework that exploits distance constraints over up to four different images (Section 2.2). Particularly, in order to get efficient optimization, it is based on Mahalanobis-like distance metrics embedded in a convex optimization scheme. We present optimization techniques, such as active set methods, to deal with a large number of constraints and make the learning scheme tractable (Section 2.3). We demonstrate the benefit on recognition performance of this type of constraints, in rich contexts such as relative attributes (Section 2.4) and hierarchical image classification (Section 2.5).

In Chapter 4, we also propose a new emerging context about webpage visual screenshot comparison. The proposed context exploits this quadruplet-wise approach to automatically discover important semantic regions in webpages and perform change detection.

Some of the material in this chapter has been published at the following conference:

- Law, M.T., Thome, N., Cord, M. (2013) Quadruplet-wise Image Similarity Learning. *IEEE International Conference on Computer Vision (ICCV)*. [Law et al., 2013]

2.1 Motivation

As explained in Section 1.4, most metric learning approaches focus on contexts where binary similarity information (such as class membership) is used to create pairwise or triplet-wise similarity constraints. We propose in this chapter to investigate meaningful relations between quadruplets of images.

We first motivate why these quadruplet-wise constraints may be useful in some contexts. For this purpose, we illustrate in Fig. 2.1 our approach in the context of relative attributes (see Section 1.2) for which the goal is to learn a projection of visual image features into a high-level semantic space. Each dimension of this high-level semantic space corresponds to the degree of presence of a given attribute (e.g., the presence of nature or large objects in the images). Four scene classes are considered in Fig. 2.1: *tall building* (T), *inside city* (I), *street* (S) and *open country* (O). Class membership information and relative orderings on classes for the attributes “Natural” and “Large objects” are also provided as training information.

In Fig. 2.1, the degrees of presence of nature and of large objects in the *street* image and the *inside-city* image are clearly not equivalent even though their corresponding classes are annotated as having equivalent presence of these attributes. The formulation of the original relative attribute problem

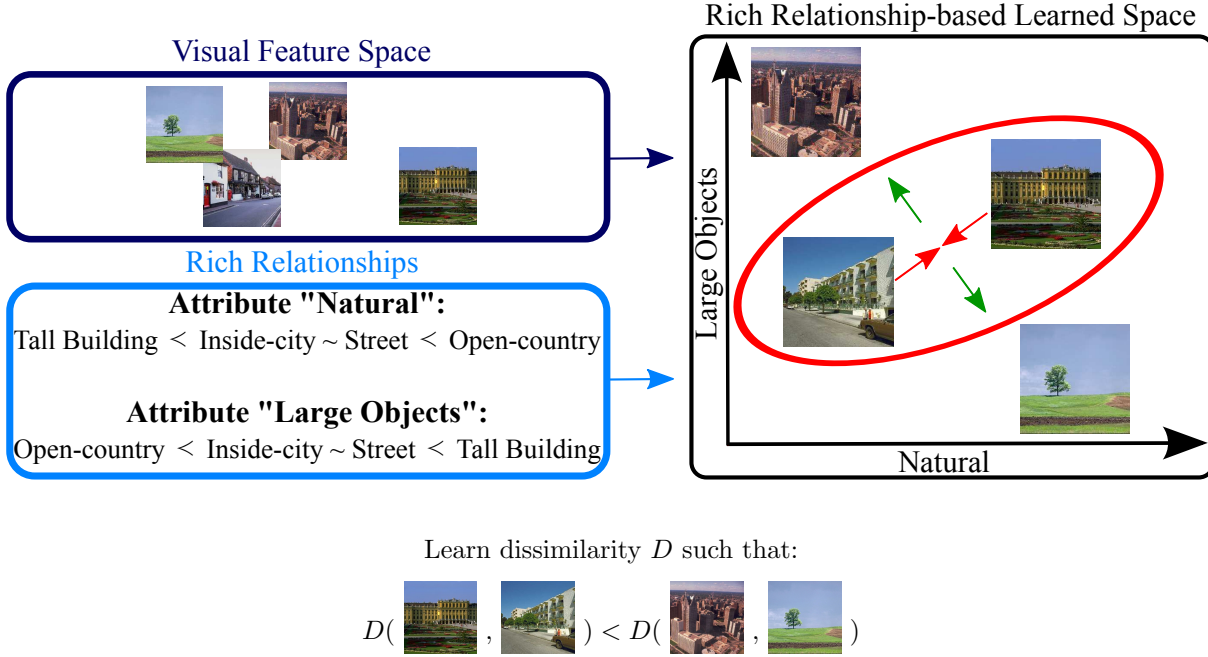


Figure 2.1: Illustration of the quadruplet-wise (Qwise) strategy in the relative attribute context. The goal is to learn a projection of scene images by exploiting rich relationships (here relative attributes) over quadruplets of images such that samples satisfy the relationship constraints in the projected space.

[Parikh and Grauman, 2011] that promotes equal scores of presence of these attributes in these images then seems limited. We argue in this chapter that this type of absolute similarity information between the two images or classes is restrictive, and thus noisy. Alternatively, a natural way to relax and exploit this equivalence information is to upper bound the difference of attribute presence by considering pairs of classes for which the difference of attribute presence is greater. Such pairs of classes are easy to find when the following ordering is given: $(e) \prec (f) \sim (g) \prec (h)$. The difference between classes (f) and (g) is smaller than the difference between (h) and (e) . Since the proposed relaxed constraints better describe relative orderings between the different classes, they are more robust to noisy information.

We propose to exploit this type of constraints, that involves quadruplets of images, in order to learn a simple form of distance metric. Unlike other quadruplet-wise approaches mentioned in Section 1.4.3 (e.g., Eq. (1.9)), we do not learn an embedding but a metric with a different type of supervision. We investigate how constraints that involve quadruplets can better exploit rich relationships between samples in different contexts.

2.2 Quadruplet-wise Similarity Learning Framework

Our goal is to learn a metric that satisfies constraints involving quadruplets of images. We describe the proposed constraints and the distance metric learning problem. The optimization scheme will be presented in Section 2.3.

2.2.1 Quadruplet-wise Constraints

We are given a set \mathcal{P} of images \mathcal{I}_i , and the target dissimilarity function $D : \mathcal{P} \times \mathcal{P} \rightarrow \mathbb{R}$ between pairs of images $(\mathcal{I}_i, \mathcal{I}_j)$, we note $D(\mathcal{I}_i, \mathcal{I}_j) = D_{ij}$. We are interested in comparing pairs of dissimilarities (D_{ij}, D_{kl}) .

Each of them involves up to four different images $(\mathcal{I}_i, \mathcal{I}_j, \mathcal{I}_k, \mathcal{I}_l)$. Two types of relations \mathcal{R} are considered between D_{ij} and D_{kl} :

1. strict inequality between dissimilarities: $D_{ij} < D_{kl}$,
2. non-strict inequality: $D_{ij} \leq D_{kl}$. Note that $D_{ij} = D_{kl}$ can be rewritten as two relations $D_{ij} \leq D_{kl}$ and $D_{ij} \geq D_{kl}$.

In order to deal with these constraints, we approximate them by creating the set of constraints \mathcal{N} in this way:

$$\forall q = (\mathcal{I}_i, \mathcal{I}_j, \mathcal{I}_k, \mathcal{I}_l) \in \mathcal{N}, D_{kl} \geq D_{ij} + \delta_q \quad (2.1)$$

where $\delta_q \in \mathbb{R}$ is a safety margin specific to the quadruplet q . The non-strict inequality constraint corresponds to $\delta_q = 0$. And the strict inequality constraint corresponds to $\delta_q > 0$, δ_q is usually set to 1.

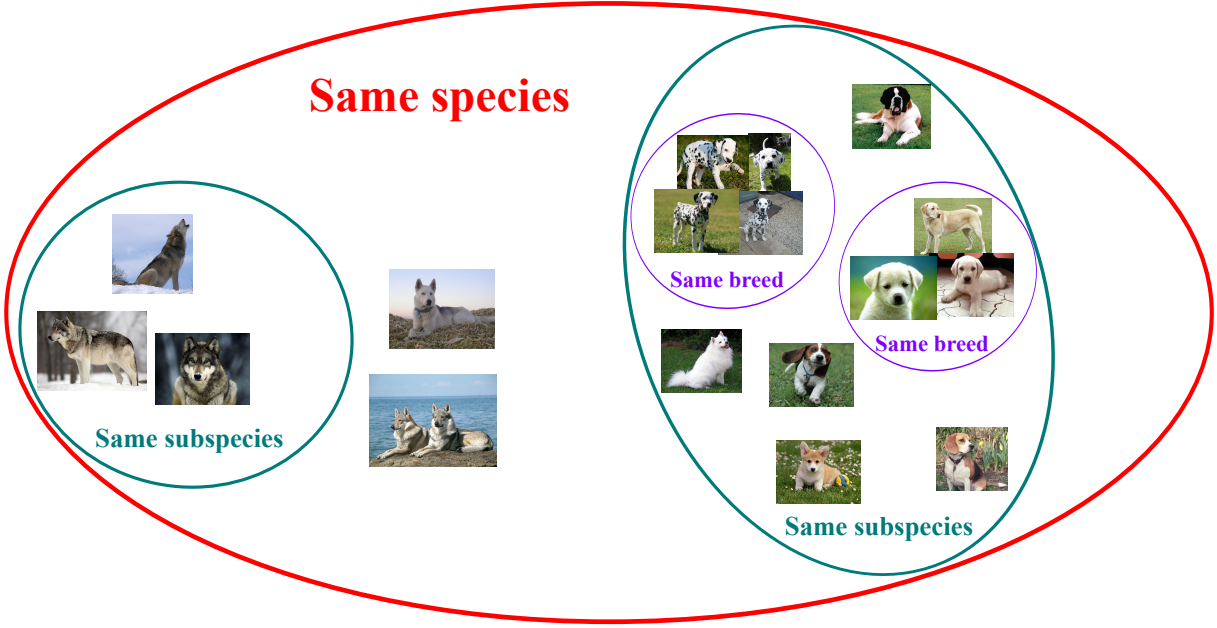
Eq. (2.1) is actually a generalization of triplet-wise and pairwise constraints. Indeed:

- every triplet-wise constraint $D_{ik} \geq D_{ij} + \delta_q$ (i.e., that involves the triplet $(\mathcal{I}_i, \mathcal{I}_j, \mathcal{I}_k)$) can be formulated by creating the quadruplet $q = (\mathcal{I}_i, \mathcal{I}_j, \mathcal{I}_i, \mathcal{I}_k) \in \mathcal{N}$.
- every pairwise constraint $D_{ij} \geq l$ that involves a dissimilar pair of images $(\mathcal{I}_i, \mathcal{I}_j) \in \mathcal{D}$, and where l is a given lower bound that represents the minimum value such that images $(\mathcal{I}_i, \mathcal{I}_j)$ are considered as dissimilar, can be formulated by creating the quadruplet $q = (\mathcal{I}_i, \mathcal{I}_i, \mathcal{I}_i, \mathcal{I}_j) \in \mathcal{N}$ with $\delta_q = l$.
- every pairwise constraint $u \geq D_{ij}$ that involves a similar pair of images $(\mathcal{I}_i, \mathcal{I}_j) \in \mathcal{S}$, and where u is a given upper bound that represents the maximum value such that images $(\mathcal{I}_i, \mathcal{I}_j)$ are considered as similar, can be formulated by creating the quadruplet $q = (\mathcal{I}_i, \mathcal{I}_j, \mathcal{I}_i, \mathcal{I}_i) \in \mathcal{N}$ with $\delta_q = -u$.

Although quadruplet-wise constraints can be inferred from pairwise approaches [Davis et al., 2007, Mignon and Jurie, 2012], the converse is not true. Indeed, if two given pairs $(\mathcal{I}_i, \mathcal{I}_j)$ and $(\mathcal{I}_k, \mathcal{I}_l)$ are in \mathcal{S} and \mathcal{D} , respectively, the following constraints $D_{ij} < D_{kl}$ can be inferred. However, the constraint $D_{ij} < D_{kl}$ does not imply that the pairs $(\mathcal{I}_i, \mathcal{I}_j)$ and $(\mathcal{I}_k, \mathcal{I}_l)$ are in \mathcal{S} and \mathcal{D} , respectively. In other words, from a quadruplet-wise constraint $D_{ij} < D_{kl}$, there is no need to determine arbitrary values of u and l such that $D_{ij} < u$ and $l < D_{kl}$ since u and l can take all the possible values (as long as $u \leq l$) and satisfy the quadruplet-wise constraint. Only the order of similarity between $(\mathcal{I}_i, \mathcal{I}_j)$ and $(\mathcal{I}_k, \mathcal{I}_l)$ is required. Since the provided constraints are less restrictive and thus less prone to noise, relative distances are particularly useful when human users that are not experts of the domain have to annotate similarity or relation information on data. A similar issue is pointed out in the context of relative attributes [Parikh and Grauman, 2011] in which boolean presence of an attribute is difficult to annotate, whereas relative comparisons are easier and more natural for humans to annotate.

Fig. 2.2 illustrates some examples of constraints for which a pairwise formulation is difficult, or at least for which constraints of relative distance comparisons seem more natural and intuitive. It shows different members of the *Canis lupus* species that are gathered together depending on their respective subspecies and breeds. By considering only pairwise similarity constraints, it is difficult to formulate the distance metric learning problem such that (1) members of the same breed are closer to each other than other members of the same subspecies are, and (2) members of the same subspecies are closer to each other than members from different subspecies. Depending on whether we consider members of the same subspecies as similar or dissimilar, the distance metric learned with pairwise constraints does not fully exploit the rich information given by the provided taxonomy. This limitation can be easily overcome by using relative distance comparison constraints as illustrated in Fig. 2.2.

We present in the following two different frameworks to learn a Mahalanobis distance metric that exploit this type of constraints. The first one considers the learning of a Mahalanobis distance metric parameterized by a *full* matrix $\mathbf{M} \in \mathbb{S}_+^d$ (i.e., any type of matrix in \mathbb{S}_+^d). The second one considers the learning of a distance metric parameterized by one or many vectors that are learned independently.



Learn dissimilarity D such that:

$$\begin{aligned}
 D\left(\begin{array}{c} \text{Dalmatian 1} \\ \text{Dalmatian 2} \end{array}\right) &< D\left(\begin{array}{c} \text{Basset Hound} \\ \text{Golden Retriever} \end{array}\right) \\
 D\left(\begin{array}{c} \text{Chihuahua} \\ \text{Bulldog} \end{array}\right) &< D\left(\begin{array}{c} \text{Poodle} \\ \text{Wolf} \end{array}\right)
 \end{aligned}$$

Figure 2.2: Illustration of the quadruplet-wise (Qwise) strategy in a class taxonomy context. The goal is to learn a projection of animals of the same species such that members of the same breed are closer to each other than members from different breeds, and members from the same subspecies are closer to each other than member from different subspecies.

2.2.2 Full matrix Mahalanobis distance metric learning

We present in this subsection the general Mahalanobis-like distance metric learning framework where we consider a distance metric parameterized by a PSD matrix $\mathbf{M} \in \mathbb{S}_+^d$. The distance between two images \mathcal{I}_i and \mathcal{I}_j represented by vectors $\mathbf{x}_i \in \mathbb{R}^d$ and $\mathbf{x}_j \in \mathbb{R}^d$ is formulated as:

$$D_{\mathbf{M}}^2(\mathcal{I}_i, \mathcal{I}_j) = \langle \mathbf{M}, \mathbf{C}_{ij} \rangle \quad (2.2)$$

where $\mathbf{C}_{ij} = \Phi(\mathcal{I}_i, \mathcal{I}_j)\Phi(\mathcal{I}_i, \mathcal{I}_j)^\top$, and typically $\Phi(\mathcal{I}_i, \mathcal{I}_j) = (\mathbf{x}_i - \mathbf{x}_j)$.

2.2.2.1 Optimization problem

The goal of our distance metric learning framework is to maximize the number of satisfied constraints in Eq. (2.1). However, the problem of maximizing the number of satisfied constraints in Eq. (2.1) is NP-hard [Joachims, 2002], we then approximate it by using slack variables. By noting each quadruplet

$q = (\mathcal{I}_i, \mathcal{I}_j, \mathcal{I}_k, \mathcal{I}_l) \in \mathcal{N}$, we optimize the following problem:

$$\begin{aligned} \min_{\mathbf{M} \in \mathbb{S}_+^d} \quad & \Omega(\mathbf{M}) + C_Q \sum_{q \in \mathcal{N}} \xi_q \\ \text{s.t.} \quad & \forall q \in \mathcal{N}, D_{\mathbf{M}}^2(\mathcal{I}_k, \mathcal{I}_l) \geq D_{\mathbf{M}}^2(\mathcal{I}_i, \mathcal{I}_j) + \delta_q - \xi_q \\ & \forall q \in \mathcal{N}, \xi_q \geq 0 \end{aligned} \quad (2.3)$$

where $\Omega(\mathbf{M})$ is a regularization term and $C_Q > 0$ a regularization parameter that controls the trade-off between fitting and regularization. The problem in Eq. (2.3) is similar to LMNN [Weinberger and Saul, 2009] (see Eq. (1.5)) with the exception that we exploit quadruplets in our constraints instead of triplets.

We will explain in Section 2.3.1 how to efficiently solve the problem in Eq. (2.3). We first propose to enrich the model with other types of constraints.

2.2.2.2 Combining pairwise and quadruplet-wise constraints

In some contexts, both absolute and relative similarity informations can be provided. We present here how to combine them in a single optimization problem.

As mentioned in Section 2.2.1, pairwise constraints can be rewritten as quadruplet-wise constraints. Nonetheless, in order to enhance the readability of the thesis, we consider to explicitly distinguish the sets of similar image pairs \mathcal{S} and of dissimilar image pairs \mathcal{D} from the set of relative distance comparisons \mathcal{N} .

Especially, if we are provided with a set of similar pairs (\mathcal{S}) and a set of dissimilar pairs (\mathcal{D}), we expect the distances of similar pairs to be smaller than a given threshold u and the distances of dissimilar pairs to be greater than another threshold l (with $u \leq l$). To know whether a test pair is similar or dissimilar, one only needs to compute its distance and compare it to $b = \frac{u+l}{2}$. The resulting absolute similarity constraints can be written in this way:

$$\forall (\mathcal{I}_i, \mathcal{I}_j) \in \mathcal{S} : D_{\mathbf{M}}^2(\mathcal{I}_i, \mathcal{I}_j) \leq u \quad (2.4)$$

$$\forall (\mathcal{I}_i, \mathcal{I}_j) \in \mathcal{D} : D_{\mathbf{M}}^2(\mathcal{I}_i, \mathcal{I}_j) \geq l \quad (2.5)$$

The integration of pairwise information in Eq. (2.3) then results in the following problem:

$$\begin{aligned} \min_{\mathbf{M} \in \mathbb{S}_+^d} \quad & \Omega(\mathbf{M}) + C_Q \sum_{q \in \mathcal{N}} \xi_q + C_P \sum_{(\mathcal{I}_i, \mathcal{I}_j) \in (\mathcal{S} \cup \mathcal{D})} \xi_{ij} \\ \text{s.t.} \quad & \forall q \in \mathcal{N}, D_{\mathbf{M}}^2(\mathcal{I}_k, \mathcal{I}_l) \geq D_{\mathbf{M}}^2(\mathcal{I}_i, \mathcal{I}_j) + \delta_q - \xi_q \\ & \forall (\mathcal{I}_i, \mathcal{I}_j) \in \mathcal{S}, D_{\mathbf{M}}^2(\mathcal{I}_i, \mathcal{I}_j) \leq u + \xi_{ij} \\ & \forall (\mathcal{I}_i, \mathcal{I}_j) \in \mathcal{D}, D_{\mathbf{M}}^2(\mathcal{I}_i, \mathcal{I}_j) \geq l - \xi_{ij} \\ & \forall q \in \mathcal{N}, \xi_q \geq 0 \\ & \forall (\mathcal{I}_i, \mathcal{I}_j) \in (\mathcal{S} \cup \mathcal{D}), \xi_{ij} \geq 0 \end{aligned} \quad (2.6)$$

which can be rewritten equivalently:

$$\begin{aligned} \min_{\mathbf{M} \in \mathbb{S}_+^d} \quad & \Omega(\mathbf{M}) + C_Q \sum_{q \in \mathcal{N}} [\delta_q + \langle \mathbf{M}, \mathbf{C}_{ij} - \mathbf{C}_{kl} \rangle]_+ \\ & + C_P \sum_{(\mathcal{I}_i, \mathcal{I}_j) \in \mathcal{S}} [\langle \mathbf{M}, \mathbf{C}_{ij} \rangle - u]_+ + C_P \sum_{(\mathcal{I}_i, \mathcal{I}_j) \in \mathcal{D}} [l - \langle \mathbf{M}, \mathbf{C}_{ij} \rangle]_+ \end{aligned} \quad (2.7)$$

where $\forall x \in \mathbb{R}, [x]_+ = \max(0, x)$, $C_Q \geq 0$ and $C_P \geq 0$. This problem is equivalent to Eq. (2.3) when $C_P = 0$ or $\mathcal{S} = \mathcal{D} = \emptyset$. It is convex w.r.t. \mathbf{M} . However, naive optimization methods to solve it can

be computationally expensive. We discuss optimization schemes to efficiently solve this problem in Section 2.3. Before that, we present an alternative distance metric formulation.

2.2.3 Simplification of the model by optimizing over vectors

In this subsection, we consider cases where a distance metric is formulated as a function of one or many vectors. The distance metric is learned by optimizing over those vectors. We particularly focus on two contexts where the optimization process may be done efficiently [Chapelle, 2007, Chapelle and Keerthi, 2010] by using this vector optimization approach and by learning a model with a relatively small number of parameters. The first one constrains the PSD matrix $\mathbf{M} \in \mathbb{S}_+^d$ to be diagonal. The second one considers multiple prior relative ordering informations about data, and learns a linear transformation that tries to satisfy all those informations.

2.2.3.1 Learning a diagonal PSD matrix

In the first context, we constrain in Eq. (2.7) the learned PSD matrix $\mathbf{M} \in \mathbb{S}_+^d$ to be a diagonal matrix. By noting $\mathbf{w} = \text{Diag}(\mathbf{M}) \in \mathbb{R}^d$ the diagonal vector of \mathbf{M} , it is easy to verify that, if \mathbf{M} is a diagonal matrix, we have the following equivalence:

$$D_{\mathbf{M}}^2(\mathcal{I}_i, \mathcal{I}_j) = \Phi(\mathcal{I}_i, \mathcal{I}_j)^\top \mathbf{M} \Phi(\mathcal{I}_i, \mathcal{I}_j) = \mathbf{w}^\top [\Phi(\mathcal{I}_i, \mathcal{I}_j) \circ \Phi(\mathcal{I}_i, \mathcal{I}_j)]$$

where \circ is the Hadamard product (element-by-element product). For convenience, we note $\Phi^{\circ 2}(\mathcal{I}_i, \mathcal{I}_j) = \Phi(\mathcal{I}_i, \mathcal{I}_j) \circ \Phi(\mathcal{I}_i, \mathcal{I}_j)$. The problem can then be rewritten as a function of \mathbf{w} .

In this context, the constraint $\mathbf{M} \in \mathbb{S}_+^d$ is equivalent to the constraint $\mathbf{w} \in \mathbb{R}_+^d$ (the elements of \mathbf{w} are non-negative). Indeed, all the diagonal elements of a square diagonal matrix are its eigenvalues and a symmetric matrix is PSD iff all its eigenvalues are non-negative. We then consider the constraint $\mathbf{w} \in \mathbb{R}_+^d$ when the learned matrix $\mathbf{M} \in \mathbb{S}_+^d$ is constrained to be diagonal.

2.2.3.2 Learning the rows of a transformation matrix

If the training annotations are M different relative orderings, and each of them is focused on a given criterion (e.g., \mathcal{I}_i is smiling more than \mathcal{I}_j , \mathcal{I}_i is more natural than \mathcal{I}_j ...), then we can learn M dissimilarity functions that try to satisfy these relative orderings. Each of these learned dissimilarity functions can be parameterized by a vector $\mathbf{w}_m \in \mathbb{R}^d$, and its corresponding function $\mathcal{D}_{\mathbf{w}_m} : \mathcal{P} \times \mathcal{P} \rightarrow \mathbb{R}$ where $\mathcal{D}_{\mathbf{w}_m}(\mathcal{I}_i, \mathcal{I}_j) = \mathbf{w}_m^\top \Phi(\mathcal{I}_i, \mathcal{I}_j)$ describes the difference of presence of the m -th criterion between \mathcal{I}_i and \mathcal{I}_j . The M parameters \mathbf{w}_m can be concatenated in a single matrix $\mathbf{L} \in \mathbb{R}^{M \times d}$ in this way:

$$\mathbf{L} = \begin{bmatrix} w_{1,1} & \dots & w_{1,d} \\ \vdots & \vdots & \vdots \\ w_{M,1} & \dots & w_{M,d} \end{bmatrix} = \begin{bmatrix} \mathbf{w}_1^\top \\ \vdots \\ \mathbf{w}_M^\top \end{bmatrix}, \quad \mathbf{w}_m^\top : m^{\text{th}} \text{ row of } \mathbf{L} \quad (2.8)$$

In the end, a transformation matrix \mathbf{L} is learned (with each row learned independently from one another). As mentioned in Section 1.3.2, learning a transformation matrix \mathbf{L} is equivalent to learning a distance metric parameterized by the matrix $\mathbf{M} = \mathbf{L}^\top \mathbf{L}$.

2.2.3.3 Unified problem formulation

In both cases mentioned above, the learning problem may be expressed as a linear combination of the parameter $\mathbf{w} \in \mathcal{C}^d$ where \mathcal{C}^d is a d -dimensional convex set in \mathbb{R}^d . In this thesis, the convex set \mathcal{C}^d is

either \mathbb{R}^d or \mathbb{R}_+^d . Without loss of generality, we consider optimizing the following dissimilarity function:

$$\mathcal{D}_{\mathbf{w}}(\mathcal{I}_i, \mathcal{I}_j) = \mathbf{w}^\top \Psi(\mathcal{I}_i, \mathcal{I}_j) \text{ s.t. } \mathbf{w} \in \mathcal{C}^d \quad (2.9)$$

where

- $\Psi = \Phi^{\circ 2}$ and $\mathcal{C}^d = \mathbb{R}_+^d$ in the case $\mathbf{M} \in \mathbb{S}_+^d$ is a diagonal matrix.
- $\Psi = \Phi$ and $\mathcal{C}^d = \mathbb{R}^d$ in the other case.

We formulate our vector optimization problem as:

$$\begin{aligned} \min_{(\mathbf{w}, b)} \quad & \frac{1}{2}(\|\mathbf{w}\|_2^2 + b^2) + C_Q \sum_{q \in \mathcal{N}} \xi_q + C_P \sum_{(\mathcal{I}_i, \mathcal{I}_j) \in (\mathcal{S} \cup \mathcal{D})} \xi_{ij} \\ \text{s.t.} \quad & \forall (\mathcal{I}_i, \mathcal{I}_j) \in \mathcal{S}, \mathcal{D}_{\mathbf{w}}(\mathcal{I}_i, \mathcal{I}_j) \leq b - 1 + \xi_{ij} \\ & \forall (\mathcal{I}_i, \mathcal{I}_j) \in \mathcal{D}, \mathcal{D}_{\mathbf{w}}(\mathcal{I}_i, \mathcal{I}_j) \geq b + 1 - \xi_{ij} \\ & \forall q \in \mathcal{N}, \mathcal{D}_{\mathbf{w}}(\mathcal{I}_k, \mathcal{I}_l) \geq \mathcal{D}_{\mathbf{w}}(\mathcal{I}_i, \mathcal{I}_j) + \delta_q - \xi_q \\ & \xi_q \geq 0, \xi_{ij} \geq 0, \mathbf{w} \in \mathcal{C}^d, b \in \mathcal{C} \end{aligned} \quad (2.10)$$

It is very similar to Eq. (2.7) when the matrix $\text{Diag}(\mathbf{w}) = \mathbf{M}$ is constrained to be diagonal, $\Omega(\mathbf{M}) = \frac{1}{2}\|\mathbf{M}\|_F^2 = \frac{1}{2}\|\mathbf{w}\|_2^2$, $u = b - 1$ and $l = b + 1$. The only difference is the inclusion of the $b^2/2$ term in the regularizer. Note that both \mathbf{w} and b are learned in Eq (2.10).

The problem is convex w.r.t. \mathbf{w} and b , and the inclusion of the $b^2/2$ term in the regularizer does not affect generalization [Keerthi and DeCoste, 2005]. The optimization process is briefly discussed in Section 2.3.2 and a detailed discussion is provided in Appendix B.

2.3 Quadruplet-wise (Qwise) Optimization

In this section, we discuss optimization details of our proposed Quadruplet-wise distance metric framework. We first focus on the case where $\mathbf{M} \in \mathbb{S}_+^d$ is a full (i.e., non-diagonal) matrix, then we discuss the case where the learned metric is parameterized by one vector of a set of vectors. Finally, we describe optimization issues that are common to both presented distance metric formulations.

2.3.1 Full matrix metric optimization

We solve our problem by using the projected subgradient method as done in [Weinberger and Saul, 2009].

Projected Subgradient Method The optimization problem in Eq. (2.7) consists in minimizing a convex function that is subject to the constraint $\mathbf{M} \in \mathbb{S}_+^d$. Since the set \mathbb{S}_+^d is convex, the problem in Eq. (2.7) is convex and can be solved by the projected subgradient method [Boyd and Vandenberghe, 2008]. The projected subgradient method is an extension of the subgradient method, which is a generalization of gradient methods for non-differentiable (and subdifferentiable) convex functions. The projected subgradient method solves the following constrained convex optimization problem:

$$\min_x f(x) \text{ subject to } x \in \mathcal{C}$$

where f is a convex function and \mathcal{C} is a convex set. Let x^t denote the value of x at iteration t , the projected subgradient method is given by a sequence of the following operation $x^{t+1} = \Pi_{\mathcal{C}}(x^t - \eta_t g^t)$ where $\Pi_{\mathcal{C}}$ is the Euclidean projection on \mathcal{C} , g^t is any subgradient of f at x^t (when f is differentiable, the subgradient g^t is unique and is the gradient of f at x^t). $\eta_t \geq 0$ is the step size at iteration t (see [Boyd and Vandenberghe, 2008] for optimal stepsize strategies in subgradient methods). The algorithm provably converges [Boyd and Vandenberghe, 2008].

Algorithm 1 Projected Subgradient Method**Require:** Sets \mathcal{N} , \mathcal{D} , \mathcal{S} (some of them can be empty)

- 1: Iteration $t = 0$
- 2: Initialize $\mathbf{M}^t \in \mathbb{S}_+^d$ (e.g., $\mathbf{M}^t = \mathbf{0}$)
- 3: Initialize the step size $\eta_t > 0$ (e.g., $\eta_t = 1$)
- 4: **repeat**
- 5: Compute ∇^t (subgradient w.r.t. \mathbf{M}^t , Eq. (2.11))
- 6: $\mathbf{M}^{t+1} \leftarrow \Pi_{\mathbb{S}_+^d}(\mathbf{M}^t - \eta_t \nabla^t)$
- 7: $t \leftarrow t + 1$
- 8: **until** $\|\mathbf{M}^t - \mathbf{M}^{t-1}\|_F^2 \leq \epsilon$
- 9: **Return** \mathbf{M}_t

Subgradient of our problem A subgradient of Eq. (2.7) at \mathbf{M} is computed as follows:

$$\nabla = \partial\Omega(\mathbf{M}) + C_P \left(\sum_{(\mathcal{I}_i, \mathcal{I}_j) \in \mathcal{S}^+} \mathbf{C}_{ij} - \sum_{(\mathcal{I}_i, \mathcal{I}_j) \in \mathcal{D}^+} \mathbf{C}_{ij} \right) + C_Q \sum_{q \in \mathcal{N}^+} (\mathbf{C}_{ij} - \mathbf{C}_{kl}) \quad (2.11)$$

where $\partial\Omega(\mathbf{M})$ is a subgradient¹⁹ of Ω at \mathbf{M} and where \mathcal{N}^+ , \mathcal{S}^+ and \mathcal{D}^+ are the subsets of violated constraints in \mathcal{N} , \mathcal{S} , \mathcal{D} , respectively, i.e., :

- $q \in \mathcal{N}^+ \iff q = (\mathcal{I}_i, \mathcal{I}_j, \mathcal{I}_k, \mathcal{I}_l) \in \mathcal{N}$ and $\delta_q + \langle \mathbf{M}, \mathbf{C}_{ij} - \mathbf{C}_{kl} \rangle > 0$
- $(\mathcal{I}_i, \mathcal{I}_j) \in \mathcal{S}^+ \iff (\mathcal{I}_i, \mathcal{I}_j) \in \mathcal{S}$ and $D_{\mathbf{M}}^2(\mathcal{I}_i, \mathcal{I}_j) > u$
- $(\mathcal{I}_i, \mathcal{I}_j) \in \mathcal{D}^+ \iff (\mathcal{I}_i, \mathcal{I}_j) \in \mathcal{D}$ and $D_{\mathbf{M}}^2(\mathcal{I}_i, \mathcal{I}_j) < l$

The whole algorithm of this subgradient method is presented in Algorithm 1 where η_t is the step size. The complexity of Algorithm 1 is linear in the number of constraints. When the input space dimensionality d is large, its complexity is dominated by the projection $\Pi_{\mathbb{S}_+^d}$ onto the PSD cone performed at each iteration (step 6, see Appendix A.3 for more details on the projection onto \mathbb{S}_+^d).

2.3.2 Vector metric optimization

To solve the vector optimization problem introduced in Eq. (2.10), we adapt the RankSVM model [Joachims, 2002]. The complexity is linear in the number of constraints and large-scale efficient solvers have been proposed such as Newton's method [Chapelle and Keerthi, 2010]. In order to exploit Newton's method, we use a Huber loss function instead of a hinge loss function like in Eq. (2.7). The optimization process is detailed in Appendix B and is a Newton adaptation of Algorithm 1 for vector optimization.

¹⁹The value of $\partial\Omega(\mathbf{M})$ depends on the choice of regularizer $\Omega(\mathbf{M})$. For instance

1. $\partial\Omega(\mathbf{M}) = \mathbf{I}_d$ if $\Omega(\mathbf{M}) = \text{tr}(\mathbf{M})$.
2. $\partial\Omega(\mathbf{M}) = \mathbf{M}$ if $\Omega(\mathbf{M}) = \frac{1}{2}\|\mathbf{M}\|_F^2$.
3. $\partial\Omega(\mathbf{M}) = \sum_{(\mathcal{I}_i, \mathcal{I}_j) \in \mathcal{S}} \mathbf{C}_{ij}$ if $\Omega(\mathbf{M}) = \langle \mathbf{M}, \sum_{(\mathcal{I}_i, \mathcal{I}_j) \in \mathcal{S}} \mathbf{C}_{ij} \rangle$ in the case of MMC [Xing et al., 2002] and LMNN [Weinberger and Saul, 2009].

2.3.3 Implementation details

Projection onto \mathbb{S}_+^d In the full matrix case (Section 2.3.1), the projection onto \mathbb{S}_+^d requires an eigendecomposition of the matrix $(\mathbf{M}_t - \eta_t \nabla_t)$, whose complexity is cubic in the dimensionality d . This can be prohibitive if d is large. However, the dimensionality d of our input data is always smaller or equal to 1000 in our experiments. On a single 3,40 GHz computer, the eigendecomposition of a $10^3 \times 10^3$ matrix takes less than 0.1 second, which is tractable for our applications.

Regularization parameter In the experiments, we use the same regularization as LMNN (i.e., the term $\sum_{(\mathcal{I}_i, \mathcal{I}_j) \in \mathcal{S}} D_{\mathbf{M}}^2(\mathcal{I}_i, \mathcal{I}_j)$) when we use LMNN as a baseline and we want to study the benefit of our proposed constraints in order to have a fair comparison. When we constrain $\mathbf{M} \in \mathbb{S}_+^d$ to be diagonal, we use the squared Frobenius norm in order to apply an efficient RankSVM [Chapelle and Keerthi, 2010] optimization scheme.

Efficient subgradient computation As one can see in Eq. (2.11), the subgradient related to the loss of each quadruplet of images $q = (\mathcal{I}_i, \mathcal{I}_j, \mathcal{I}_k, \mathcal{I}_l) \in \mathcal{N}$ is:

$$\partial [\delta_q + \langle \mathbf{M}, \mathbf{C}_{ij} - \mathbf{C}_{kl} \rangle]_+ = \begin{cases} \mathbf{0} & \text{if } q \notin \mathcal{N}^+ \\ (\mathbf{C}_{ij} - \mathbf{C}_{kl}) & \text{if } q \in \mathcal{N}^+ \end{cases}$$

The value of the subgradient does not depend on the degree to which the constraint associated to the quadruplet $q \in \mathcal{N}$ is violated, but depends only on whether q is in \mathcal{N}^+ or not. Then let $h(\mathcal{N}^+)$ be a subgradient associated to the set \mathcal{N}^+ , i.e., $h(\mathcal{N}^+) = \sum_{q \in \mathcal{N}^+} (\mathbf{C}_{ij} - \mathbf{C}_{kl})$. Let \mathcal{N}_t^+ be the set of violated constraints in \mathcal{N} at iteration t . We note that:

$$h(\mathcal{N}_{t+1}^+) = h(\mathcal{N}_t^+) - h(\mathcal{N}_t^+ \setminus \mathcal{N}_{t+1}^+) + h(\mathcal{N}_{t+1}^+ \setminus \mathcal{N}_t^+)$$

Since the sets $(\mathcal{N}_t^+ \setminus \mathcal{N}_{t+1}^+)$ and $(\mathcal{N}_{t+1}^+ \setminus \mathcal{N}_t^+)$ are very small in practice, it is more efficient to store the matrix $h(\mathcal{N}_t^+)$ and compute $h(\mathcal{N}_t^+ \setminus \mathcal{N}_{t+1}^+)$ and $h(\mathcal{N}_{t+1}^+ \setminus \mathcal{N}_t^+)$ to obtain $h(\mathcal{N}_{t+1}^+)$ than naively computing $\sum_{q \in \mathcal{N}^+} (\mathbf{C}_{ij} - \mathbf{C}_{kl})$ for which the complexity is $O(|\mathcal{N}_{t+1}^+|d^2)$. Note that the same technique can be used for the sets \mathcal{S} and \mathcal{D} when they are not empty.

A small adaptation needs to be done for the vector metric optimization (see Section 2.3.2) to exploit this subgradient computation technique since we use Huber loss functions instead of a hinge loss. As the Huber loss function is composed of two linear parts (sets $\beta_{i,y}^0$ and $\beta_{i,y}^L$ in Appendix B.2) and a quadratic part, this technique for the hinge loss can be applied to the linear parts of the Huber loss function, which represent nearly all the domain of L_i^h .

Active set strategy We describe here an active set strategy to deal with large number of constraints. Since the number of possible quadruplets can be very large, it is computationally prohibitive and sub-optimal to use all the quadruplets. To overcome this limitation, we propose to add to our optimization schemes an *active set* strategy that exploits the fact that the great majority of training quadruplets do not incur margin violations. Only a small fraction of the quadruplets in \mathcal{N} are in \mathcal{N}^+ . In a similar manner as in LMNN [Weinberger and Saul, 2009], we check all the quadruplets and maintain an active list of those with margin violations: a full re-check is performed every 10-20 iterations, depending on fluctuations of the set \mathcal{N}_t^+ . For intermediate iterations, we only check for margin violations from among those active quadruplets accumulated over previous iterations. When the optimization converges for a given active set \mathcal{N}_t^+ , the most active constraints that are not in \mathcal{N}_t^+ are added in \mathcal{N}_{t+1}^+ , note that $\mathcal{N}_t^+ \subset \mathcal{N}_{t+1}^+$. If all the possible active constraints are already in \mathcal{N}_t^+ , then we have reached an optimal solution for the global (and convex) optimization problem. Otherwise, some remaining active constraints are added to the current set \mathcal{N}_t until convergence.

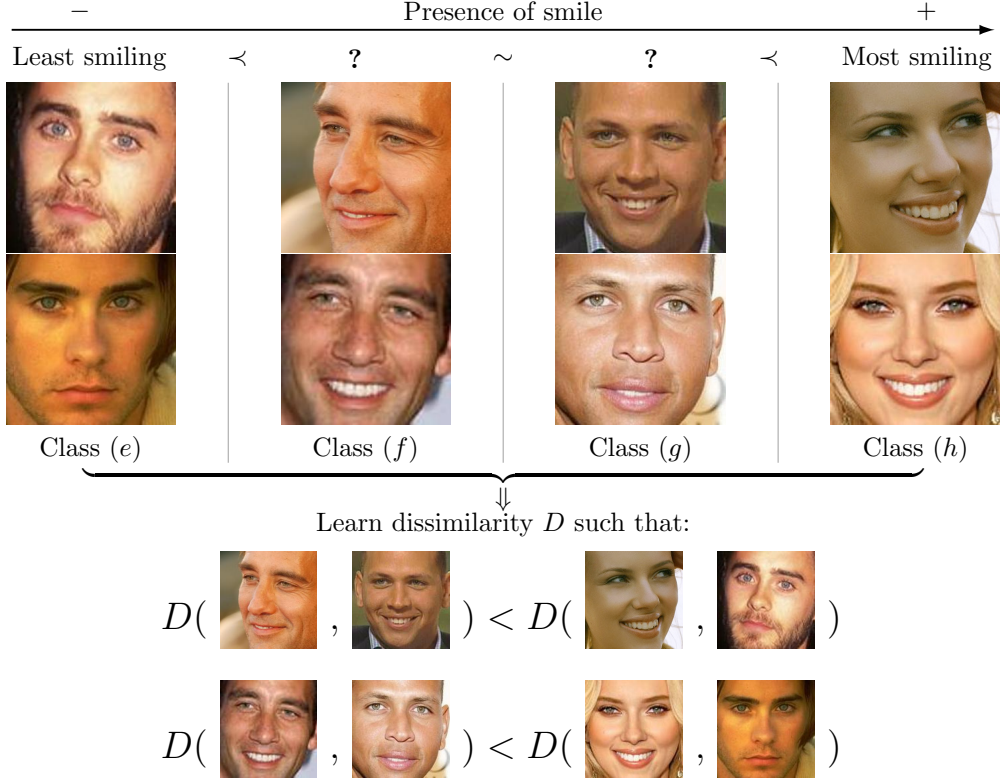


Figure 2.3: Quadruplet-wise (Qwise) strategy on 4 face classes ranked according to the degree of presence of smile. Qwise strategy defines quadruplet-wise constraints to express that dissimilarities between examples from (f) and (g) should be smaller than dissimilarities between examples from (e) and (h).

2.4 Experimental Validation on Relative Attributes

In this section, we present and compare different strategies to sample quadruplet-wise constraints in the context of relative attributes.

Relative attributes have been introduced in [Parikh and Grauman, 2011]. Attributes are human-nameable concepts used to describe images. For instance, in Fig. 2.3, the attribute a_m = “presence of smile” allows to rank 4 celebrity classes from the least to the most smiling. Instead of considering attributes as boolean values as done in [Lampert et al., 2009] (i.e., the concept is present in the image or not), Parikh and Grauman [Parikh and Grauman, 2011] consider relative orderings between classes of images (e.g., the concept “presence of smile” is more present in class (h) than in class (e)). They learn for each attribute a_m a vector $\mathbf{w}_m \in \mathbb{R}^d$ such that the score $\mathbf{w}_m^\top \mathbf{x}_i \in \mathbb{R}$ represents the degree of presence of a_m in the image \mathcal{I}_i .

Let M be the total number of attributes that are considered for a given dataset. Once the optimal weight vectors \mathbf{w}_m are learned for all the attributes a_m with $m \in \{1, \dots, M\}$, each image \mathcal{I}_i is described by a high level feature representation:

$$\mathbf{h}_i = [\mathbf{w}_1^\top \mathbf{x}_i, \dots, \mathbf{w}_m^\top \mathbf{x}_i, \dots, \mathbf{w}_M^\top \mathbf{x}_i]^\top \in \mathbb{R}^M$$

This corresponds to learning a linear transformation parameterized by the matrix $\mathbf{L} \in \mathbb{R}^{M \times d}$ such that $\mathbf{h}_i = \mathbf{L} \mathbf{x}_i$ where the m^{th} row of \mathbf{L} is \mathbf{w}_m^\top (see Eq. (2.8)). As explained in Section 2.2.2, their problem can be cast as a metric learning problem since they learn a linear transformation.

To learn \mathbf{w}_m , they use original training sets about relative ordering between classes such as the one

OSR Attributes	Relative Ordering of Classes
Natural	$T \prec I \sim S \prec H \prec C \sim O \sim M \sim F$
Open	$T \prec F \prec I \sim S \prec M \prec H \sim C \sim O$
Perspective	$O \prec C \prec M \sim F \prec H \prec I \prec S \prec T$
Large-Objects	$F \prec O \prec M \prec I \sim S \prec H \sim C \prec T$
Diagonal-Plane	$F \prec O \prec M \prec C \prec I \sim S \prec H \prec T$
Close-Depth	$C \prec M \prec O \prec T \sim I \sim S \sim H \sim F$
PubFig Attributes	Relative Ordering of Classes
Masculine-Looking	$S \prec M \prec Z \prec V \prec J \prec A \prec H \prec C$
White	$A \prec C \prec H \prec Z \prec J \prec S \prec M \prec V$
Young	$V \prec H \prec C \prec J \prec A \prec S \prec Z \prec M$
Smiling	$J \prec V \prec H \prec A \sim C \prec S \sim Z \prec M$
Chubby	$V \prec J \prec H \prec C \prec Z \prec M \prec S \prec A$
Visible-Forehead	$J \prec Z \prec M \prec S \prec A \sim C \sim H \sim V$
Bushy-Eyebrows	$M \prec S \prec Z \prec V \prec H \prec A \prec C \prec J$
Narrow-Eyes	$M \prec J \prec S \prec A \prec H \prec C \prec V \prec Z$
Pointy-Nose	$A \prec C \prec J \sim M \sim V \prec S \prec Z \prec H$
Big-Lips	$H \prec J \prec V \prec Z \prec C \prec M \prec A \prec S$
Round-Face	$H \prec V \prec J \prec C \prec Z \prec A \prec S \prec M$

Table 2.1: Relative orderings used in [Parikh and Grauman, 2011] for the OSR dataset (categories: coast (C), forest (F), highway (H), inside-city (I), mountain (M), open-country (O), street (S) and tall-building (T)) and the PubFig dataset (categories: Alex Rodriguez (A), Clive Owen (C), Hugh Laurie (H), Jared Leto (J), Miley Cyrus (M), Scarlett Johansson (S), Viggo Mortensen (V) and Zac Efron (Z)).

presented in Fig. 2.3: $(e) \prec (f) \sim (g) \prec (h)$. In [Parikh and Grauman, 2011], only pairwise relations are considered for learning:

- $(e) \prec (f)$ meaning that images in class (f) have stronger presence of the attribute a_m than images in class (e) .
- $(f) \sim (g)$ meaning that images in (f) and (g) have equivalent strength of presence of the attribute a_m .

In [Parikh and Grauman, 2011], the training information concerning the degree of presence of an attribute in an image is provided at a class level: pairwise constraints based on classes may be noisy or irrelevant, leading to less than optimal learning scheme. Considering triplet-wise constraints (e.g., class (x) is more similar to (y) than to (z)) could be helpful but also generates inconsistent constraints in some cases: in Fig. 2.3 (second row), Owen (f) seems to be smiling more like Johansson (h) than like Rodriguez (g) . To further exploit the available ordered set of classes and overcome these limitations, we consider relations between quadruplets of images to relax pairwise relations. Two types of Qwise constraints may be derived from the provided training set.

2.4.1 Integrating quadruplet-wise constraints

Following our vector formalism defined in Section 2.2.3.2, we consider to learn for each attribute a_m the signed dissimilarity function $D_{\mathbf{w}_m}$ such that $D_{\mathbf{w}_m}(\mathcal{I}_i, \mathcal{I}_j) = \mathbf{w}_m^\top \Psi(\mathcal{I}_i, \mathcal{I}_j)$, with $\Psi(\mathcal{I}_i, \mathcal{I}_j) = (\mathbf{x}_i - \mathbf{x}_j)$ and $\mathbf{w} \in \mathbb{R}^d$. The sign of $D_{\mathbf{w}_m}(\mathcal{I}_i, \mathcal{I}_j)$ determines the relative ordering of presence of the attribute a_m between the images \mathcal{I}_i and \mathcal{I}_j . For instance, $D_{\mathbf{w}_m}(\mathcal{I}_i, \mathcal{I}_j) > 0$ means that the presence of a_m is stronger in \mathcal{I}_i than in \mathcal{I}_j .

2.4.1.1 Replacing ordered pairs by quadruplets

The first type of relation that we consider in this section is: $(e) \prec (f) \prec (g) \prec (h)$ in order to relax the relation $(f) \prec (g)$ exploited in [Parikh and Grauman, 2011]. We do the following assumption: any

image pair from the extreme border classes (e) and (h) is more dissimilar than any image pair from the intermediate classes (f) and (g). This information can be written:

$$\forall (\mathcal{I}_i, \mathcal{I}_j, \mathcal{I}_k, \mathcal{I}_l) \in (g) \times (f) \times (h) \times (e) \quad D_{kl} > D_{ij} \quad (2.12)$$

By sampling such quadruplets from the whole set of relative orderings over classes (i.e., Table 2.1, see experiments for details), we build our Qwise set \mathcal{N} such that for all quadruplet q in \mathcal{N} , we have $\delta_q = 1$ in Eq. (2.10).

2.4.1.2 Flexible constraints instead of equivalence constraints

The second type of relation that we consider is: $(e) \prec (f) \sim (g) \prec (h)$ in order to relax the relation $(f) \sim (g)$. To take into account the fact that the dissimilarity D_{ij} between \mathcal{I}_i and \mathcal{I}_j is signed, we consider the following constraint²⁰: $D_{kl} > |D_{ij}|$ where $(\mathcal{I}_k, \mathcal{I}_l) \in (h) \times (e)$. In order to have a convex problem, we rewrite it as two constraints:

$$\begin{cases} D_{kl} \geq D_{ij} + 1 \\ D_{kl} \geq -D_{ij} + 1 \end{cases} \quad (2.13)$$

From Eq. (2.13), we then generate two quadruplets in \mathcal{N} .

2.4.2 Classification experiments

In order to evaluate and compare our Qwise scheme, we follow a classification framework inspired from [Parikh and Grauman, 2011] for scene and face recognition on the OSR [Oliva and Torralba, 2001] and Pubfig [Kumar et al., 2009] datasets.

Datasets: We experiment with the two datasets used in [Parikh and Grauman, 2011]: Outdoor Scene Recognition (OSR) [Oliva and Torralba, 2001] containing 2688 images from 8 scene categories and a subset of Public Figure Face (PubFig) [Kumar et al., 2009] containing 771 images from 8 face categories. We use the image features made publicly available by [Parikh and Grauman, 2011]: a 512-dimensional GIST [Oliva and Torralba, 2001] descriptor for OSR and a concatenation of the GIST descriptor and a 45-dimensional Lab color histogram for PubFig. Relative orderings of classes according to some semantic attributes are also available (see Table 2.1).

2.4.2.1 Recognition with Gaussian Models

We study here the impact of our constraints on the original relative attribute problem.

Baseline: As a baseline, we use the model proposed in [Parikh and Grauman, 2011] that exploits relative attribute orderings between classes (see Table 2.1) to generate pairwise constraints. A multivariate Gaussian model is learned to perform recognition, as explained below.

Qwise Method: We use for **OSR** and **Pubfig** the quadruplet-wise constraints defined in Section 2.4.1. The Qwise scheme uses relative attribute information to learn a linear transformation. Particularly, we propose two different QWise strategies named **QWSL** and **OQWSL**:

- **QWSL**: this method exploits the same pairwise ordered constraints as [Parikh and Grauman, 2011] (e.g., $(e) \prec (f)$) and relaxes pairwise equivalence constraints (i.e., in Section 2.4.1.2, we consider the relation $(e) \prec (f) \sim (g) \prec (h)$ instead of $(f) \sim (g)$). By relaxing only restrictive pairwise equivalence constraints, this method is more robust to the annotation problems described in Fig 2.3.

²⁰It is not necessary to discuss the sign of D_{kl} since \mathcal{I}_k was annotated to have stronger presence of a_m than \mathcal{I}_l . We infer $D_{kl} > 0$.

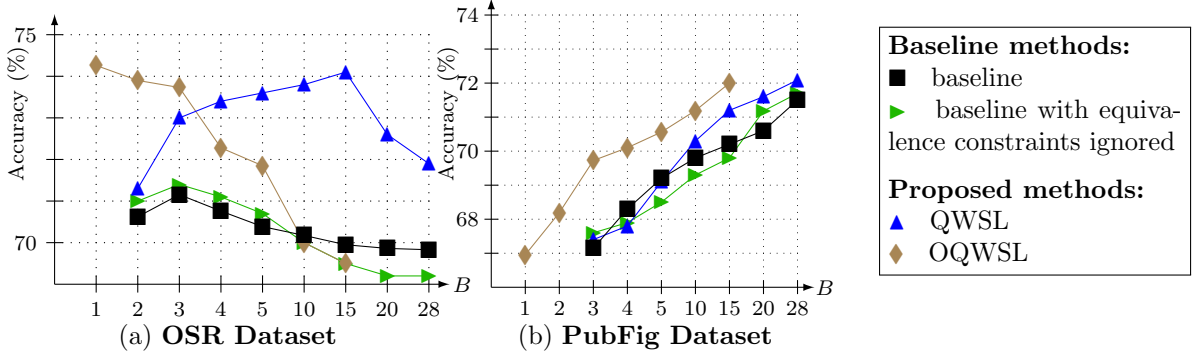


Figure 2.4: Recognition performance of the baseline [Parikh and Grauman, 2011] and the proposed methods on OSR dataset (a) and PubFig dataset (b) as a function of B (the number of pairs of classes used to generate relative constraints per attribute). Accuracies smaller than 69% are not reported for $B = 1$ on OSR. Accuracies smaller than 66% are not reported for $B = 1$ or $B = 2$ on PubFig.

- *OQWSL*: this method exploits solely quadruplet-wise constraints for training. The pairwise equivalence constraints are relaxed in the same way as QWSL, and pairwise ordered constraints are replaced by quadruplet-wise constraints (i.e., in Section 2.4.1.1, we consider the relation $(e) \prec (f) \prec (g) \prec (h)$ instead of $(f) \prec (g)$). On some datasets, the pairwise ordered annotations performed by humans may be noisy in the same way as equivalence constraints. The purpose of this method is to relax pairwise constraints generated by these possibly noisy annotations.

Learning setup: We use the same experimental setup as [Parikh and Grauman, 2011] to learn our Qwise metric. $N = 30$ training images are used per class, the rest is for testing. Let B be the number of pairs of classes that we select to learn the projection direction \mathbf{w}_m of attribute a_m . From each of the B selected pairs of classes, we extract $N \times N$ image pairs or quadruplets to create training constraints. To carry out fair comparisons, we generate one Qwise constraint for each pairwise constraint generated by [Parikh and Grauman, 2011] using the strategies described in Section 2.4.1. In this way, we have the same number of constraints. Once all the M projection directions \mathbf{w}_m are learned, a Gaussian distribution is learned for each class c_s of images: the mean $\boldsymbol{\mu}_s \in \mathbb{R}^M$ and covariance matrix $\boldsymbol{\Sigma}_s \in \mathbb{R}^{M \times M}$ are estimated using the \mathbf{h}_i of all the training images \mathcal{I}_i in c_s . A test image \mathcal{I}_t is assigned to the class corresponding to the highest likelihood. The performance is measured as the average classification accuracy across all classes over 10 random train/test splits.

Concerning the values of B , when at least one of the two images \mathcal{I}_i and \mathcal{I}_j belongs to extreme border classes (e.g., the most or least smiling classes), a pair of images $(\mathcal{I}_k, \mathcal{I}_l)$ such that $D_{kl} > D_{ij}$ cannot be sampled. We ignore the constraint in this case: since we cannot generate Qwise constraint from a pairwise constraint that involves extreme border classes, the maximum possible value for B is $\binom{C-2}{2} = 15$ for OQWSL where $C = 8$ is the number of classes. Otherwise, the maximum possible value for B is $\binom{C}{2} = 28$.

Results: The comparison of our proposed methods and the baseline [Parikh and Grauman, 2011] is illustrated in Fig. 2.4 for the OSR dataset and PubFig dataset.

- *Pairwise baseline study*: we first study for the baseline [Parikh and Grauman, 2011] the impact of the pairwise equivalence constraints (i.e., $(f) \sim (g)$) on recognition performance to better analyze the benefit of our Qwise constraints. On both OSR and PubFig, recognition performance is comparable when pairwise equivalence constraints are exploited and when they are not. This proves that equivalence constraints are not informative and do not appropriately exploit the provided equivalence information. In the following, we study the impact on recognition induced by the integration of our proposed Qwise constraints:

- *OSR*: On OSR, our methods reach an accuracy of 74.3% and 74.1%, which is 3% better than the optimal baseline accuracies. QWSL is more robust as B increases, it seems to benefit both from the precision

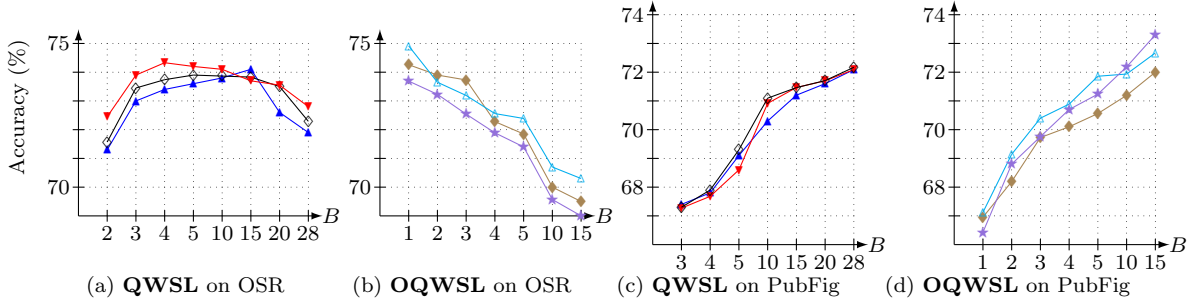


Figure 2.5: Recognition performance of our proposed methods for different neighbor sampling strategies (see text) on OSR dataset ((a) & (b)) and PubFig dataset ((c) & (d)) as a function of B (the number of pairs of classes used to generate relative constraints per attribute). Accuracies smaller than 69% are not reported for $B = 1$ on OSR. Accuracies smaller than 66% are not reported for $B = 1$ or $B = 2$ on PubFig.

Proposed methods:					
▲	QWSL-1	◆	OQWSL-1	▲	OQWSL-2
▼	QWSL-2	◆	OQWSL-2	▲	OQWSL-3
◇	QWSL-3	◆	OQWSL-3	▲	OQWSL-3

of strict order pairwise constraints and from the flexibility applied on problematic equivalent pairs of classes. OQWSL performs surprisingly well with a set of 4 classes ($B = 1$) per attribute, attesting that our Qwise scheme performs well with a small number of constraints.

- *PubFig*: On PubFig, since there are not many equivalence constraints (see Table 2.1), QWSL mostly uses the same pairwise constraints as the baselines and then performs similarly. OQWSL reaches 72% accuracy, which is 2% better than baselines with comparable B (i.e., comparable number of constraints). Moreover, when combining OQWSL and pairwise ordered constraints for extreme border classes, our method reaches 74.5% accuracy.

The recognition performance of all the baselines and proposed methods decreases with large values of B on OSR but increases on PubFig, which suggests that the provided annotations of OSR are noisy, or at least not reliable. QWSL is more robust and performs at least as well as baselines on both datasets. However, OQWSL is clearly better than all the other methods on PubFig with comparable B .

In conclusion, our approach outperforms the baselines on both OSR and PubFig with a margin of 3% accuracy, reaching state-of-the-art results in this original setup²¹ [Parikh and Grauman, 2011].

This proves that relaxing noisy pairwise constraints by intuitive quadruplet-wise constraints introduces robustness and compensates for labeling imprecisions described in Section 2.4.1.

Impact of the distance of surrounding classes to create quadruplets: We have a totally ordered set of classes per attribute to describe relations. We only studied the case where we upper bound the dissimilarity between two classes with their nearest neighbor classes in the ordered set. What happens if we choose more distant classes in the set to create quadruplets? Fig. 2.5 shows that our methods are very robust to the distance of surrounding classes. In the figures, the methods (O)QWSL-1, (O)QWSL-2, (O)QWSL-3 correspond to different sampling strategies to generate a given quadruplet $q = (\mathcal{I}_i, \mathcal{I}_j, \mathcal{I}_k, \mathcal{I}_l)$ from a given pair $(\mathcal{I}_i, \mathcal{I}_j)$. For a given $p \in \{1, 2, 3\}$, (O)QWSL- p corresponds to sampling the images \mathcal{I}_k and \mathcal{I}_l from the p^{th} closest classes of the classes of \mathcal{I}_i and \mathcal{I}_j .²²

Except in Fig 2.5 (b) where OQWSL-3 performs little worse than OQWSL-1, choosing further neighbors gives better results than choosing nearest neighbors. Our best accuracies are obtained by doing so: QWSL-2 in Fig. 2.5 (a), OQWSL-2 in Fig. 2.5 (b) and OQWSL-3 in Fig. 2.5 (d). Our performances are about 4% and 1.5% better than the optimal baselines accuracies on OSR and PubFig respectively (3.5% better on PubFig with comparable B). The reason of this phenomenon seems to be the high intra-class

²¹A different setup is used in [Parkash and Parikh, 2012] where additional feedback improves recognition.

²²For instance, if we have $(k) \prec (i) \prec (e) \prec (f) \sim (g) \prec (h) \prec (j) \prec (l)$, the classes (i) and (j) and the second closest classes to (f) and (g) . The classes (k) and (l) are their third closest classes.

variance. In general, using two close classes seems to be the right choice to learn a good margin between classes. However, if the generated training constraints are noisy due to annotation limitations (here because annotations are performed on whole classes instead of individual images), the quality of the learned projection direction \mathbf{w} is affected.

In conclusion, Qwise constraints allow to refine relations between samples and can improve recognition.

2.4.2.2 Comparison of different classification models

The relative attribute problem learns a high-level representation of images that reflects the relative degrees of presence of attributes between classes. Nevertheless, the learned transformation is not explicitly optimized so that a global distance metric measures semantical similarities between images. In particular, if we are interested in obtaining a global metric that accurately describes class membership, one can exploit the learned image representations as input data to train a metric-based classifier.

Note that learning for each class a multivariate Gaussian distribution $\mathcal{N}(\boldsymbol{\mu}_s, \boldsymbol{\Sigma}_s)$ can be seen as learning a Mahalanobis distance metric $D_{\boldsymbol{\Sigma}_s^{-1}}(\mathbf{x}, \boldsymbol{\mu}_s)$ (see Eq. (1.1)). We propose to compare the performances of our learned representations when combined with another metric learning approach: LMNN [Weinberger and Saul, 2009]. LMNN exploits only class membership information in order to learn a Mahalanobis-like distance metric. For each image, LMNN tries to satisfy the condition that members of a predefined set of target neighbors (of the same class) are closer than samples from other classes. In [Weinberger and Saul, 2009], those neighbors are chosen using the ℓ_2 -distance in the input space.

Setup: we propose a strategy called **Qwise + LMNN** for which the high level features $\mathbf{h}_i \in \mathbb{R}^M$ learned with our method are used as input of LMNN.

As baselines, we denote:

- *LMNN*: the methods for which a k -NN classifier is used (since LMNN is designed for k -NN classification). In its basic setup, we use low-level features (i.e., GIST or GIST+lab features) as input of LMNN.
- *LMNN-G*: the methods for which a linear transformation is learned (using the LMNN method) but used with a multivariate Gaussian model instead of a k -NN classifier. We propose these methods in order to have the same classifier as [Parikh and Grauman, 2011] and be fair in comparison.
- *RA + LMNN* is a combination of [Parikh and Grauman, 2011] and [Weinberger and Saul, 2009] that first uses relative attribute annotations to learn a representation of images in attribute space, and second, learns a metric in attribute space with LMNN.

We use the publicly available codes of [Parikh and Grauman, 2011] and [Weinberger and Saul, 2009].

	OSR	Pubfig
LMNN	$71.2 \pm 2.0\%$	$71.5 \pm 1.6\%$
LMNN-G	$70.7 \pm 1.9\%$	$69.9 \pm 2.0\%$
RA (Parikh's code)	$71.3 \pm 1.9\%$	$71.3 \pm 2.0\%$
RA + LMNN	$71.8 \pm 1.7\%$	$74.2 \pm 1.9\%$
Qwise	$74.1 \pm 2.1\%$	$74.5 \pm 1.3\%$
Qwise + LMNN	$74.3 \pm 1.9\%$	$77.6 \pm 2.0\%$

Table 2.2: Test classification accuracies on the OSR and Pubfig datasets for different methods.

Results: Table 2.2 reports the classification scores for the different baselines, Qwise, and Qwise+LMNN. On OSR and Pubfig, our method reaches an accuracy of 74.1% and 74.5%, respectively (see previous results). It outperforms the baselines [Parikh and Grauman, 2011] and [Weinberger and Saul, 2009] on both datasets by a margin of 3% accuracy. Moreover, performance is further improved when relative attributes and LMNN are combined. Particularly, an improvement of about 3% is obtained on Pubfig,

reaching 77.6%. Relative attribute annotations (used for Qwise learning) and class membership information (used for LMNN) then seem complementary.

In conclusion, we have proposed and compared different strategies to sample constraints and compensate for labeling imprecisions. Relaxing strong equivalence constraints by quadruplet-wise constraints improves recognition in the context of relative attributes.

2.5 Experimental Validation on Hierarchical Information

In this section, the goal is to learn a distance metric that is relevant to a given hierarchical object class taxonomy. More precisely, our objective is to learn a metric such that images from close (e.g., sibling) classes with respect to the class semantic hierarchy are more similar than images from more distant classes. Our strategy is illustrated in Fig. 2.2 where different subclasses of the general class *Canis lupus* are gathered together depending on their subspecies and their breed, which corresponds to subclasses and subsubclasses in the taxonomy, respectively.

We show the benefit of exploiting full matrix metrics over diagonal matrix metrics in the context of k -NN classification. The experiments are performed on datasets where billions of constraints can be generated. To have a tractable framework, we use the optimization strategies mentioned in Section 2.3.

2.5.1 Formulation of our metric and constraints

Constraints: Given a semantic taxonomy expressed by a tree of classes, let us consider two sibling classes c_a and c_b and a class c_d that is not their sibling (we call it a cousin class). We generate two types of quadruplet-wise constraints in order to:

(1) Enforce the dissimilarity between two images from the same class to be smaller than between two others from sibling classes. If $(\mathcal{I}_i, \mathcal{I}_j)$ are both sampled from c_a , and $(\mathcal{I}_k, \mathcal{I}_l)$ are sampled from $c_a \times c_b$, we want $D_{ij} < D_{kl}$. These constraints are similar to the ones exploited by LMNN [Weinberger and Saul, 2009] with the exception that we use quadruplets of images (i.e., $\mathcal{I}_i = \mathcal{I}_k$ in LMNN) and that LMNN does not exploit taxonomy information: i.e., we sample \mathcal{I}_l from a sibling class of c_a whereas LMNN samples \mathcal{I}_l from any class different from c_a .

(2) Enforce the dissimilarity between two images from sibling classes to be smaller than between two images from cousin classes. If $(\mathcal{I}_i, \mathcal{I}_j)$ are sampled from $c_a \times c_b$ and $(\mathcal{I}_k, \mathcal{I}_l)$ from $c_a \times c_d$, we want $D_{ij} < D_{kl}$. These constraints are strongly related to the taxonomy information and allow to discriminate images from sibling classes better than from any other class. They follow the idea that semantically close objects should be closer with the learned distance metric.

In order to limit the number of training constraints, we sample the image \mathcal{I}_j such that \mathcal{I}_j is one of the k nearest neighbors of \mathcal{I}_i : \mathcal{I}_j is sampled in the same class in the case (1) and in a sibling class in the case (2).

Distance metric: in this section, we consider both the diagonal PSD matrix and the full matrix distance metric formulations described in Section 2.2.

2.5.2 Experiments

2.5.2.1 Datasets and classification task

Classification task: In order to validate the Qwise ability to learn a powerful metric using a class hierarchy, we focus on the local subtree classification task described in [Verma et al., 2012]. In this section, the goal is to discriminate classes (leafs of a hierarchical subtree) amongst a hierarchical subtree that contains all the considered classes.

Subtree Dataset	Non-linear SVM	TaxEmb	Verma et al.	Qwise (Diag. Matrix)	Qwise (Full Matrix)
Amphibian	38%	38%	41%	43.5%	43.5%
Fish	34%	37%	39%	41%	41.6%
Fruit	22.5%	20%	23.5%	21.1%	21.1%
Furniture	44%	41%	46%	48.8%	48.9%
Geological Formation	50.5%	50.5%	52.5%	56.1%	56.1%
Musical Instrument	30.5%	23%	32.5%	32.9%	32.9%
Reptile	21.5%	18.5%	22%	23.0%	23.1%
Tool	27.5%	24.5%	29.5%	26.4%	26.7%
Vehicle	30.5%	22.5%	27%	34.7%	34.7%
Average Accuracy	33.2%	30.6%	34.8%	36.4%	36.5%

Table 2.3: Standard classification accuracy for the various datasets.

Datasets: We use the same 9 datasets as in [Verma et al., 2012] (which are all subsets of ImageNet [Deng et al., 2009]): *Amphibian*, *Fish*, *Fruit*, *Furniture*, *Geological Formation*, *Musical Instrument*, *Reptile*, *Tool*, *Vehicle*. Each of these 9 datasets contains 8 to 40 different classes and from 8000 to 54000 images each. We use the train, validation and test sets defined in [Verma et al., 2012], and also the same publicly available features²³: 1000 dimensional SIFT-based Bag-of-Words (BoW) [Sivic and Zisserman, 2003].

2.5.2.2 Optimal strategy

We learn a PSD matrix $\mathbf{M} \in \mathbb{S}_+^d$ that exploits the constraints described in Section 2.5.1 and that we decompose²⁴ as $\mathbf{M} = \mathbf{L}^\top \mathbf{L}$. The matrix \mathbf{L} is used to project input data in another representation space which is the input space of another classifier. We choose a standard classifier (linear SVM) to perform classification.

When we constrain $\mathbf{M} \in \mathbb{S}_+^d$ to be diagonal, we formulate our metric $D_{\mathbf{M}}^2(\mathcal{I}_i, \mathcal{I}_j) = \mathcal{Q}_{\mathbf{w}}(\mathcal{I}_i, \mathcal{I}_j) = \mathbf{w}^\top \Psi(\mathcal{I}_i, \mathcal{I}_j)$ where $\Psi(\mathcal{I}_i, \mathcal{I}_j) = (\mathbf{x}_i - \mathbf{x}_j) \circ (\mathbf{x}_i - \mathbf{x}_j)$ and $\mathbf{w} = \text{Diag}(\mathbf{M})$. Once the diagonal PSD matrix $\mathbf{M} \geq \mathbf{0}$ is learned, we project the input space using the linear transformation parameterized by the diagonal matrix $\mathbf{M}^{1/2} = \mathbf{L} \in \mathbb{R}^{d \times d}$ such that $\forall i \in \{1, \dots, d\}, \mathbf{L}_{ii} = \sqrt{\mathbf{M}_{ii}}$ (note that $\mathbf{L}^\top \mathbf{L} = \mathbf{M}$).

Table 2.3 presents for the 9 different datasets the test classification accuracies:

- reported in [Verma et al., 2012] for different methods (TaxEmb [Weinberger and Chapelle, 2008], a non-linear SVM and the method proposed in [Verma et al., 2012]). The model of [Verma et al., 2012] and TaxEmb [Weinberger and Chapelle, 2008] also exploit class taxonomy information to learn hierarchical similarity metrics or an embedding. It is worth mentioning that Verma et al. [Verma et al., 2012] have a complex learning framework: they learn a local metric parameterized by a full PSD matrix for each class (leaf of the subtree), which can lead to overfitting.

- of our two methods: the first one constrains the learned matrix $\mathbf{M} \in \mathbb{S}_+^d$ to be diagonal, the second one does not. Our Qwise-learning model is simpler than [Verma et al., 2012] since we learn only one global metric for each subtree. Moreover, when we use a diagonal matrix model, the number of parameters only grows linearly with the input space dimension. Both proposed methods obtain surprisingly very similar results with a global accuracy of $36.4 \sim 36.5\%$, which beats the method of Verma et al. [Verma et al., 2012] by 1.6%. The similar performances of the full and diagonal matrix models seem to be due to the linear SVM classifier which implicitly decorrelates training data by ignoring irrelevant features and giving special importance to discriminant features. Both proposed methods outperform all the reported methods, globally and on each dataset except Fruit and Tool. All these results validate the fact that the proposed constraints are useful when richer information compared to class membership information is provided.

²³<http://www.image-net.org/challenges/LSVRC/2010/>

²⁴We use the eigendecomposition $\mathbf{M} = \mathbf{U}\mathbf{D}\mathbf{U}^\top$ where \mathbf{D} is a diagonal matrix, and we formulate $\mathbf{L} = \mathbf{D}^{1/2}\mathbf{U}^\top$.

Model	Amph.	Fish	Fruit	Furn.	Geol. F.	Mus. I.	Rept.	Tool	Vehi.	AVG
Euclidean distance	35.5	33.9	16.9	36.6	43.3	27.0	17.2	24.5	20.2	28.3
LMNN Diag. Matrix	39.0	37.4	19.5	39.4	47.2	27.5	19.8	23.8	22.9	30.8
LMNN Full Matrix	41.8	38.3	21.1	41.1	49.5	28.5	21.2	24.0	28.0	32.6
Qwise Diag. Matrix	39.3	37.6	20.6	40.0	47.6	28.0	20.7	23.8	24.8	31.4
Qwise Full Matrix	41.8	38.5	21.7	41.6	51	29.3	21.8	24.2	29.3	33.2

Table 2.4: Standard classification accuracy for the various datasets using the k -NN classification framework, with $k = 10$.

Model	Amph.	Fish	Fruit	Furn.	Geol. F.	Mus. I.	Rept.	Tool	Vehi.	AVG
Euclidean distance	50.1	35.3	32.1	42.2	45.1	28.5	21.3	26.2	29.1	34.4
LMNN Diag. Matrix	53.0	42.0	34.2	42.7	48.5	30.2	22.4	25.5	32.2	36.7
LMNN Full Matrix	56.0	42.3	34.5	44.1	51.1	31.7	22.4	25.7	32.8	37.8
Qwise Diag. Matrix	54.8	42.5	39.1	44.8	50.0	33.1	24.4	25.6	33.2	38.6
Qwise Full Matrix	56.7	43.6	39.7	46.9	53.2	34.1	25.5	26.1	34.7	40.1

Table 2.5: Classification accuracy that takes class information into account for the various datasets using the k -NN classification framework (see text), with $k = 10$.

2.5.2.3 Further analysis with k -NN classification

We further study the impact of our proposed constraints in a k -NN classification context. For this purpose, we also learn a metric that exploits the constraints described in Section 2.5.1. Each test image is assigned to the class with maximum number of nearest neighbors w.r.t. the learned metric.

Table 2.4 reports the average classification accuracy across all classes for different k -NN methods:

- the Euclidean distance which corresponds to the Mahalanobis-like distance metric parameterized by the unlearned identity matrix $\mathbf{M} = \mathbf{I}_d$. We report the results for 10 nearest neighbor classification (which performs better than 1-NN, 5-NN and 50-NN).
- LMNN [Weinberger and Saul, 2009] that is a popular metric learning approach for classification. It does not exploit taxonomy information.
- our two proposed methods: the first one learns a diagonal PSD distance matrix, the second one learns a full PSD distance matrix as described in Section 2.2.2.

All the learned models outperform the Euclidean distance metric in this setup for the mentioned datasets. Full matrix models that exploit correlations between features outperform metric learning models that learn a diagonal distance matrix. We note that our proposed methods, which exploit hierarchical taxonomy information, slightly outperform LMNN that uses only class membership information. It is worth mentioning that this gain is not straightforward since our proposed constraints focus on preserving semantic distances w.r.t. the provided taxonomy rather than performing k -NN classification task. In order to better observe the preservation of relationships between classes using our learned metric, we use another evaluation criterion that takes into account the relationship between the predicted class and the true class instead of only focusing on the correct assignment of an image to its true class.

The proposed accuracy metric can be written as the average accuracy across all classes $1/C \sum_{c=1}^C \text{Acc}_c$ where C is the number of considered categories. The accuracy for each class c is $\text{Acc}_c = 1 - \frac{1}{m} \sum_{t=1}^m \Delta(c, \hat{y}_t^c)$ where c and \hat{y}_t^c denote the true and predicted class labels of the t^{th} test example; m denotes the total number of test examples in the class c . In the standard classification accuracy and the proposed evaluation metrics, each correct prediction has zero loss (i.e., $\Delta(c, \hat{y}_t^c) = 0$ when $c = \hat{y}_t^c$). However:

- $\Delta(a, \hat{y}_t^c) = 1$ iff $a \neq c$ for the standard classification accuracy.
- for the proposed metric: $\Delta(a, \hat{y}_t^c) = 0.5$ when a is a sibling class of \hat{y}_t^c in the hierarchical taxonomy. $\Delta(y_t, \hat{y}_t) = 1$ otherwise.

In this way, we can measure and interpret the ability of models to preserve semantic relationships. Table 2.5 reports the recognition scores when using the proposed accuracy metric. When the evaluation metric considers semantic closeness between categories, the gap between our method and LMNN is more important. Our proposed method outperforms all the tested methods. This demonstrates that the proposed constraints allow to better fit semantic relationships between classes. This result corroborates the claim of [Verma et al., 2012] that exploiting class taxonomy to learn a metric is beneficial for recognition.

2.6 Conclusion

In this chapter, we have proposed a general and efficient Mahalanobis distance metric learning framework that exploits constraints over quadruplets of images. Our approach is a generalization of pairwise and triplet-wise approaches, it can also describe relations between data that are not possible with classic approaches. Moreover, it can easily combine relative and absolute distance constraints. In many contexts, relations between pairs of samples seem intuitive and prove to be reliable information to improve recognition when combined with or when replacing pairwise or triplet-wise approaches. We experimentally show in different scenarios (i.e., relative attributes and metric learning on class hierarchy) that it is specifically adapted to incorporate knowledge from rich or complex semantic label relations. In the context of relative attributes, we have shown that some pairwise comparisons of images are limited and can be improved by relaxing them with quadruplet-wise constraints. A meaningful high-level representation of images has then been learned and used in the context of image classification. In the context of hierarchical classification, class taxonomies have been used to better describe semantical relationships between images, and thus improve recognition performance. We will complete these experiments with another application in Chapter 4. Furthermore, our approach can be used in contexts where billions of constraints are generated thanks to an active set strategy. Future work includes the adaptation in our framework of other efficient methods to deal with huge numbers of constraints, such as the 1-slack cutting plane method used for structural SVMs.

Chapter 3

Fantope Regularization

Chapter Abstract This chapter introduces a regularization method to explicitly control the rank of a learned symmetric positive semidefinite distance matrix in Mahalanobis distance metric learning. For this purpose, we propose to incorporate in the objective function a regularization term that minimizes the sum of the k smallest eigenvalues of the learned distance matrix. It is equivalent to minimizing the trace of the product of the distance matrix with a matrix in the convex hull of rank- k projection matrices, called a Fantope. Based on this new regularization method, we derive an optimization scheme to efficiently learn the distance matrix.

We first present classic methods to control the rank of the learned model in Mahalanobis distance metric learning (Section 3.1). We then introduce our proposed regularizer and an algorithm to solve our resulting objective problem (Section 3.2). We provide a theoretical justification for the algorithm (Section 3.3). We experimentally demonstrate the effectiveness of the method on synthetic and challenging real-world datasets of face verification and image classification with relative attributes (Section 3.4), on which our method outperforms state-of-the-art metric learning algorithms.

Some of the material in this chapter has been published at the following conference:

- Law, M. T., Thome, N., and Cord, M. (2014). Fantope Regularization in Metric Learning. *IEEE Conference on Computer Vision and Pattern Recognition (CVPR)* [Law et al., 2014b]

3.1 Introduction

In the previous chapter, we focused on the generation of meaningful constraints to improve recognition when rich information on the dataset is provided. This chapter is dedicated to the control of the complexity of the learned distance metric model.

Mahalanobis distance metric learning approaches infer a symmetric positive semidefinite matrix and hence a linear transformation of the data. The number of independent parameters of the learned model is proportional to both the dimensionality of the input space and the rank of the learned PSD matrix. Controlling the rank of the learned model has several theoretical and practical advantages. First, it is a powerful way to limit overfitting, especially because the number of independent parameters of the model can be quadratic in the input space dimensionality if its rank is not controlled. It also allows to better exploit correlations between features. In practice, low-rank models often perform better than high-rank models, particularly in contexts with high-dimensional input space. Finally, it has practical interest since it allows to efficiently store data projected in a low-dimensional space, which also speeds up the computation of Euclidean distances in this space.

Nonetheless, the formulation of Mahalanobis distance metric learning problems to obtain a low-rank solution remains an open problem. Indeed, minimizing a convex function subject to a rank constraint is NP-hard [Natarajan, 1995]. Diverse approaches have then been proposed to learn a low-rank solution. The most popular ones in metric learning are (1) using the nuclear norm (i.e., the sum of singular values)

of the learned matrix as a convex regularization term and (2) writing the metric learning problem as a function of a low-rank transformation matrix and optimizing the problem with respect to this matrix.

In the first case, the nuclear norm $\|\mathbf{X}\|_*$ has been widely used as a regularization term in metric learning [Shen et al., 2009, McFee and Lanckriet, 2010, Lim et al., 2013] since it is the convex envelope of $\text{rank}(\mathbf{X})$ on the set $\{\mathbf{X} \in \mathbb{R}^{m \times n} : \|\mathbf{X}\| \leq 1\}$ [Fazel, 2002]. The nuclear norm can also be thought of as a convex relaxation of the number of non-zero singular values (i.e., the rank). However, although it promotes low-rank solutions, it does not allow to explicitly control the rank of the learned matrix. As with the ℓ_1 norm that penalizes the largest elements of a vector more than the smallest ones, trace norm penalizes the largest singular values more than the smallest ones. This can be problematic to approximate the rank function and describe high correlations between data.

On the other hand, decomposing the learned model $\mathbf{M} \in \mathbb{S}_+^d$ as $\mathbf{M} = \mathbf{L}^\top \mathbf{L}$ where $\mathbf{L} \in \mathbb{R}^{e \times d}$ and optimizing over the transformation matrix \mathbf{L} prevents solutions of rank greater than e . It also makes the optimization of the problem efficient as it avoids to project \mathbf{M} onto \mathbb{S}_+^d at each iteration. However, it makes the problem nonconvex, and the gradient formulation makes the rank of the learned matrix nonincreasing (see Section 1.5.2.1) at each descent iteration. Since methods that optimize over \mathbf{L} [Mignon and Jurie, 2012, Mensink et al., 2013] do not use a regularization term, their method usually rely on *early stopping* to limit overfitting.

Other distance metric learning approaches such as LMNN [Weinberger and Saul, 2009] and ITML [Davis et al., 2007] do not promote low-rank solutions and are thus prone to overfitting when the dimensionality of the input space is large.

This chapter introduces a novel type of regularization which allows to explicitly control the rank of the learned symmetric PSD matrix $\mathbf{M} \in \mathbb{S}_+^d$. The regularization term that we propose minimizes the sum of the k smallest eigenvalues of a symmetric PSD matrix. It is minimized when the rank of the learned matrix is smaller than or equal to $(d-k)$. As in the truncated nuclear norm [Hu et al., 2013], it minimizes the sum of the k smallest singular values of the matrix since the singular values of a PSD matrix are also its eigenvalues (see Appendix A). However, the problem formulated in [Hu et al., 2013] requires the truncated nuclear norm to be combined with some specific type of smooth convex loss function in order to be optimized efficiently. On the other hand, our formulation of the truncated nuclear norm with respect to eigenvalues, although restricted to the domain \mathbb{S}_+^d , can be efficiently optimized when our regularization term is combined with any type of (subdifferentiable) convex loss function.

3.2 Regularization Scheme

We formulate our metric learning problem in a classic way (see Section 1.3):

$$\min_{\mathbf{M}} \mu R(\mathbf{M}) + \ell(\mathbf{M}, \mathcal{N}) \text{ s.t. } \mathbf{M} \in \mathbb{S}_+^d \quad (3.1)$$

where $R(\mathbf{M})$ is the regularization term, $\ell(\mathbf{M}, \mathcal{N})$ is a (convex) loss function over a training set \mathcal{N} , and $\mu \geq 0$ a regularization parameter.

We propose a regularization term that reaches its minimum when the rank of the learned PSD matrix is smaller than or equal to a fixed target rank. We formulate the regularization term $R(\mathbf{M})$ as the sum of the k smallest eigenvalues of $\mathbf{M} \in \mathbb{S}_+^d$:

$$R(\mathbf{M}) = \sum_{i=d-k+1}^d \lambda(\mathbf{M})_i \quad (3.2)$$

Since the rank of the PSD matrix $\mathbf{M} \in \mathbb{S}_+^d$ is the number of its non-zero eigenvalues and all the eigenvalues of $\mathbf{M} \in \mathbb{S}_+^d$ are non-negative, the proposed regularization term $R(\mathbf{M})$ allows an explicit control over the rank of \mathbf{M} :

$$R(\mathbf{M}) = 0 \Leftrightarrow \text{rank}(\mathbf{M}) \leq d - k \quad (3.3)$$

We explain in the following how to express $R(\mathbf{M})$ in a convenient way.

3.2.1 Regularization term linearization

The sum of the k smallest eigenvalues of \mathbf{M} can be written as $\text{tr}(\mathbf{W}\mathbf{M}) = \langle \mathbf{W}, \mathbf{M} \rangle$ where $\mathbf{W} \in \mathbb{S}_+^d$ is the orthogonal projector on the eigenvectors of \mathbf{M} with k smallest eigenvalues. We describe in this subsection how to construct such an orthogonal projection matrix \mathbf{W} .

Let $\mathbf{M} = \mathbf{V}_\mathbf{M} \text{Diag}(\lambda(\mathbf{M})) \mathbf{V}_\mathbf{M}^\top$ be the eigendecomposition of $\mathbf{M} \in \mathbb{S}_+^d$ where $\mathbf{V}_\mathbf{M}$ is an orthogonal matrix. Let us construct $\mathbf{w} = (w_1, \dots, w_d)^\top \in \mathbb{R}^d$ such that:

$$w_i = \begin{cases} 0 & \text{if } 1 \leq i \leq d-k \text{ (the first } d-k \text{ elements)} \\ 1 & \text{if } d-k+1 \leq i \leq d \text{ (the last } k \text{ elements)} \end{cases}$$

We then express \mathbf{W} as:

$$\mathbf{W} = \mathbf{V}_\mathbf{M} \text{Diag}(\mathbf{w}) \mathbf{V}_\mathbf{M}^\top \quad (3.4)$$

It is simple to verify that $R(\mathbf{M}) = \text{tr}(\mathbf{W}\mathbf{M})$ is the sum of the k smallest eigenvalues of $\mathbf{M} \in \mathbb{S}_+^d$:

$$\begin{aligned} R(\mathbf{M}) &= \text{tr}(\mathbf{W}\mathbf{M}) = \text{tr}(\mathbf{V}_\mathbf{M} \text{Diag}(\mathbf{w}) \mathbf{V}_\mathbf{M}^\top \mathbf{V}_\mathbf{M} \text{Diag}(\lambda(\mathbf{M})) \mathbf{V}_\mathbf{M}^\top) \\ &= \mathbf{w}^\top \lambda(\mathbf{M}) = \sum_{i=d-k+1}^d \lambda(\mathbf{M})_i \end{aligned}$$

Since the last k elements of $\lambda(\mathbf{M})$ (the k smallest eigenvalues of \mathbf{M}) equal 0 iff $\text{rank}(\mathbf{M}) \leq d-k$, one can deduce the expected property given in Eq. (3.3) that $R(\mathbf{M}) = 0$ iff the rank of \mathbf{M} is smaller or equal to $d-k$.

As one can see in Eq. (3.4), the value of \mathbf{W} such that $R(\mathbf{M}) = \text{tr}(\mathbf{W}\mathbf{M})$ depends on the value \mathbf{M} .

3.2.2 Optimization scheme

The regularization term $R(\mathbf{M})$ has been introduced in the previous subsection, we now explicit the formulation of the loss function $\ell(\mathbf{M}, \mathcal{N})$ and the objective function.

Loss Function We focus on quadruplet-wise constraints, introduced in the previous chapter of this thesis, that encompass pairwise and triplet-wise constraints. We briefly recall them in this paragraph. They involve distance comparisons of the form $D(\mathcal{I}_k, \mathcal{I}_l) > D(\mathcal{I}_i, \mathcal{I}_j)$ for any quadruplet of images $q = (\mathcal{I}_i, \mathcal{I}_j, \mathcal{I}_k, \mathcal{I}_l)$. Our goal is to learn a metric $D_\mathbf{M}$ parameterized by \mathbf{M} that satisfies the following constraint for all q in a training set \mathcal{N} :

$$\forall q \in \mathcal{N}, D_\mathbf{M}^2(\mathcal{I}_k, \mathcal{I}_l) \geq \delta_q + D_\mathbf{M}^2(\mathcal{I}_i, \mathcal{I}_j) \quad (3.5)$$

where δ_q is a safety margin specific to each quadruplet q and our learned distance metric can be written $D_\mathbf{M}^2(\mathcal{I}_i, \mathcal{I}_j) = \langle \mathbf{M}, \mathbf{C}_{ij} \rangle$ (see Chapter 2 for details).

Our quadruplet-wise constraints in Eq. (3.5) using $q = (\mathcal{I}_i, \mathcal{I}_j, \mathcal{I}_k, \mathcal{I}_l) \in \mathcal{N}$ can be rewritten equivalently:

$$\forall q \in \mathcal{N}, \langle \mathbf{M}, \mathbf{C}_{kl} - \mathbf{C}_{ij} \rangle \geq \delta_q \quad (3.6)$$

Once these constraints have been established, we define a global loss $\ell(\mathbf{M}, \mathcal{N}) = \sum_{q \in \mathcal{N}} \ell_\mathbf{M}(q)$ that accumulates losses over all the constraints in Eq.(3.6). We design the loss for a single quadruplet: $\ell_\mathbf{M}(q) = \max(0, \delta_q + \langle \mathbf{M}, \mathbf{C}_{ij} - \mathbf{C}_{kl} \rangle)$.

Algorithm 2 Metric Learning with Fantope Regularization**input** : Training constraints \mathcal{N} , hyper-parameter μ and step size $\eta > 0$.**output** : $\mathbf{M} \in \mathbb{S}_+^d$

- 1: Initialize $\mathbf{M}^1 \in \mathbb{S}_+^d$, iteration $n = 1$
- 2: **repeat**
- 3: $\mathbf{W}^n \leftarrow \mathbf{V}_{\mathbf{M}^n} \text{Diag}(\mathbf{w}) \mathbf{V}_{\mathbf{M}^n}^\top$ (Eq. (3.4))
- 4: Compute $\nabla_{\mathbf{M}^n}$ (Eq. (3.8))
- 5: $\mathbf{M}^{n+1} \leftarrow \Pi_{\mathbb{S}_+^d}(\mathbf{M}^n - \eta \nabla_{\mathbf{M}^n})$
- 6: $n \leftarrow n + 1$
- 7: **until** stopping criterion (e.g., convergence)

Optimization By including our regularization term and $\ell(\mathbf{M}, \mathcal{A})$, our optimization problem in Eq. (3.1) can be written:

$$\begin{aligned} \min_{\mathbf{M}} \quad & \mu \langle \mathbf{W}, \mathbf{M} \rangle + \sum_{q \in \mathcal{N}} \max(0, \delta_q + \langle \mathbf{M}, \mathbf{C}_{ij} - \mathbf{C}_{kl} \rangle) \\ \text{s.t.} \quad & \mathbf{M} \in \mathbb{S}_+^d, \mathbf{W} = \mathbf{V}_{\mathbf{M}} \text{Diag}(\mathbf{w}) \mathbf{V}_{\mathbf{M}}^\top \end{aligned} \quad (3.7)$$

In order to solve Eq. (3.7), we present a method that alternately updates the values of \mathbf{M} and \mathbf{W} since the value of \mathbf{W} depends on the value of \mathbf{M} .

Although the objective function defined in Eq. (3.7) is nonconvex, it is convex w.r.t. \mathbf{M} when \mathbf{W} is fixed. We then propose to perform a subgradient method over \mathbf{M} with \mathbf{W} fixed. We alternate the update of \mathbf{M} and \mathbf{W} by fixing one of these matrices and updating the other. \mathbf{M} is updated by performing a projected subgradient method iteration (see Section 2.2.2).

Algorithm 2 illustrates our method. Let \mathbf{M}^n be the value of \mathbf{M} at the n -th iteration, \mathbf{W}^n is constructed such that it is the orthogonal projector on the eigenvectors of \mathbf{M}^n with k smallest eigenvalues (step 3). A subgradient at \mathbf{M} of Eq. (3.7) with $\mathbf{W} = \mathbf{W}^n$ fixed is computed (step 4):

$$\nabla_{\mathbf{M}^n} = \mu \mathbf{W}^n + \sum_{q \in \mathcal{N}^+} (\mathbf{C}_{ij} - \mathbf{C}_{kl}) \quad (3.8)$$

where \mathcal{N}^+ is the subset of constraints in \mathcal{N} that are not satisfied (Eq. (3.6)). \mathbf{M}^{n+1} is determined by projecting $(\mathbf{M}^n - \eta \nabla_{\mathbf{M}^n})$ onto \mathbb{S}_+^d (step 5). The process stops when the objective value stops decreasing.

The fact that the value of \mathbf{W} depends on the value \mathbf{M} is not clearly visible in our proposed algorithm. We demonstrate in the next section that $\nabla_{\mathbf{M}^n}$ is the gradient of our objective function when it is differentiable at \mathbf{M}^n .

3.3 Theoretical Analysis

In this section, we introduce different useful mathematical concepts to study the theoretical properties of R . Particularly, we show that R is a concave function. From this observation, we exhibit its corresponding (super-)gradient.

3.3.1 Concavity analysis

Definition of Fantope We show in this subsection that R (the sum of the k smallest eigenvalues) is a concave function. For this purpose, we introduce the convex nonempty hull of the set of projection matrices of rank- p [Overton and Womersley, 1992, Overton and Womersley, 1993]. It is called a Fantope [Dattorro, 2005], we denote it \mathbb{F}_p^d :

$$\begin{aligned}\mathbb{F}_p^d &= \text{conv}(\{\mathbf{V}\mathbf{V}^\top \mid \mathbf{V} \in \mathbb{R}^{d \times p}, \mathbf{V}^\top \mathbf{V} = \mathbf{I}_p\}) \\ &= \{\mathbf{F} \in \mathbb{S}_+^d \mid \mathbf{0} \preceq \mathbf{F} \preceq \mathbf{I}_d, \text{tr}(\mathbf{F}) = p\} \\ &= \{\mathbf{I}_d - \mathbf{W} \mid \mathbf{W} \in \mathbb{F}_{d-p}^d\}\end{aligned}\tag{3.9}$$

where $\text{conv}(\mathcal{X})$ denotes the convex hull of the set \mathcal{X} of points. To describe it simply, the second row of Eq. (3.9) indicates that \mathbb{F}_p^d is the set of all symmetric matrices for which:

- all the eigenvalues have values between 0 and 1
- and the trace is p .

Fantope and sum of the largest eigenvalues Once the Fantope is defined, we introduce a function whose properties are well known. Its relation w.r.t. R will be explicitated in the following.

We denote $g_p(\mathbf{M})$ the sum of the p largest eigenvalues of a symmetric matrix $\mathbf{M} \in \mathbb{S}^d$. It can be expressed as:

$$g_p(\mathbf{M}) \stackrel{(a)}{=} \max_{\mathbf{V}^\top \mathbf{V} = \mathbf{I}_p} \langle \mathbf{M}, \mathbf{V}\mathbf{V}^\top \rangle \stackrel{(b)}{=} \max_{\mathbf{A} \in \mathbb{F}_p^d} \langle \mathbf{M}, \mathbf{A} \rangle \tag{3.10}$$

Identity (a) is an extremal property known as *Ky Fan's maximum principle* [Fan, 1949]. The proofs of identities (a) and (b) are given in [Overton and Womersley, 1992]. The sum of the p largest eigenvalues of $\mathbf{M} \in \mathbb{S}^d$ is a convex function in \mathbf{M} [Overton and Womersley, 1992], this is obvious from Eq. (3.10) since it is the pointwise maximum of a set of convex functions.

Fantope and sum of the smallest eigenvalues Now that g_p is defined, we remark that R can be written as a function of g_{d-k} :

$$\begin{aligned}R(\mathbf{M}) &= \sum_{i=d-k+1}^d \lambda(\mathbf{M})_i = \sum_{i=1}^d \lambda(\mathbf{M})_i - \sum_{i=1}^{d-k} \lambda(\mathbf{M})_i \\ &= \text{tr}(\mathbf{M}) - g_{d-k}(\mathbf{M})\end{aligned}\tag{3.11}$$

As the trace function is linear, it is both convex and concave. From Eq. (3.10), we see that R is the sum of two concave functions (i.e., tr and $-g_{d-k}$), it is then a concave function.

Since the k smallest eigenvalues of \mathbf{M} are also the opposite of the k largest eigenvalues of $-\mathbf{M}$, $R(\mathbf{M})$ can also be written:

$$R(\mathbf{M}) = -g_k(-\mathbf{M}) = -\max_{\mathbf{A} \in \mathbb{F}_k^d} \langle -\mathbf{M}, \mathbf{A} \rangle = \min_{\mathbf{A} \in \mathbb{F}_k^d} \langle \mathbf{M}, \mathbf{A} \rangle \tag{3.12}$$

3.3.2 (Super-)Gradient of the regularizer

We describe here how to compute the (super-)gradient of $R : \mathbb{S}_+^d \rightarrow \mathbb{R}_+$ at some point \mathbf{M} .

Theorem 1. *Every matrix $\mathbf{F} \in \operatorname{argmin}_{\mathbf{A} \in \mathbb{F}_k^d} \langle \mathbf{M}, \mathbf{A} \rangle$ is a supergradient of the concave function R at \mathbf{M} .*

Proof: By definition, each matrix $\mathbf{G} \in \mathbb{S}^d$ that satisfies:

$$\forall \mathbf{X} \in \mathbb{S}_+^d, R(\mathbf{M}) + \langle \mathbf{G}, \mathbf{X} - \mathbf{M} \rangle \geq R(\mathbf{X})$$

is a supergradient of the concave function R at \mathbf{M} . Since $\forall \mathbf{F} \in \operatorname{argmin}_{\mathbf{A} \in \mathbb{F}_k^d} \langle \mathbf{M}, \mathbf{A} \rangle$, we have $\langle \mathbf{F}, \mathbf{M} \rangle = R(\mathbf{M})$ and $\forall \mathbf{X} \in \mathbb{S}_+^d, \langle \mathbf{F}, \mathbf{X} \rangle \geq R(\mathbf{X}) = \min_{\mathbf{A} \in \mathbb{F}_k^d} \langle \mathbf{X}, \mathbf{A} \rangle$. We then have the property: $\forall \mathbf{X} \in \mathbb{S}_+^d, R(\mathbf{M}) + \langle \mathbf{F}, \mathbf{X} \rangle \geq \langle \mathbf{F}, \mathbf{M} \rangle + R(\mathbf{X}) \implies R(\mathbf{M}) + \langle \mathbf{F}, \mathbf{X} - \mathbf{M} \rangle \geq R(\mathbf{X})$. \square

Definition 3.3.1. (*Superdifferential*) The superdifferential of the concave function R at \mathbf{M} , denoted $\partial R(\mathbf{M})$, is the set of all the supergradients of R at \mathbf{M} . If $\partial R(\mathbf{M})$ is a singleton, then R is differentiable at \mathbf{M} and the single element in $\partial R(\mathbf{M})$ is the gradient of R at \mathbf{M} .

We show here that the superdifferential of R at \mathbf{M} is $\operatorname{argmin}_{\mathbf{A} \in \mathbb{F}_k^d} \langle \mathbf{M}, \mathbf{A} \rangle$.

Property 3.3.2. ([Overton and Womersley, 1993], Corollary 3.5) The subdifferential of the sum of the $d - k$ largest eigenvalues of \mathbf{M} is the set $\{\mathbf{A} \in \mathbb{F}_{d-k}^d \mid \langle \mathbf{A}, \mathbf{M} \rangle = g_{d-k}(\mathbf{M})\} = \operatorname{argmax}_{\mathbf{A} \in \mathbb{F}_{d-k}^d} \langle \mathbf{A}, \mathbf{M} \rangle$.

From this property and from Eq. (3.11), we deduce that the superdifferential of our regularization function R at \mathbf{M} is the set $\partial R(\mathbf{M}) = \operatorname{argmin}_{\mathbf{A} \in \mathbb{F}_k^d} \langle \mathbf{M}, \mathbf{A} \rangle$.

Property 3.3.3. ([Overton and Womersley, 1993], Corollary 3.10) if $\lambda(\mathbf{M})_{d-k} > \lambda(\mathbf{M})_{d-k+1}$, the function g_{d-k} is differentiable at \mathbf{M} (and the solution $\mathbf{Z} \in \operatorname{argmax}_{\mathbf{A} \in \mathbb{F}_{d-k}^d} \langle \mathbf{M}, \mathbf{A} \rangle$ is unique).

From this property, if $\lambda(\mathbf{M})_{d-k} > \lambda(\mathbf{M})_{d-k+1}$, the unique solution $\mathbf{F} \in \operatorname{argmin}_{\mathbf{A} \in \mathbb{F}_k^d} \langle \mathbf{M}, \mathbf{A} \rangle$ is the gradient of R at \mathbf{M} . Otherwise, all the possible supergradients of R at \mathbf{M} are solutions of $\operatorname{argmin}_{\mathbf{A} \in \mathbb{F}_k^d} \langle \mathbf{M}, \mathbf{A} \rangle$. The interested reader that wants to explicitly construct all the possible solutions of $\operatorname{argmin}_{\mathbf{A} \in \mathbb{F}_k^d} \langle \mathbf{M}, \mathbf{A} \rangle$ can refer to [Overton and Womersley, 1993].

Proposed regularization scheme The matrix \mathbf{W} (constructed as in Eq. (3.4)) used to compute the sum of the k smallest eigenvalues of \mathbf{M} is a rank- k projection matrix, it then belongs to \mathbb{F}_k^d (convex hull of rank- k projection matrices). Since we have shown that $\langle \mathbf{M}, \mathbf{W} \rangle = R(\mathbf{M})$, we deduce $\mathbf{W} \in \operatorname{argmin}_{\mathbf{A} \in \mathbb{F}_k^d} \langle \mathbf{M}, \mathbf{A} \rangle$. It is then the gradient of R at \mathbf{M} if $\lambda(\mathbf{M})_{d-k} \neq \lambda(\mathbf{M})_{d-k+1}$, and a supergradient of R at \mathbf{M} otherwise. Algorithm 2 can then be seen as a (projected) gradient method over our objective function for points where it is differentiable.²⁵ In the general case (e.g., when the optimization problem is not differentiable at some given point \mathbf{M}^n), our algorithm can be seen as a subgradient method iteration over a convex upper bound²⁶ of Eq. (3.1) at \mathbf{M}^n . Our method then allows to optimize over Eq. (3.1) although it does not necessarily leads to its global optimum since Eq. (3.1) is not a convex problem.

Generalization of trace(-norm) regularization Fantope regularization is a generalization of trace regularization. Indeed, for every matrix $\mathbf{M} \in \mathbb{S}^d$, $\operatorname{tr}(\mathbf{M}) = \operatorname{tr}(\mathbf{I}_d \mathbf{M})$. Since $\mathbb{F}_d^d = \{\mathbf{I}_d\}$, trace regularization is equivalent to a Fantope regularization where $\operatorname{tr}(\mathbf{W}\mathbf{M})$ is the sum of the d smallest eigenvalues of \mathbf{M} (i.e., $\mathbf{W} = \mathbf{V}_\mathbf{M} \operatorname{Diag}(\mathbf{1}) \mathbf{V}_\mathbf{M}^\top = \mathbf{I}_d$).

²⁵ $\nabla_{\mathbf{M}^n}$ (see Eq. (3.8)) is the gradient of Eq. (3.1) if both R and $\ell(\cdot, \mathcal{N})$ are differentiable at \mathbf{M}^n , i.e., :

- R is differentiable at \mathbf{M}^n if $\lambda(\mathbf{M}^n)_{d-k} \neq \lambda(\mathbf{M}^n)_{d-k+1}$.
- $\ell(\cdot, \mathcal{N})$ is differentiable at \mathbf{M}^n if $\forall q \in \mathcal{N}, D_{\mathbf{M}^n}^2(\mathcal{I}_k, \mathcal{I}_l) \neq \delta_q + D_{\mathbf{M}^n}^2(\mathcal{I}_i, \mathcal{I}_j)$.

²⁶ Indeed, for all fixed matrix $\mathbf{F} \in \mathbb{F}_k^d$, we have the following property: $\forall \mathbf{M} \in \mathbb{S}_+^d, \langle \mathbf{M}, \mathbf{F} \rangle \geq \min_{\mathbf{A} \in \mathbb{F}_k^d} \langle \mathbf{M}, \mathbf{A} \rangle = R(\mathbf{M}) \geq 0$.

Regularization	Acc.	rank(\mathbf{M})	$\ \mathbf{M} - \mathbf{T}\ _F^2$
No Regularization	89.3%	31	1.07
Subgradient Descent over \mathbf{L}	92.7%	10	0.44
Trace	95.1%	4	0.38
Fantope	97.5%	10	0.04
Fantope and Trace	98.0%	10	0.03

Table 3.1: Toy experiment results. Fantope regularization allows to approximate the target matrix \mathbf{T} better than other methods.

3.4 Experimental Validation

3.4.1 Synthetic example

We propose to start exploring the behavior of our Fantope regularization method using a synthetic dataset with a target metric $D_{\mathbf{T}}$ parameterized by a known low-rank distance matrix $\mathbf{T} \in \mathbb{S}_+^d$. For this purpose, we create a random symmetric positive definite matrix $\mathbf{A} \in \mathbb{S}_+^e$ with $\text{rank}(\mathbf{A}) = e$ and $e < d$, and define the target PSD distance matrix $\mathbf{T} \in \mathbb{S}_+^d$: $\mathbf{T} = \begin{pmatrix} \mathbf{A} & \mathbf{0} \\ \mathbf{0} & \mathbf{0} \end{pmatrix}$ with $\text{rank}(\mathbf{T}) = \text{rank}(\mathbf{A}) = e$. We generate a set \mathcal{X} of feature vectors $\mathbf{x}_i \in \mathbb{R}^d$ from a uniform distribution in $[0, 1[$ for each component. The distance between two feature vectors \mathbf{x}_i and \mathbf{x}_j is given by: $D_{\mathbf{T}}^2(\mathbf{x}_i, \mathbf{x}_j) = (\mathbf{x}_i - \mathbf{x}_j)^T \mathbf{T} (\mathbf{x}_i - \mathbf{x}_j)$. In order to build a training set \mathcal{N} , we randomly sample pairs of distances using quadruplets in \mathcal{X}^4 and get the ground-truth using $D_{\mathbf{T}}^2$, so that: $\forall(\mathbf{x}_i, \mathbf{x}_j, \mathbf{x}_k, \mathbf{x}_l) \in \mathcal{N}, D_{\mathbf{T}}^2(\mathbf{x}_k, \mathbf{x}_l) > D_{\mathbf{T}}^2(\mathbf{x}_i, \mathbf{x}_j)$. The set \mathcal{N} is used to learn our matrix \mathbf{M} by solving Eq. (3.1) where $\delta_q = 1$ and $\mathbf{W} \in \mathbb{S}_+^d$ such that $\text{rank}(\mathbf{W}) = (d - e)$ as defined in Eq. (3.4).

A test set \mathcal{T} and a validation set \mathcal{V} are generated in the same way as \mathcal{N} . To illustrate the relevance of the proposed method, we focus on having a small e and large d : we set $e = 10$, $d = 50$, $|\mathcal{N}| = 10^4$, $|\mathcal{V}| = |\mathcal{T}| = 10^6$ and $|\mathcal{X}| = 8000$. In this setting, 80% of the features are noisy.

Evaluation Metrics We compute the number of satisfied constraints on the test set \mathcal{T} , the accuracy being measured as the percentage of satisfied constraints on \mathcal{T} . We also compare the similarity between the learned PSD matrix $\mathbf{M} \in \mathbb{S}_+^d$ and the target matrix $\mathbf{T} \in \mathbb{S}_+^d$. The similarity between \mathbf{M} and \mathbf{T} is measured as the distance $\|\mathbf{M} - \mathbf{T}\|_F^2 = \sum_{i,j} (M_{i,j} - T_{i,j})^2$. \mathbf{M} and \mathbf{T} are rescaled so that their largest element is 1.

Results To evaluate the impact of Fantope regularization, we compare the following metric learning schemes:

- No Regularization*: setting $\mu = 0$ in Eq. (3.1), and applying a subgradient descent over $\mathbf{M} \in \mathbb{S}_+^d$ ²⁷.
- Subgradient Descent over \mathbf{L}* : setting $\mu = 0$, Eq. (3.1) is solved using a subgradient descent over $\mathbf{L} \in \mathbb{R}^{e \times d}$ where $\mathbf{M} = \mathbf{L}^T \mathbf{L}$ ²⁸. This approach is different from our proposed method since it cannot return a solution whose rank is greater than $d - k$, whereas our method can.
- Trace(-norm) Regularization*: setting $\mu > 0$ and $\mathbf{W} = \mathbf{I}_d$.
- Fantope Regularization*: setting $\mu > 0$.
- Fantope and Trace Regularization*: replacing the regularization term $\mu \text{tr}(\mathbf{W}\mathbf{M})$ by $R(\mathbf{M}) = \gamma \text{tr}(\mathbf{M}) + \mu \text{tr}(\mathbf{W}\mathbf{M})$.

For each method, the hyper-parameters $\gamma > 0$ and $\mu > 0$ are determined based on the validation set \mathcal{V} .

²⁷This scheme usually leads to high-rank solutions prone to overfitting.

²⁸This method is often used in the Computer Vision literature [Mensink et al., 2013, Mignon and Jurie, 2012]. Although the problem is not convex w.r.t. \mathbf{L} , this method controls the rank of \mathbf{M} and avoids overfitting since $\text{rank}(\mathbf{M}) = \text{rank}(\mathbf{L}) \leq e$ with $e < d$.

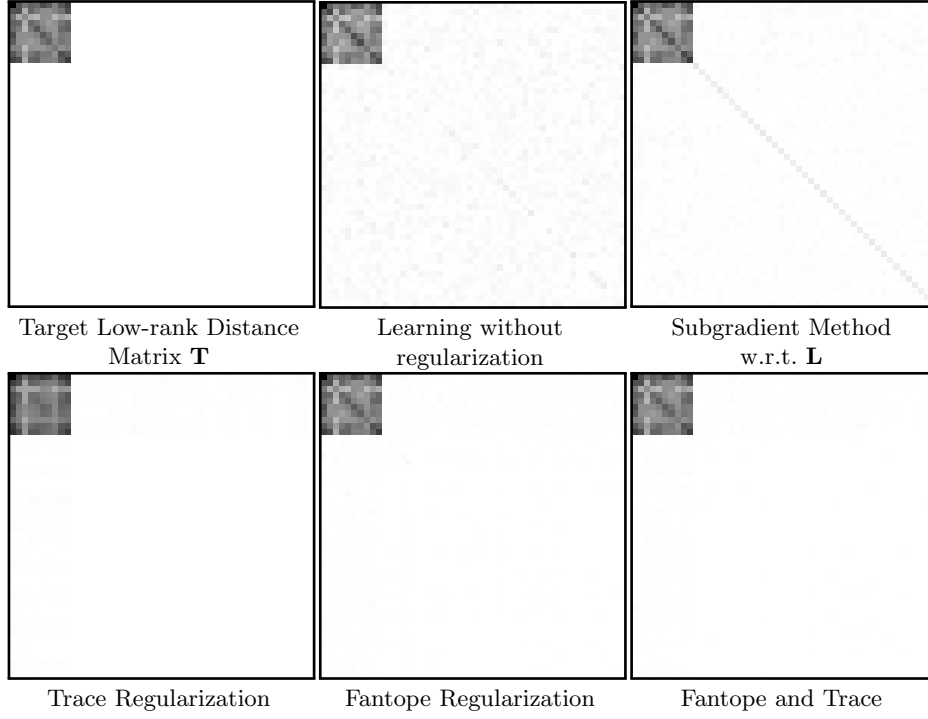


Figure 3.1: Target distance matrix \mathbf{T} and the learned PSD distance matrices \mathbf{M} . Higher absolute values are darker.

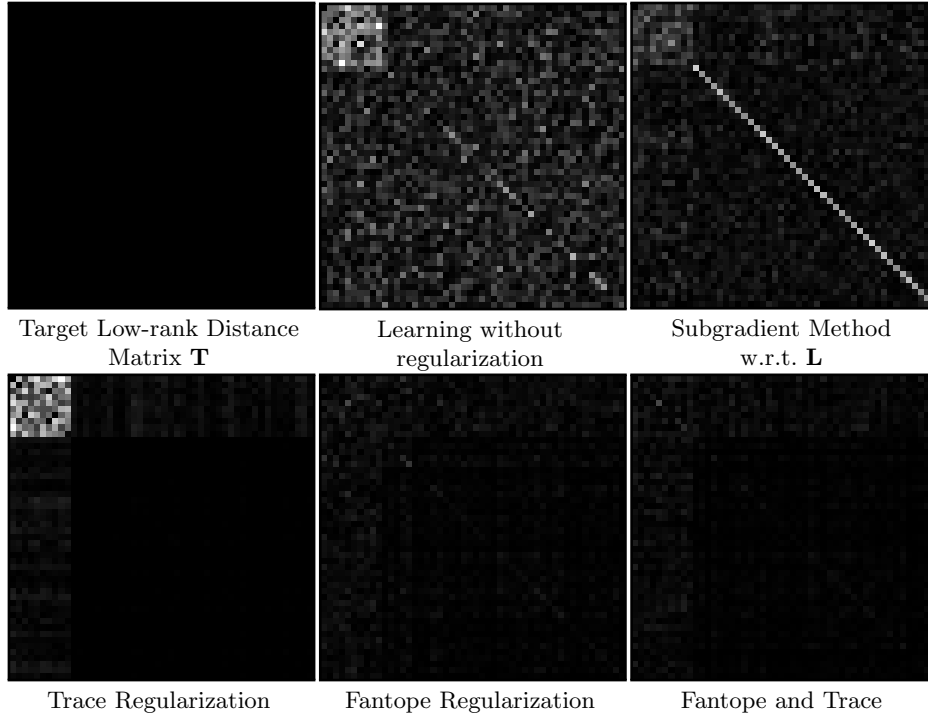


Figure 3.2: Difference between the matrices and the target PSD distance matrix \mathbf{T} . Smaller differences are darker.

Table 3.1 reports the accuracies and distances between \mathbf{T} and the learned matrices \mathbf{M} . Methods without explicit regularization obtain the worst results (89.3% and 92.7% accuracy). Trace regularization ignores most of the noisy features but learns a matrix whose rank is a lot smaller than the target rank $e = 10$. That leads to an accuracy of 95.1% and illustrates the fact that trace regularization cannot fine-control the rank of the solution matrix, although it promotes low-rank solutions. Finally, Fantope regularization outperforms the other methods by reaching 97.5% accuracy (and 98% when combined with trace regularization). In addition, the rank of the learned matrix corresponds exactly to the target rank.

Fig. 3.1 illustrates the target PSD distance matrix \mathbf{T} and the PSD distance matrices \mathbf{M} learned with the different methods reported in the toy experiment. Higher absolute values are darker.

Fig. 3.2 illustrates (the absolute value of each element of) the difference between the distance matrices and the target PSD matrix \mathbf{T} . A zero difference is represented by a black square whereas larger differences are brighter. All the 6 images of the figure are rescaled with the same scale factor.

The distance matrix learned with trace regularization ignores noisy features but does not approximate the submatrix \mathbf{A} of the target matrix \mathbf{T} correctly because trace regularization penalizes large eigenvalues too much. On the other hand, methods without regularization do not ignore noisy features. Fantope regularization allows to learn a matrix very similar to the target distance matrix \mathbf{T} . Our proposed method is then ideal for this type of experiment.

3.4.2 Real-world experiments

We evaluate the proposed metric learning regularization method in two different Computer Vision applications. The first experiment is a face verification task, for which the similarity constraints come from relations between pairs of face images that are either similar or dissimilar. In the second experiment, we evaluate recognition performance on image classification with relative attributes [Parikh and Grauman, 2011]. In this context, we work with features defined in attribute space.

3.4.2.1 Face verification: LFW

In the face verification task, we are provided with pairs of face images. The goal is to learn a classifier that determines whether image pairs are similar (represent the same person) or dissimilar (represent two different persons). Some examples of similar and dissimilar pairs are provided in Fig. 3.3 and Fig. 3.4, respectively.

Dataset and evaluation metric We use the publicly available *Labeled Faces in the Wild* (LFW) dataset [Huang et al., 2007]. It contains more than 13,000 images of faces collected from the Web and can be considered as the current state-of-the-art face recognition benchmark. We focus in this chapter on the “restricted” paradigm where we are only provided with two sets of pairs of images: set \mathcal{S} of similar pairs (same person) and set \mathcal{D} of dissimilar images (different person). We follow the standard evaluation protocol that uses *View 2* data for training and testing (10 predefined folds of 600 image pairs each), and *View 1* for validation.

To generate our constraints, we use \mathcal{S} and \mathcal{D} and we set the upper bound $u = 0.5$ and the lower bound $l = 1.5$ following the scheme explained in Section 3.2.2. The distance of a test pair is compared to the threshold $\frac{l+u}{2} = 1$ to determine whether the pair is similar or dissimilar.

Image representation We use the same input features and setup as popular metric learning methods [Davis et al., 2007, Guillaumin et al., 2009, Mignon and Jurie, 2012] that were already tested on this dataset. We strictly follow the setup described in [Mignon and Jurie, 2012]. We use the SIFT descriptors [Lowe, 2004] computed by [Guillaumin et al., 2009] available on their website. Each face image is represented by 27 SIFT descriptors. Those 27 descriptors are concatenated in a single histogram, and a element-wise square-root is performed on this histogram to return face image representations \mathbf{x}_i .

Initialization of the distance matrix $\mathbf{M} \in \mathbb{S}_+^d$ Let e be the target rank of the learned matrix $\mathbf{M} \in \mathbb{S}_+^d$. To initialize the PSD matrix \mathbf{M} , we first compute the matrix $\mathbf{L} \in \mathbb{R}^{e \times d}$ that is composed of the coefficients

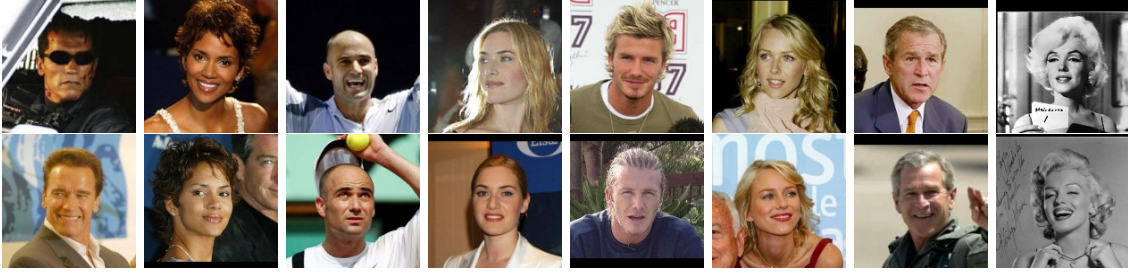


Figure 3.3: Examples of similar pairs in the Labeled Faces in the Wild (LFW) dataset.



Figure 3.4: Examples of dissimilar pairs in the Labeled Faces in the Wild (LFW) dataset.

Regularization Method	Accuracy (in %)
Trace-norm Regularization	77.6 ± 0.7
Fantope Regularization	82.3 ± 0.5

Table 3.2: Accuracies (mean and standard error) obtained on LFW in the “restricted” setup with our learning framework in different regularization settings.

for the e most dominant principal components of the training data. \mathbf{M} is then initialized by computing $\mathbf{M} = \mathbf{L}^\top \mathbf{L}$.

We now provide a quantitative evaluation of our method in the described setup. The target rank e of our regularization term is fixed to $e = 40$, as in [Mignon and Jurie, 2012].

Impact of regularization We compare here the impact of Fantope regularization over trace regularization. Table 3.2 shows classification accuracies when solving Eq. (3.1) with both regularization methods. Fantope regularization outperforms trace regularization by a large margin (82.3% *vs.* 77.6%). This illustrates the importance of having an explicit control over the rank of the distance matrix. In the following, we combine trace and Fantope regularization by replacing the regularization term $R(\mathbf{M}) = \mu \text{tr}(\mathbf{W}\mathbf{M})$ by $R(\mathbf{M}) = \gamma \text{tr}(\mathbf{M}) + \mu \text{tr}(\mathbf{W}\mathbf{M})$, with $\gamma \ll \mu$.

State-of-the-art results We now compare Fantope Regularization to other popular metric learning algorithms. Table 3.3 shows performances of ITML [Davis et al., 2007], LDML [Guillaumin et al., 2009] and PCCA [Mignon and Jurie, 2012] reported in [Guillaumin et al., 2009] and [Mignon and Jurie, 2012] in the linear metric learning setup. These methods are the most popular metric learning methods when the task is to decide whether a pair is similar or dissimilar. Fantope regularization, which reaches $82.3 \pm 0.5\%$ accuracy, outperforms ITML and LDML and is comparable to PCCA on LFW in this setup. We explain in the following how our method can reach $83.5 \pm 0.5\%$.

Impact of early stopping It is worth mentioning that the accuracy of 82.2% obtained with PCCA [Mignon and Jurie, 2012] is achieved by performing *early stopping*. Table 3.4 reports the accuracies we obtained on LFW by testing the code of PCCA [Mignon and Jurie, 2012] kindly provided by its authors,

Method	Accuracy (in %)
ITML [Guillaumin et al., 2009]	76.2 ± 0.5
LDML [Guillaumin et al., 2009]	77.5 ± 0.5
PCCA [Mignon and Jurie, 2012]	82.2 ± 0.4
Proposed Method	83.5 ± 0.5

Table 3.3: Results (mean and standard error) on LFW in the “restricted” setup of state-of-the-art linear metric learning algorithms and of our method with *early stopping*.

Number of iterations	10	30	100	1000	10^4
Accuracy (in %)	79.2 ± 0.5	82.2 ± 0.5	79.3 ± 0.5	75.8 ± 0.5	63.2 ± 0.5

Table 3.4: Accuracy of Mignon’s code [Mignon and Jurie, 2012] on LFW as a function of the number of iterations of gradient descent. The performance of PCCA [Mignon and Jurie, 2012] greatly depends upon the *early stopping* criterion.

as a function of the number of iterations of gradient descent. 82.2% is the accuracy obtained with 30 iterations. We can notice that the PCCA performance decreases for larger numbers of iterations (e.g., 75.8% and 63.2% with 1000 and 10000 iterations, respectively). As in [Mignon and Jurie, 2012], we integrated this *early stopping* criterion in our method and determined the maximum number of iterations of subgradient descent from the validation set *View 1*. We reach an accuracy of $83.5 \pm 0.5\%$. To the best of our knowledge, this is the best result obtained for linear metric learning methods in the same setup (same input features). As a conclusion, our regularization scheme makes our method much more robust than PCCA [Mignon and Jurie, 2012] to *early stopping*.

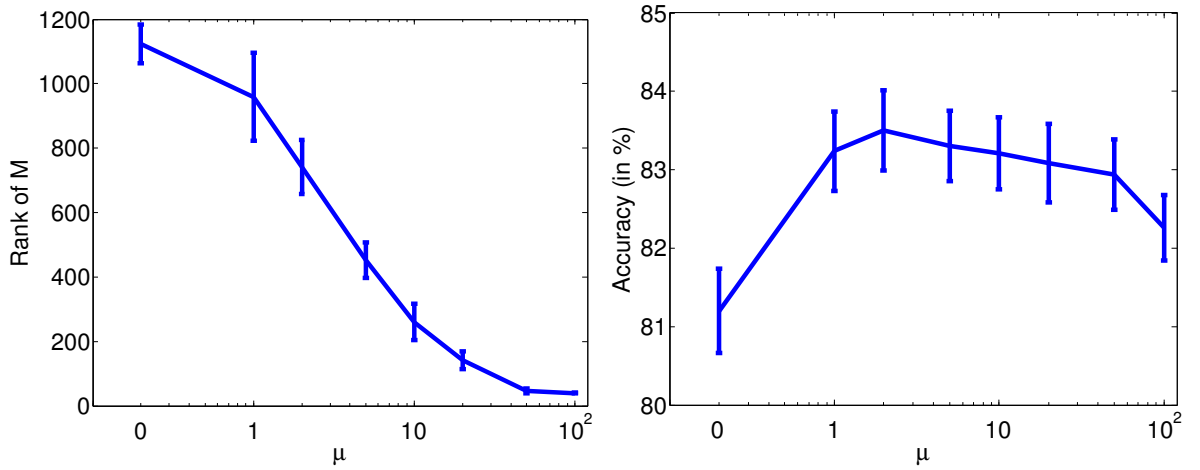


Figure 3.5: (left) Rank and (right) accuracy of the learned metric on LFW in the “restricted” setup as a function of the hyper-parameter μ with *early stopping*. The expected rank is $e = 40$. The proposed regularization controls rank(\mathbf{M}) while improving accuracy when compared to the absence of regularization ($\mu = 0$).

Impact of the hyper-parameter μ Fig. 3.5 illustrates the impact of the Fantope regularization on the rank of the solution matrix $\mathbf{M} \in \mathbb{S}_+^d$ and on the accuracy on LFW as we modify the value of the regularization parameter μ when we perform *early stopping*. We observe that μ has a real impact on the rank of the solution matrix: the rank of \mathbf{M} decreases as μ increases and reaches the expected rank $e = 40$ for high values of μ . On the other hand, the accuracy of the method first increases and eventually

Classification model	OSR	PubFig
RA [Parikh and Grauman, 2011]	69.7 ± 1.5	70.6 ± 1.8
RA + LMNN	71.7 ± 1.7	74.3 ± 1.9
RA + LMNN + Trace	72.4 ± 2.0	75.0 ± 1.6
RA + LMNN + Fantope (ours)	73.7 ± 1.8	77.5 ± 1.6
Qwise + LMNN + Fantope (ours)	75.0 ± 2.0	77.6 ± 1.1

Table 3.5: Test accuracies (mean and standard deviation in %) obtained on the OSR and Pubfig datasets. Fantope regularization improves recognition in the classification task.

decreases as μ increases. Nonetheless, the recognition performed with high values of μ (82.3%) is still better than without regularization (81.2% with $\mu = 0$).

3.4.2.2 Metric learning in attribute space

In this subsection, we focus on the image classification task where the goal is to assign an image to a predefined class. Particularly, we focus on the case where classes are described with relative attributes (for more details on relative attributes, see Section 2.4). Each image \mathcal{I}_i is described by a vector $\mathbf{x}_i \in \mathbb{R}^d$ where d is the number of attributes. The j -th element of \mathbf{x}_i represents the score (degree) of presence of the j -th attribute in \mathbf{x}_i .

Experiment setup To evaluate and compare our Fantope regularization approach, we follow the same classification framework as [Parikh and Grauman, 2011] for scene and face recognition on the OSR [Oliva and Torralba, 2001] and PubFig [Kumar et al., 2009] datasets. The framework and the datasets are described in Section 2.4.

Baselines We use two baselines already described in the previous chapter:

- RA: The relative attribute learning problem [Parikh and Grauman, 2011] that uses relative attribute annotations on classes to compute high-level representations of images $\mathbf{x}_i \in \mathbb{R}^d$, a Gaussian distribution is learned for each class.
- RA + LMNN: High-level representations $\mathbf{x}_i \in \mathbb{R}^d$ are used as input features of the LMNN classifier [Weinberger and Saul, 2009].

We use the publicly available codes of [Parikh and Grauman, 2011] and [Weinberger and Saul, 2009].

Integration of regularization We modify the code of LMNN to integrate trace and Fantope regularization, the stopping criterion is the convergence of the algorithm (i.e., the objective function stops decreasing).

Learning setup We use the same experimental setup as [Parikh and Grauman, 2011]. $N = 30$ training images are used per class to learn the representations \mathbf{x}_i and classifiers, the rest is for testing. The performance is measured as the average classification accuracy across all classes over 30 random train/test splits.

Results Table 3.5 reports accuracies of baselines and our proposed regularization method on both OSR and PubFig datasets. Fantope regularization applied to LMNN significantly improves recognition over baselines, particularly on PubFig. It outperforms the classic LMNN algorithm (without regularization) with a margin of 2 and 3% on OSR and PubFig, respectively. Trace-norm regularization also outperforms the absence of regularization. These results validate the importance of a proper regularization.

The Qwise strategy presented in Chapter 2 combined with Fantope regularization improves recognition only on the OSR dataset. RA + LMNN + Fantope and Qwise + LMNN already perform similarly on PubFig (see Table 2.2). We recall that PubFig has a very small number of pairwise equivalence constraints, it then seems that Fantope regularization implicitly counterbalances noisy ordered pairwise annotation

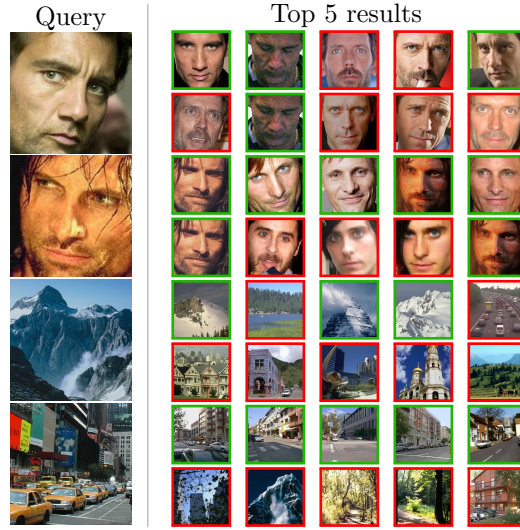


Figure 3.6: Some results of similarity search on the PubFig and OSR datasets. We show for each query the 5 nearest neighbors returned by our method (first row) and by LMNN (second row). Results in green correspond to images in the same class as the query whereas results in red are images from different classes.

problems on this dataset by reducing the complexity of the model, and thus better exploiting correlations between data.

Fantope regularization finds a low e -dimensional subspace where distances can be computed with $e < d$ (e.g., $e = 8$ with $d = 11$ on PubFig) and allows to exploit correlations between features better than methods that learn a high-rank distance matrix. In this case, each feature corresponds to the score of presence of an attribute in images. Notably, by considering the learned matrix $\mathbf{M} \in \mathbb{S}_+^d$ as a covariance matrix, the most correlated attributes w.r.t. the Pearson product-moment correlation coefficient are “smiling”, “chubby” and “male-looking” on the PubFig dataset. This result is expected since the women of the PubFig dataset (Scarlett Johansson and Miley Cyrus) are annotated in [Parikh and Grauman, 2011] as more chubby and smiling more than most men of the dataset. On the OSR dataset, the attributes “close depth”, “open” and “perspective”, which are all related to the notion of depth, are also strongly correlated.

Fig. 3.6 illustrates on some examples how our scheme is effective to learn semantics. Particularly on PubFig, the learned metric gives priority to semantical similarity rather than visual similarity: the images retrieved by the classic LMNN are more visually similar than the images returned by our Fantope regularization. However, they are more often in different categories than the category of the query.

3.5 Discussion

We discuss how the proposed metric learning framework can exploit the concavity property of the regularization term to adapt other efficient optimization techniques.

Difference of convex functions First, we remark that Eq. (3.1) can be rewritten as a difference of two convex functions v and w :

$$\min_{\mathbf{M} \in \mathbb{S}_+^d} v(\mathbf{M}) - w(\mathbf{M}) \Leftrightarrow \min_{\mathbf{M} \in \mathbb{S}_+^d} \ell(\mathbf{M}, \mathcal{N}) + \mu R(\mathbf{M}) \quad (3.13)$$

where $v(\mathbf{M}) = \ell(\mathbf{M}, \mathcal{N})$ and $w(\mathbf{M}) = -\mu R(\mathbf{M})$. In the same way as many machine learning methods that exploit a nonconvex regularization term [Candès et al., 2008, Rakotomamonjy et al., 2011, Hu et al., 2013], a majorization-minorization [Hunter and Lange, 2004] method can be used.

Definition 3.5.1. (*Majorization-minimization*) A majorization-minimization algorithm for minimizing a function $\varphi : \mathbb{S}_+^d \rightarrow \mathbb{R}$ classically consists of the iteration:

$$\mathbf{M}^{n+1} := \underset{\mathbf{M} \in \mathbb{S}_+^d}{\operatorname{argmin}} \hat{\varphi}(\mathbf{M}, \mathbf{M}^n) \quad (3.14)$$

where $\hat{\varphi}(\mathbf{M}, \mathbf{M}^n)$ is a convex upper bound to φ that is tight at \mathbf{M}^n , i.e., $\forall \mathbf{M} \in \mathbb{S}_+^d, \hat{\varphi}(\mathbf{M}, \mathbf{M}^n) \geq \varphi(\mathbf{M})$ and $\hat{\varphi}(\mathbf{M}, \mathbf{M}) = \varphi(\mathbf{M})$.

In our case, we can formulate $\varphi(\mathbf{M}) = \mu R(\mathbf{M}) + \ell(\mathbf{M}, \mathcal{N})$ and $\hat{\varphi}(\mathbf{M}, \mathbf{M}^n) = \mu \langle \mathbf{M}, \mathbf{W}^n \rangle + \ell(\mathbf{M}, \mathcal{N})$ where $\mathbf{W}^n \in \operatorname{argmin}_{\mathbf{W} \in \mathbb{F}_k^d} \langle \mathbf{M}^n, \mathbf{W} \rangle$.²⁹ In other words, the matrix \mathbf{W}^n is fixed in the regularization term³⁰ of $\hat{\varphi}(\cdot, \mathbf{M}^n)$. For convenience, we write the convex function $\hat{\varphi}(\mathbf{M}, \mathbf{M}^n) = \hat{\varphi}_n(\mathbf{M})$.

Algorithm 3 presents a majorization-minimization adaptation of our problem.

Algorithm 3 Basic majorization-minimization scheme

input : $\mathbf{M}^1 \in \mathbb{S}_+^d$ (initial estimate); N (number of iterations)

output : $\mathbf{M}^{N+1} \in \mathbb{S}_+^d$ (final estimate)

for $n = 1$ to N **do**

 Compute a tight surrogate $\hat{\varphi}_n$ of φ at \mathbf{M}^n

$\mathbf{M}^{n+1} \in \operatorname{argmin}_{\mathbf{M} \in \mathbb{S}_+^d} \hat{\varphi}_n(\mathbf{M})$

end for

Projection onto the PSD cone A classic way (see the survey in [Kulis, 2012]) to solve distance metric learning problems is to use the projected gradient method. However, this method is computationally inefficient for large values of d since the projection onto \mathbb{S}_+^d performed at each iteration is cubic in d .

To deal with this problem, many distance metric learning algorithms can be written as the following constrained convex optimization problems (e.g., Eq. (3.13)):

$$\min_{\mathbf{X} \in \mathbb{S}^d, \mathbf{Z} \in \mathbb{S}_+^d} f(\mathbf{X}) + \tilde{I}_{\mathbb{S}_+^d}(\mathbf{Z}) \text{ s.t. } \mathbf{X} = \mathbf{Z} \quad (3.15)$$

where f is a convex function and the convex function $\tilde{I}_{\mathbb{S}_+^d}$ is called the indicator function of the set \mathbb{S}_+^d :

$$\tilde{I}_{\mathbb{S}_+^d}(\mathbf{Z}) = \begin{cases} 0 & \text{if } \mathbf{Z} \in \mathbb{S}_+^d \\ +\infty & \text{if } \mathbf{Z} \notin \mathbb{S}_+^d \end{cases}$$

Efficient algorithms, such as the *Alternating Direction Method of Multipliers* (ADMM) ([Boyd et al., 2011] Section 5), can be used to optimize the kind of problem described in Eq. (3.15). ADMM alternates between the optimization over \mathbf{X} and \mathbf{Z} , it relaxes the constraint $\mathbf{X} \in \mathbb{S}_+^d$ by $\mathbf{X} \in \mathbb{S}^d$ and then does not require to perform costly projection at each gradient descent.

²⁹Although the solution of $\mathbf{W}^n \in \operatorname{argmin}_{\mathbf{W} \in \mathbb{F}_k^d} \langle \mathbf{M}^n, \mathbf{W} \rangle$ is not unique in general (i.e., if $\lambda(\mathbf{M})_{d-k} \neq \lambda(\mathbf{M})_{d-k+1}$), we assume that the choice of \mathbf{W}^n is unique for a given \mathbf{M}^n . This allows a unique choice of the convex function $\hat{\varphi}(\cdot, \mathbf{M}^n)$ for a given \mathbf{M}^n .

³⁰We recall that for all fixed matrix $\mathbf{F} \in \mathbb{F}_k^d$, the function $\langle \cdot, \mathbf{F} \rangle$ is a convex upperbound of R since we have the following property: $\forall \mathbf{M} \in \mathbb{S}_+^d, \langle \mathbf{M}, \mathbf{F} \rangle \geq \min_{\mathbf{A} \in \mathbb{F}_k^d} \langle \mathbf{M}, \mathbf{A} \rangle = R(\mathbf{M}) \geq 0$.

Dealing with large number of constraints If some pairs of images are involved in many training constraints, structural metric learning [McFee and Lanckriet, 2010] approaches can be adapted to learn to rank pairs that are involved in lots of constraints. This reduces the number of training constraints since the newly created constraints involve rankings between (a large number of) pairs instead of only four images at a time.

3.6 Conclusion

We have proposed a new regularization scheme for metric learning that explicitly controls the rank of the learned distance matrix. The proposed regularization term, which minimizes the sum of the smallest eigenvalues of the learned matrix, reaches its minimum value when the rank of the matrix is smaller than or equal to a target threshold. Unlike traditional nuclear norm heuristics, which take into account all the singular values, our approach achieves a better approximation of the rank function. Our method actually generalizes nuclear norm regularization for PSD matrices. Although the new objective function is no longer convex, it is formulated as a difference of convex functions. It can be solved either by classic gradient descent method as proposed in this chapter, or with a majorization-minimization approach. Indeed, the definition of our regularization term allows the formulation of a linear upper bound which is simple to optimize. We demonstrate that the proposed regularization greatly improves recognition on both synthetic and real-world datasets, showing the relevance of this new regularization to limit overfitting. Future work includes a generalization of this regularization approach to better approximate the rank function.

Chapter 4

Discovering Important Semantic Regions in Webpages

Chapter Abstract This chapter illustrates how our quadruplet-wise distance metric learning framework can be applied in the context of webpage understanding. In particular, we train a distance metric by exploiting temporal relationships between successive versions of a same webpage to detect important semantical change regions and ignore unimportant ones. Our learned metric also allows to determine whether semantical changes occurred between two versions of the same webpage or not.

Three main contributions can be claimed in this chapter in the context of webpage analysis: 1) We propose an unsupervised and a semi-supervised metric learning schemes that exploit fully automatically generated quadruplet-wise constraints. 2) The formalization of our metric allows to visually segment webpages and detect spatial regions wherein important changes occur. 3) We show the good performance on different websites of our change detection algorithm learned without human supervision. We also demonstrate that the performance of our approach can be improved with very little human effort and structural information. We show that our method is robust to noise (e.g., advertisement and menus) and works on different types of pages.

We first present challenges related to webpage change detection (Section 4.1), and introduce our framework (Section 4.2). We present how to compute similarities between webpage screenshots (Section 4.3) and provide experimental results on real websites (Section 4.4).

Some of the material in this chapter has been published at the following conferences:

- Law, M.T., Thome, N., Gançarski, S., and Cord, M. (2012). Structural and visual comparisons for web page archiving. *ACM Symposium on Document Engineering (DocEng)*. [Law et al., 2012b]
- Law, M.T., Thome, N., Cord, M. (2013) Quadruplet-wise Image Similarity Learning. *IEEE International Conference on Computer Vision (ICCV)*. [Law et al., 2013]

4.1 Introduction

This chapter focuses on an unusual Computer Vision task, which is webpage change detection in the contexts of Web crawling and archiving. In this context, change detection aims at determining whether a change that occurred between two successive versions of a page is important enough to increase the frequency of crawling of the page or not. Particularly, a change detection algorithm has to understand the semantic structure of the document by ignoring unimportant changes (e.g., advertisement changes) and detecting important semantical changes (e.g., the change of the main news in a news page).

Fig. 4.1 and Fig. 4.2 illustrate two pairs of successive versions of webpages. In Fig. 4.1, the change of advertisement (yellow region) is the only observable change. Since it does not change the content shared by the webpage, the two versions are considered as similar. A human (or indexing robot) does not need



Figure 4.1: A pair of successive versions of the New York Times homepage wherein only the advertisement (yellow region) is different. The change of advertisement does not affect the information shared by the page, the two versions are thus considered as similar.

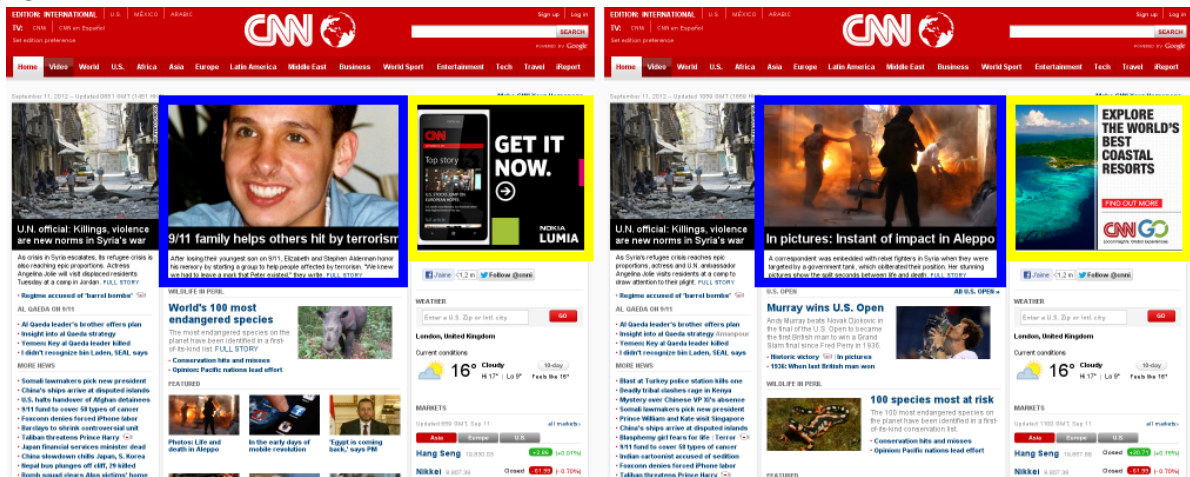


Figure 4.2: A pair of successive versions of the CNN homepage. The change of news title (blue region), which is the main information shared by the page, makes the two versions dissimilar and is thus considered as an important change.

to visit these two versions since the shared content is the same. On the contrary, in Fig. 4.2, although an advertisement (yellow region) has also changed, the main news shared by the webpage (blue region) is different. The versions then both need to be visited and indexed, and are considered as dissimilar. In this thesis, we denote a webpage version as a full rendered page with included resources (images...).

Change detection to monitor Internet information and activity With the explosion of information on the World Wide Web, keeping track of the constant changes in media is a challenging task. Several applications and domains that want to keep track of those changes focus on temporal aspects of (usually textual) information on the Web. Some examples of such applications are large-scale information monitoring and delivery systems [Douglass et al., 1998, Liu et al., 2000, Lim and Ng, 2001, Fleca and Masciari, 2003, Jacob et al., 2004], active databases [Jacob et al., 2004], servicing of continuous queries [Abiteboul, 2002], Web cache optimization [Cho and Garcia-Molina, 2000], and Web archiving [Ben Saad and Gangarski, 2011, Pehlivan et al., 2010]. All these applications use change detection methods at semi-structured data level.

In some of these tasks [Cho and Garcia-Molina, 2000, Ben Saad and Gançarski, 2011], change detection is exploited to determine crawling strategies which are optimized for the corresponding application. Many papers [Cho and Garcia-Molina, 2000, Ntoulas et al., 2004, Jatowt et al., 2007, Adar et al., 2009b, Ben Saad and Gançarski, 2011] then focus on observing the change pattern behaviors of websites. The reported results are quite variable because the similarity metrics used to observe changes (e.g., Dice’s coefficient of words in [Adar et al., 2009b]) are different. In order to determine a good crawling strategy, the choice of an appropriate webpage change detection metric is thus a challenging task. In this chapter, we are interested in learning an appropriate metric by exploiting visual information.

Proposed method We propose to exploit our quadruplet framework to learn a metric that detects regions wherein important changes occur. Our approach considers webpage screenshots as images and computes distances between their visual representations. Our learned metric is subsequently used to detect semantic changes between page versions (e.g., the one illustrated in Fig. 4.2). To guide the learning process, our method can integrate annotations provided by humans. Each of these annotations indicates whether two page versions are similar or dissimilar. This type of proposed annotations requires significantly less human interaction than classic methods [Song et al., 2004, Ben Saad and Gançarski, 2011] which require the importance score of each region for each page version.

Several papers that extract meaningful information in webpages admit the importance of visual information [Song et al., 2004, Luo et al., 2009, Spengler and Gallinari, 2010] since the layout is taken into account when pages are created. In order to exploit visual information, these approaches actually integrate visual descriptors from the structure (e.g., position, width, border of regions or font colors) rather than computer vision based features. Moreover, according to [Kohlschütter et al., 2010], four different levels of features can be extracted: individual text blocks, the complete HTML document, the rendered document image, and the complete website. A major argument usually mentioned against using the rendered document image is that template statistics need to be learned separately for each website since each website uses a different layout. We propose in this chapter to learn a semantic distance metric that does not require human interaction, but exploits temporal relationships. In this way, learning template statistics is cheap.

Context of the thesis chapter The idea of learning a visual distance metric to compare semantic changes between page versions came from a collaboration of our department at LIP6 with digital preservation organizations (such as the British Library³¹, the national library of the United Kingdom, or Internet Memory Foundation³²) in the European FP7 project SCAPE³³ (Scalable Preservation Environments). The goal of SCAPE project was to develop scalable tools for digital preservation.

Change detection for webpage archiving had already been investigated at LIP6 [Pehlivan et al., 2010, Ben Saad and Gançarski, 2011] to compare pages via their DOM trees after rendering. In order to extend previous works that exploited visual content via the structural architecture of pages, we propose to integrate computer vision methods in this webpage analysis task.

4.2 Constraint Formalization

4.2.1 Automatic generation of constraints

Our approach relies on an assumption on the behavior of many websites, which we call *monotony of changes*. This assumption lies on the way pages are usually modified: when a content is added to a page, it is usually added to the recent content that was present in the last version of the page. The significant information that disappears usually does not reappear on the page. For a page version captured at some

³¹<http://www.bl.uk/>

³²<http://internetmemory.org/en/>

³³<http://www.scape-project.eu/>

given time, its similarity of significant content with successive versions then decreases over time. Indeed, the content of the version gradually disappears from the page and new significant content that is added is different. However, advertisements tend to disappear and reappear frequently.

Monotony of changes in a webpage is illustrated in Fig. 4.3 where four successive versions of the same webpage v_{t-1} , v_t , v_{t+1} , v_{t+2} are crawled with a sufficiently high frequency (each hour). Although the four versions are different, one human eye can compare visual dissimilarities between them. For instance, v_t seems more similar to v_{t+1} than to v_{t+2} . Similarly, v_t and v_{t+1} are more similar than v_{t-1} and v_{t+2} are. From this observation, we can generate a set \mathcal{B} of quadruplets of versions $(v_t, v_{t+1}, v_r, v_s) \in \mathcal{B}$ where $r \leq t < s$, and we would like our visual dissimilarity function D to satisfy the maximum number of the following constraints:

$$\forall (v_t, v_{t+1}, v_r, v_s) \in \mathcal{B} : D(v_t, v_{t+1}) \leq D(v_r, v_s) \quad (4.1)$$

In order to satisfy these constraints, the metric D has to ignore random and periodic changes, which are often caused by advertisements. Fig. 4.3 illustrates a case where a car advertisement (at the right of the page) is identical in v_{t-1} , v_t and v_{t+2} and different in v_{t+1} . By ignoring that advertisement region, it is easier for D to satisfy the constraints in Eq. (4.1).

Nonetheless, a trivial solution to satisfy all the constraints in Eq. (4.1) is a pseudometric such that: $\forall (v_i, v_j), D(v_i, v_j) = 0$. To avoid this degenerate solution, one can assume that there exists a change period $\gamma > 1$ such that for all $r \leq t < r + \gamma$ we have the strict inequality $D(v_t, v_{t+1}) < D(v_r, v_{r+\gamma})$. In other words, we assume that there exists a change period γ of the page such that the changes that occurred between the two versions v_r and $v_{r+\gamma}$ are more important than between directly successive versions v_t and v_{t+1} where $r \leq t < r + \gamma$. Although v_t and v_{t+1} may be dissimilar, their dissimilarity is assumed smaller than the dissimilarity between v_r and $v_{r+\gamma}$. Different ways to determine the parameter γ exist. It can be determined with prior knowledge about the page or it can be chosen heuristically following the observation in Adar et al. [Adar et al., 2009a]: human users tend to visit more frequently webpages that often change. In other words, human users can be considered as intelligent web crawlers with a good crawling strategy. For example, a page that is visited everyday by a lot of unique visitors can be assumed to be different everyday (in this case $\gamma = 24$ hours). This popularity information can be obtained from services that provide detailed statistics about the visits to a website (e.g., Google Analytics).

In the same way as \mathcal{B} , we create a set \mathcal{A} (with $\mathcal{A} \cap \mathcal{B} = \emptyset$) and we want the maximum number of the following constraints to be satisfied:

$$\forall (v_t, v_{t+1}, v_r, v_s) \in \mathcal{A} : D(v_t, v_{t+1}) + 1 \leq D(v_r, v_s) \quad (4.2)$$

where 1 is a safety margin, $r \leq t$ and $s \geq r + \gamma \geq t + 1$. Quadruplets of versions that violate Eq. (4.2) penalize content that does not change much in some regions although a change in the whole page is expected. This type of static content usually corresponds to menus and the algorithm learns to ignore these areas. Note that γ determines whether a quadruplet belongs to \mathcal{B} or \mathcal{A} , and thus its corresponding constraint (Eq. (4.1) or (4.2)). Since constraints satisfied in Eq. (4.2) are also satisfied in Eq. (4.1), choosing a value of γ greater than the actual change period of the page is not problematic.

There is a straight connection between these two equations and our quadruplet-wise distance metric learning formulation given in Chapter 2. Any quadruplet q in \mathcal{B} can be formulated as $q \in \mathcal{N}$ with $\delta_q = 0$ and any quadruplet q in \mathcal{A} can be formulated as $q \in \mathcal{N}$ with $\delta_q = 1$.

4.2.2 Similarity information provided by human users

Additionally to the automatically generated constraints based on monotony of changes, richer information of whether a pair of versions is similar or dissimilar can be integrated. It can be provided by human users or automatically determined (e.g., by exploiting RSS feeds).

Let \mathcal{S} be the set of pairs of versions annotated as (or assumed) similar and \mathcal{D} the set of dissimilar version pairs, an interesting property of the function D would be that it satisfies the following constraints:

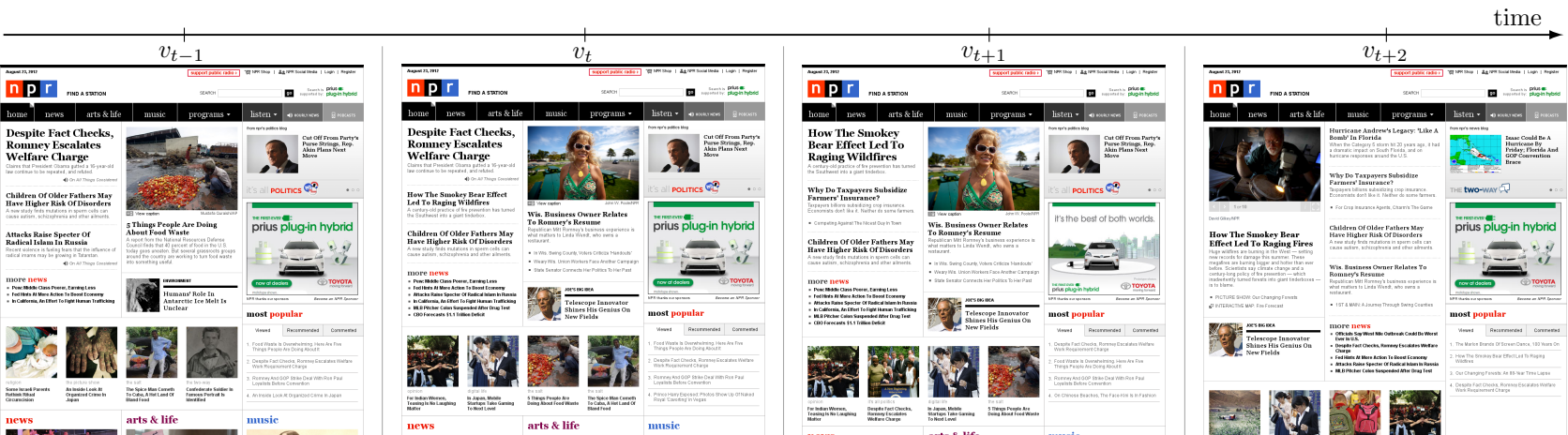


Figure 4.3: Four successive versions of the NPR homepage. Although it is hard and expensive to ask human users to annotate whether version pairs are similar or not, it is cheaper to infer that the dissimilarity between v_t and v_{t+1} , or even v_{t-1} and v_{t+1} is smaller than the dissimilarity between v_{t-1} and v_{t+2} .

$$\forall (v_r, v_s) \in \mathcal{S} : D(v_r, v_s) + 1 \leq b \quad (4.3)$$

$$\forall (v_r, v_s) \in \mathcal{D} : b + 1 \leq D(v_r, v_s) \quad (4.4)$$

where 1 is a safety margin and $b \in \mathbb{R}$ a learned threshold.

These two types of constraints (Eq. (4.3) and Eq. (4.4)) follow the classic approach in metric learning that minimizes the distance of similar pairs while separating dissimilar pairs (in our case, keeping their distances beyond the threshold b). To know whether a test pair (v_r, v_s) is similar or not, one only has to study the sign of $D(v_r, v_s) - b$, which is positive for dissimilar pairs and negative for similar pairs.

4.2.3 Distance metric formulation

We integrate the constraints mentioned from Eq. (4.1) to (4.4) in the distance metric learning framework described in Chapter 2 by generating the training set $\mathcal{N} = \mathcal{A} \cup \mathcal{B}$. We consider the diagonal and full matrix Mahalanobis-like distance metrics that we formulate as follows:

- the distance metric $\mathcal{D}_{\mathbf{w}}$ is parameterized by the d -dimensional vector $\mathbf{w} \in \mathbb{R}_+^d$. This metric tries to satisfy the ideal properties of the target function D (Eq. (4.1) to (4.4)). $\mathcal{D}_{\mathbf{w}}$ is a linear combination of d distances between versions v_i and v_j over d different spatial regions (one distance per region). These d distances are concatenated in the vector $d_{regions}(v_i, v_j) \in \mathbb{R}^d$. The computation of $d_{regions}$ is detailed in Sections 4.3.1 and 4.3.2. We formulate $\mathcal{D}_{\mathbf{w}}$ as:

$$\mathcal{D}_{\mathbf{w}}(v_i, v_j) = \mathbf{w}^\top d_{regions}(v_i, v_j) \quad (4.5)$$

where $\mathbf{w} \in \mathbb{R}_+^d$ is the weight vector: the value of the k -th element of \mathbf{w} corresponds to the importance of change assigned to the k -th region of the page. An element of \mathbf{w} close to 0 means that the corresponding region is ignored, whereas an element with a relatively high absolute value has more impact on the global dissimilarity function $\mathcal{D}_{\mathbf{w}}$. By avoiding \mathbf{w} to have negative elements, the learned metric tends to ignore unimportant changes rather than penalizing them (which would mean negative scores in order to minimize the learned function).

- the metric $D_{\mathbf{M}}$ is parameterized by the symmetric PSD matrix $\mathbf{M} \in \mathbb{S}_+^d$. $D_{\mathbf{M}}$ is written:

$$D_{\mathbf{M}}^2(v_i, v_j) = \mathbf{c}_{ij}^\top \mathbf{M} \mathbf{c}_{ij} \quad (4.6)$$

where $\mathbf{c}_{ij} = (d_{regions}(v_i, v_j))^{\circ \frac{1}{2}}$ and $\circ \frac{1}{2}$ is the Hadamard square root (element-wise square root).

4.3 Visual and Structural Comparisons of Webpages

We present in this section:

- different ways to compute the vector of visual distances between v_i and v_j : $d_{regions}(v_i, v_j)$.
- how to learn a multimodal metric that combines the learned visual metric with structural metrics.

4.3.1 Regular grid segmentation

We propose to regularly segment page regions. Our method computes the GIST [Oliva and Torralba, 2001] descriptors of screen captures, we consider screen captures of page versions as images. In our experiments, we consider only the visible part of webpages without scrolling since it generally contains the most useful information [Song et al., 2004]. Our image sizes are then about 1000×1000 pixels. The bottom part of webpage screen captures is cropped so that the maximum height of the capture is 1000 pixels.

GIST descriptor segments images by an m by m grid. We formulate $d_{regions}(v_i, v_j) \in \mathbb{R}^{m^2}$ (see Section 4.2.3) as an m^2 -dimensional vector where each element corresponds to the squared ℓ_2 -distance between bins that fall into the same cell of the grids of the screenshots of v_i and v_j . GIST descriptor was proven to provide very high accuracy for near-duplicate detection [Douze et al., 2009], which is close to our context of successive versions of the same document. The high efficiency, small memory usage and estimation of coarsely localized information of the global GIST descriptor, allowing to scale up to very large datasets [Douze et al., 2009], motivated this choice. Examples of our regular $m \times m$ segmentations are illustrated in Fig. 4.4 with 8×8 and 10×10 grids.

4.3.2 Structural segmentation

Instead of using a regular grid segmentation, the structure of webpages may be analyzed to compute $d_{regions}(v_i, v_j)$. We use the webpage segmenter of [Sanoja and Gançarski, 2012] that analyzes pages based on their DOM tree information (after rendering). The tool returns rectangular regions (see Fig. 4.9) that correspond to visually different semantic entities. In this way, $d_{regions}(v_i, v_j)$ corresponds to a vector of visual distances between semantical blocks determined by the structure of the page.

By assuming that the structure of a page does not change much with time, we randomly choose a version and segment it. The resulting segmentation is applied to all the versions of the corresponding webpage. For each version, GIST [Oliva and Torralba, 2001] descriptors of the captured rectangular regions are computed and ℓ_2 -normalized in order to avoid being biased towards larger regions. $d_{regions}(v_i, v_j) \in \mathbb{R}^d$ is the concatenation of the Euclidean distances between the descriptors of the d regions returned by the automatic segmenter.

4.3.3 Integration of structural distance metrics

In addition to visual information, we can use structural information of webpages. We use two discriminant structural distance metrics³⁴: (1) the Jaccard distance $d_{\mathcal{L}}$ between hyperlinks of two versions and (2) the Jaccard distance $d_{\mathcal{I}}$ between image URLs of the two versions. The smaller $d_{\mathcal{L}}(v_i, v_j)$ the more similar v_i and v_j are. We proved in [Law et al., 2012b] that these structural distance metrics are scalable and discriminant for change detection.

The combination of visual and structural metrics is a process in two steps. First, the visual metric $\mathcal{D}_{\mathbf{w}}$ is learned as explained in Section 4.2 (for simplicity of explanation, we only consider the diagonal matrix distance metric case). Second, a multimodal metric \mathcal{D}_{hybrid} that combines visual and structural metrics is learned. \mathcal{D}_{hybrid} is formulated as the linear combination:

$$\mathcal{D}_{hybrid}(v_i, v_j) = \alpha_1 \mathcal{D}_{\mathbf{w}}(v_i, v_j) + \alpha_2 \mathcal{D}_{\mathcal{L}}(v_i, v_j) + \alpha_3 \mathcal{D}_{\mathcal{I}}(v_i, v_j) \quad (4.7)$$

where the coefficients $\alpha_i \geq 0$ are learned with a linear classifier (SVM in our case). In the second step, the visual and structural distance metrics are fixed.

4.4 Experimental Results

We present in this section experimental results of our method. We mainly investigate how our learned metric performs in change detection task when human supervision is missing, or when it is provided. We also investigate strategies that exploit only visual information or the combination of visual and structural information.

³⁴We also tried to include the Jaccard distance of words (similar to Dice’s coefficient of words used in [Adar et al., 2009b], with the exception that it satisfies the properties of a distance metric) but it degraded performances. We assume it is because random textual content has more impact than random hyperlinks on the differences between sets of words or hyperlinks of v_i and v_j , making this metric less stable.

4.4.1 Dataset

Since there is no public dataset that provides both the source code of pages and their visual rendering, we created our own dataset. For this purpose, we hourly crawled different types of popular websites as done in [Adar et al., 2009a, Ben Saad and Gañarski, 2011] for approximately 50 days: the version v_{t+1} is visited 1 hour after v_t . The chosen websites were already used in other papers on Web crawling. For the sake of diversity and to validate the genericness of our approach, the crawled webpages³⁵ are:

- the homepages of some news websites (e.g., CNN, BBC, National Public Radio (NPR), New York Times (NYT)),
- the finance section of Yahoo! News,
- the music section of NPR (that is not often updated) and
- educational webpages: the homepage of Boston's University and the open courseware page of the Massachusetts Institute of Technology (MIT).

To evaluate our approach with quantitative results, we annotated pairs of versions of some of these websites ($\sim 1,200$ per site). To simplify the manual labeling process, we select only homepages of NCC, BBC, NPR and New York Times that are easier to annotate, and we choose as similarity criterion the presence of change of the main news in the page. Only the successive version pairs (v_t, v_{t+1}) of the CNN, BBC, NPR and New York Times homepages were annotated. We distinguish 4 labels of annotation:

- *identical*: the two versions are identical.
- *similar*: an unimportant change occurs (e.g., an advertisement change, see Fig. 4.1).
- *dissimilar*: the main news of the page changes. Particularly, we consider a version pair (v_t, v_{t+1}) as dissimilar only if textual news information is added in the page between v_t and v_{t+1} . We give more details about the annotation criterion in Section 4.4.4.
- *ambiguous*: the decision of labeling the version pair as similar or dissimilar is difficult.

4.4.2 Setup parameter

GIST setup To represent each page screenshot as a vector, we use GIST [Oliva and Torralba, 2001] descriptors built from 8 oriented edge responses at 4 different scales combined to a spatial resolution of $m \times m$. We use the publicly available code of Oliva and Torralba [Oliva and Torralba, 2001] in MATLAB to compute GIST descriptors. They can be computed independently (and then in parallel)³⁶.

Computation time The whole process of computation of distances between GIST descriptors, generation of constraints and learning of the diagonal matrix distance \mathcal{D}_w takes 0.7 seconds on a 3.4GHz machine in MATLAB. It takes 4.5 seconds in the full matrix distance case.

4.4.3 Evaluation protocol

Train/Test split The dataset is composed of versions crawled each hour for about 50 days. For each annotated page (e.g., the homepage of CNN), we create 10 train/test splits: for each split, we use 5 successive days for training, the 45 remaining days for test. We minimize the number of common versions used for training among the different splits, i.e., the first training split contains the first 5 days, the second one the 6th to 10th days, the third one the 11th to 15th days...

³⁵ www.cnn.com, www.bbc.co.uk, www.npr.org, www.nytimes.com, finance.yahoo.com, www.npr.org/music, www.bu.edu, ocw.mit.edu

³⁶ The computation time of the GIST descriptor of a page version (of $\sim 1000 \times 1000$ pixels) using a 10×10 grid is 3.2 seconds.



Figure 4.4: Important change maps for the homepages of BBC, CNN, NYTimes, NPR, Boston’s University, the open courseware page of the MIT, the finance section of Yahoo! News and the music section of NPR. (left) Webpage screenshot, with relevant area (news) in blue, unimportant parts (menu and advertisement) in green and purple, respectively. (right) Spatial weights of important change learned by our method with versions crawled during 5 days and without human annotations (higher values are darker).

Version pairs labeled as ambiguous are ignored in the test evaluation process. However, they are used to automatically generate quadruplet-wise constraints in the training process. The identical versions are also ignored for test because their distance would be 0 (i.e., the lowest possible value) with any distance metric; since they are easy examples (e.g., they would be the first retrieved similar pairs in the average precision evaluation), the performance measures would return very high scores by using them for test.

Performance measures We use two performance measures widely used in information retrieval and image classification: average precision and classification accuracy.

Average Precision (AP) By considering the binary class problem similar/dissimilar, we compute the average precision for the similar class AP_S by ranking distance values of test pairs of successive versions (v_t, v_{t+1}) in ascending order and the average precision for the dissimilar class AP_D by ranking distance values of test pairs in descending order. The Mean Average Precision (MAP) is the mean of AP_S and AP_D .

Classification Accuracy The reported accuracy is the mean of the accuracies of the class of similar pairs (S) and of the class of dissimilar pairs (D).

Average precision is particularly useful to measure how much the relative orderings of distances are respected by the distance metric. Classification accuracy is useful to determine optimal crawling strategies since it can measure how frequently a webpage changes within a given period.

4.4.4 Learning results without human supervision

We present in this subsection qualitative and quantitative results when no human supervision is integrated in the learning process (i.e., $D \cup S = \emptyset$).

4.4.4.1 Qualitative Results

A first qualitative evaluation is illustrated in Fig. 4.4. The figure shows maps learned for the 8 webpages mentioned in Section 4.4.1 without human annotations. In order to learn the importance maps of important change regions, we sample version quadruplets (v_t, v_{t+1}, v_r, v_s) using Eq. (4.1) and Eq. (4.2) so that $r \geq t - 6$, $s \leq t + 7$, $\gamma = 4$, and images are segmented as a 10×10 or 8×8 grid. Training sets to learn these maps contain screenshots of pages hourly visited during 5 days. In terms of training constraints, we deal with less than 10,000 constraints in our experiments, which makes the learning of the diagonal matrix metric \mathcal{D}_w very fast. The maps plot the relative values of the learned $w \in \mathbb{R}_+^d$. The highest positive values, represented by dark regions, correspond to important change regions of the page (e.g., news title). Menus and advertisements are ignored by the map as expected.

We also tested our method on governmental sites but their change frequency is so low (the page often remains unchanged in 5 days) that a map cannot be learned in only 5 days. This is consistent with the observations of Adar et al. [Adar et al., 2009b]: government domain addresses do not change as frequently or as much as pages in other domains do, and this may reflect the fact that this type of site provides richer and less transient content which only requires small, infrequent updates.

A second qualitative evaluation is illustrated in Fig. 4.5. The figure shows the eigenvector \mathbf{v}_1 of the largest eigenvalue λ_1 of \mathbf{M} when we learn a full matrix metric D_M . The matrix $\mathbf{M}' = \lambda_1 \mathbf{v}_1 \mathbf{v}_1^\top$ is the projection of \mathbf{M} onto rank-1 symmetric PSD matrices, and is thus the nearest rank-1 matrix of \mathbf{M} in the ℓ_2 norm. Since we have $D_{M'}^2(v_i, v_j) = \lambda_1 (\mathbf{v}_1^\top \mathbf{c}_{ij})^2$, the vector \mathbf{v}_1 weighs the importance of spatial regions of the webpage. As shown in Fig. 4.5, the vector \mathbf{v}_1 correctly detects important change regions and ignores menus and advertisements.

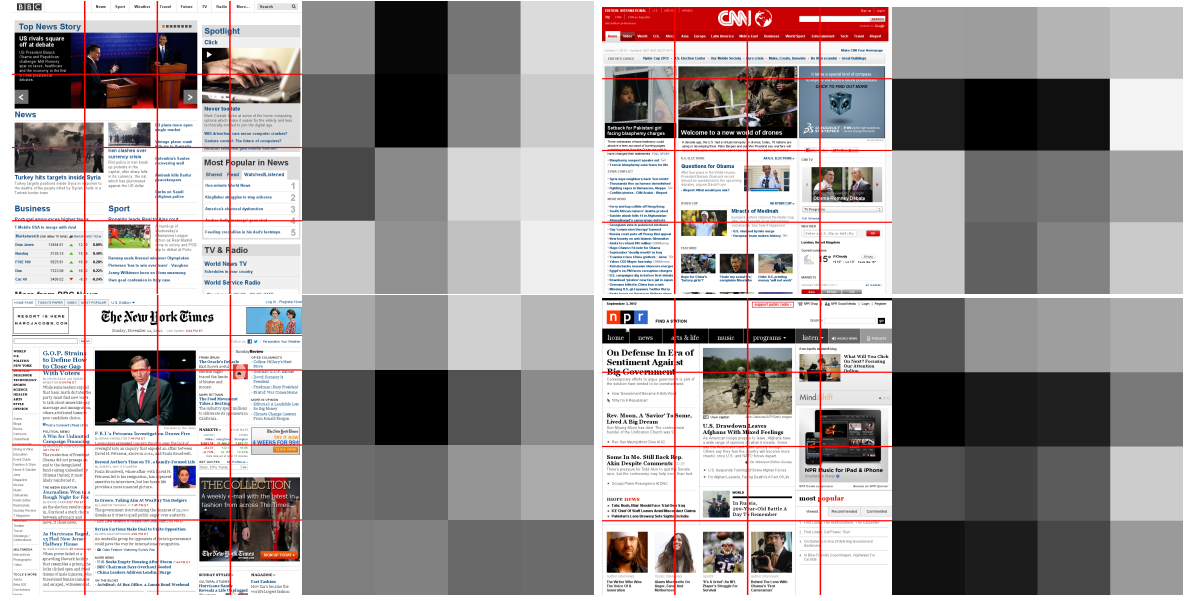


Figure 4.5: Important change maps for the homepages of BBC, CNN, New York Times and NPR. (left) Webpage screenshot with webpage regular segmentation blocks (red lines). (right) Absolute values of the eigenvector of the dominant eigenvalue of the distance non-diagonal matrix learned by our method with versions crawled during 5 days and without human supervision (higher values are darker).

4.4.4.2 Quantitative results

Average precision Table 4.1 compares the average precision scores obtained using different distance metrics:

- the Euclidean distance often used for the GIST descriptor [Oliva and Torralba, 2001].
- a triplet-based method for which the set \mathcal{N} is used to generate triplet-wise constraints.
- our learned visual metric $\mathcal{D}_{\mathbf{w}}$ parameterized by a vector $\mathbf{w} \in \mathbb{R}_+^d$.
- our learned visual metric $D_{\mathbf{M}}$ parameterized by the non-diagonal matrix $\mathbf{M} \in \mathbb{S}_+^d$.

More precisely, Table 4.1 presents the recognition scores when screenshot images of webpages are segmented as m^2 regions (i.e., $d_{regions}(v_i, v_j) \in \mathbb{R}^{m^2}$) where $m = 4, 8$ and 10 . All the metrics benefit from greater values of m , which means that they need to focus on highly detailed small regions of pages. Moreover, the Euclidean distance metric is outperformed by all the learned metrics although its performance is good, which means that the Euclidean distance is appropriate for change detection. The triplet-based method which exploits a small number of constraints is outperformed by quadruplet-wise methods that exploit a larger number of meaningful constraints. The full matrix distance metric $D_{\mathbf{M}}$ outperforms all the other methods. Particularly, it outperforms the diagonal matrix distance metric $\mathcal{D}_{\mathbf{w}}$ due to the exploitation of correlations between the different spatial regions.

The relatively low $AP_{\mathcal{D}}$ for the BBC homepage is explained by the similarity criterion used to label version pairs. In particular, we consider that two versions are dissimilar only if their textual news content is different. Fig. 4.6 illustrates a recurring example on BBC where a *breaking news* logo appears for a very recent news (the left picture) and vanishes one hour later (the right picture). The *breaking news* logo, that repeatedly appears in and vanishes from the only region where important changes occur, generates false detections. It returns high distance values for some pairs although the textual information is unchanged. In a context where any new image about an important event has to be archived, the example illustrated in Fig. 4.6 would be considered as dissimilar, and the $AP_{\mathcal{D}}$ of BBC would be higher.

National Public Radio (NPR)						
Grid Resolution	Visual Euclidean Distance			Proposed Visual Dissimilarity \mathcal{D}_w		
	AP_S	AP_D	MAP	AP_S	AP_D	MAP
4×4	$93.2 \pm 0.3\%$	$79.6 \pm 0.7\%$	$86.4 \pm 0.5\%$	$96.5 \pm 1.6\%$	$89.1 \pm 4.5\%$	$92.8 \pm 3.0\%$
8×8	$94.8 \pm 0.3\%$	$84.9 \pm 0.6\%$	$89.9 \pm 0.4\%$	$98.0 \pm 0.8\%$	$92.5 \pm 1.9\%$	$95.2 \pm 1.4\%$
10×10	$96.3 \pm 0.2\%$	$89.5 \pm 0.5\%$	$92.9 \pm 0.3\%$	$98.6 \pm 0.2\%$	$94.3 \pm 0.6\%$	$96.5 \pm 0.4\%$
Grid Resolution	Triplet-based method			Proposed Visual Dissimilarity D_M		
	AP_S	AP_D	MAP	AP_S	AP_D	MAP
4×4	$95.8 \pm 1.8\%$	$86.4 \pm 3.8\%$	$91.1 \pm 2.8\%$	$97.6 \pm 0.3\%$	$91.6 \pm 0.9\%$	$94.6 \pm 0.6\%$
8×8	$96.2 \pm 0.9\%$	$91.7 \pm 2.3\%$	$94.0 \pm 1.6\%$	$98.5 \pm 0.5\%$	$93.2 \pm 2.1\%$	$95.8 \pm 1.3\%$
10×10	$98.0 \pm 0.6\%$	$92.5 \pm 1.1\%$	$95.2 \pm 0.9\%$	$98.7 \pm 0.2\%$	$94.5 \pm 0.7\%$	$96.6 \pm 0.4\%$
New York Times						
Grid Resolution	Visual Euclidean Distance			Proposed Visual Dissimilarity \mathcal{D}_w		
	AP_S	AP_D	MAP	AP_S	AP_D	MAP
4×4	$68.3 \pm 0.9\%$	$75.1 \pm 0.7\%$	$71.7 \pm 0.6\%$	$77.3 \pm 6.0\%$	$84.2 \pm 5.8\%$	$80.7 \pm 5.9\%$
8×8	$70.3 \pm 1.0\%$	$78.7 \pm 0.5\%$	$74.5 \pm 0.6\%$	$83.9 \pm 5.7\%$	$90.9 \pm 4.7\%$	$87.4 \pm 5.2\%$
10×10	$69.8 \pm 0.9\%$	$79.5 \pm 0.4\%$	$74.6 \pm 0.5\%$	$85.5 \pm 5.4\%$	$92.3 \pm 4.1\%$	$88.9 \pm 4.6\%$
Grid Resolution	Triplet-based method			Proposed Visual Dissimilarity D_M		
	AP_S	AP_D	MAP	AP_S	AP_D	MAP
4×4	$77.0 \pm 5.5\%$	$82.7 \pm 4.9\%$	$79.9 \pm 5.2\%$	$86.3 \pm 5.0\%$	$92.8 \pm 3.2\%$	$89.5 \pm 4.1\%$
8×8	$81.9 \pm 4.2\%$	$87.8 \pm 3.9\%$	$84.9 \pm 4.1\%$	$89.3 \pm 6.1\%$	$93.0 \pm 3.4\%$	$91.2 \pm 4.8\%$
10×10	$83.2 \pm 1.4\%$	$89.1 \pm 2.7\%$	$86.1 \pm 2.0\%$	$91.6 \pm 4.4\%$	$94.7 \pm 2.4\%$	$93.1 \pm 3.4\%$
CNN						
Grid Resolution	Visual Euclidean Distance			Proposed Visual Dissimilarity \mathcal{D}_w		
	AP_S	AP_D	MAP	AP_S	AP_D	MAP
4×4	$66.1 \pm 0.6\%$	$81.1 \pm 0.5\%$	$73.6 \pm 0.4\%$	$75.0 \pm 5.0\%$	$90.1 \pm 4.3\%$	$82.5 \pm 4.6\%$
8×8	$68.0 \pm 0.6\%$	$84.3 \pm 0.6\%$	$76.2 \pm 0.5\%$	$81.5 \pm 4.2\%$	$94.3 \pm 2.0\%$	$87.9 \pm 3.1\%$
10×10	$68.1 \pm 0.6\%$	$85.9 \pm 0.6\%$	$77.0 \pm 0.5\%$	$82.7 \pm 4.1\%$	$94.6 \pm 1.8\%$	$88.6 \pm 2.9\%$
Grid Resolution	Triplet-based method			Proposed Visual Dissimilarity D_M		
	AP_S	AP_D	MAP	AP_S	AP_D	MAP
4×4	$73.8 \pm 4.5\%$	$88.4 \pm 3.3\%$	$81.1 \pm 3.9\%$	$76.5 \pm 15.5\%$	$92.2 \pm 8.3\%$	$84.3 \pm 11.9\%$
8×8	$77.6 \pm 3.8\%$	$91.1 \pm 2.2\%$	$84.4 \pm 3.0\%$	$88.3 \pm 1.0\%$	$96.6 \pm 0.3\%$	$92.5 \pm 0.6\%$
10×10	$78.8 \pm 1.9\%$	$91.7 \pm 1.7\%$	$85.2 \pm 1.8\%$	$87.9 \pm 3.1\%$	$96.6 \pm 0.6\%$	$92.2 \pm 1.9\%$
BBC						
Grid Resolution	Visual Euclidean Distance			Proposed Visual Dissimilarity \mathcal{D}_w		
	AP_S	AP_D	MAP	AP_S	AP_D	MAP
4×4	$90.5 \pm 0.3\%$	$75.7 \pm 0.7\%$	$83.1 \pm 0.5\%$	$92.8 \pm 0.8\%$	$78.5 \pm 1.9\%$	$85.6 \pm 1.4\%$
8×8	$90.6 \pm 0.2\%$	$75.4 \pm 0.6\%$	$83.0 \pm 0.4\%$	$91.9 \pm 0.7\%$	$77.2 \pm 1.7\%$	$84.5 \pm 1.2\%$
10×10	$91.1 \pm 0.3\%$	$76.7 \pm 0.6\%$	$83.9 \pm 0.4\%$	$92.8 \pm 0.4\%$	$79.3 \pm 1.3\%$	$86.1 \pm 0.8\%$
Grid Resolution	Triplet-based method			Proposed Visual Dissimilarity D_M		
	AP_S	AP_D	MAP	AP_S	AP_D	MAP
4×4	$91.5 \pm 1.2\%$	$76.7 \pm 1.0\%$	$84.1 \pm 1.1\%$	$92.8 \pm 0.5\%$	$80.0 \pm 1.3\%$	$86.4 \pm 0.9\%$
8×8	$91.7 \pm 0.9\%$	$76.5 \pm 1.1\%$	$84.1 \pm 1.0\%$	$93.0 \pm 1.1\%$	$82.7 \pm 2.0\%$	$87.8 \pm 1.5\%$
10×10	$92.5 \pm 0.4\%$	$80.1 \pm 1.0\%$	$86.3 \pm 0.6\%$	$93.0 \pm 0.6\%$	$82.5 \pm 1.3\%$	$87.7 \pm 1.0\%$

Table 4.1: Test average precisions with the classic Euclidean distance and with learned metrics in the fully unsupervised setup. The proposed visual dissimilarity D_M obtains the best scores for all webpages.

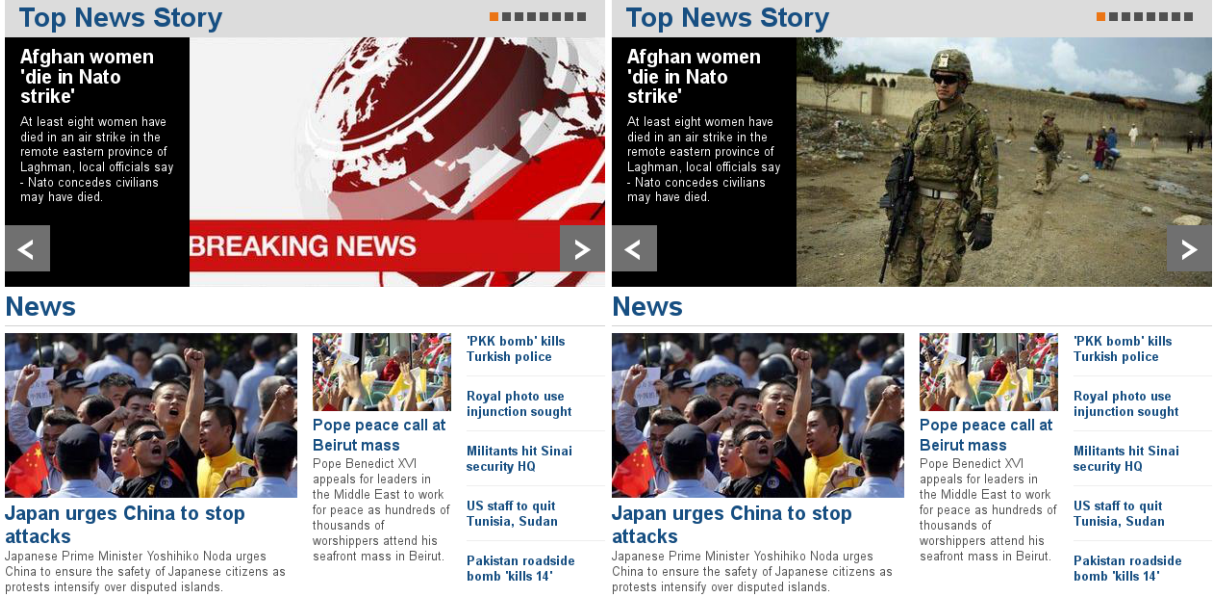


Figure 4.6: The important region of two successive versions of the BBC homepage. A specificity of the BBC website is that it always uses its “breaking news” logo to introduce recent breaking news and removes it after a short period. In this case, since the textual content of the main news is unchanged, we consider the two versions are similar. However, in a Web archiving context, these two versions are considered as dissimilar since a relevant visual information is updated. Our algorithm tends to detect a visual change in the important change region although the news is the same.

Classification accuracy We now present a strategy to learn a change detection metric without human supervision. For this purpose, we automatically generate our sets \mathcal{S} and \mathcal{D} (see Section 4.2.2) to discriminate similar pairs of versions from dissimilar pairs. For the sake of clarity and of scalability of the method, we present in the following only the results obtained with the diagonal Qwise visual distance metric $\mathcal{D}_{\mathbf{w}}$. The relative quantitative performances of other models follow the same trend as in Table 4.1.

When human annotations to distinguish similar pairs from dissimilar pairs are not provided (i.e., $\mathcal{S} \cup \mathcal{D} = \emptyset$), a distance metric $\mathcal{D}_{\mathbf{w}}$ can be learned from the training set $\mathcal{N} = \mathcal{A} \cup \mathcal{B}$ composed solely of automatically generated quadruplets of successive versions. However, no threshold (i.e., b in Eq. (4.3) and Eq. (4.4)) is learned to distinguish similar pairs from dissimilar pairs. In other words, distances between version pairs can be compared with one another but our learned metric cannot determine whether important changes occurred in a given version pair or not. We present how to learn a algorithm that can detect whether semantic changes occurred or not without exploiting information provided by human users. In particular, we propose to learn a change detection algorithm that exploits the metric $\mathcal{D}_{\mathbf{w}}$ learned from the set \mathcal{N} to automatically generate the training sets \mathcal{S} (class -1) and \mathcal{D} (class +1).

Since the average precision scores for the different websites are high, we assume that the metric $\mathcal{D}_{\mathbf{w}}$ learned in Eq. (2.10) provides lowest distance values for similar pairs and highest values for dissimilar pairs. The training pairs in \mathcal{S} and \mathcal{D} can then be automatically inferred from the training set of page versions in \mathcal{N} . Let k be the cardinality of the created sets \mathcal{S} and \mathcal{D} ($k = |\mathcal{S}| = |\mathcal{D}|$). The k version pairs (v_t, v_{t+1}) (among the $24 \times 5 = 120$ possible pairs) with highest values of $\mathcal{D}_{\mathbf{w}}(v_t, v_{t+1})$ form \mathcal{D} , whereas the k version pairs with values $\mathcal{D}_{\mathbf{w}}(v_t, v_{t+1})$ closest to 0 (and that are not completely identical) form \mathcal{S} . Once these sets are created, we learn a linear SVM that discriminates pairs in \mathcal{S} from pairs in \mathcal{D} .

Fig. 4.7 and Table 4.2 report classification accuracies in the unsupervised setup described above. We learn a linear SVM with the automatically created sets \mathcal{S} and \mathcal{D} using the $|\mathcal{S}| = |\mathcal{D}| = k = 25$ version pairs with lowest and highest distances.

Fig. 4.7 illustrates that change detection gets improved as the grid resolution increases. At a grid

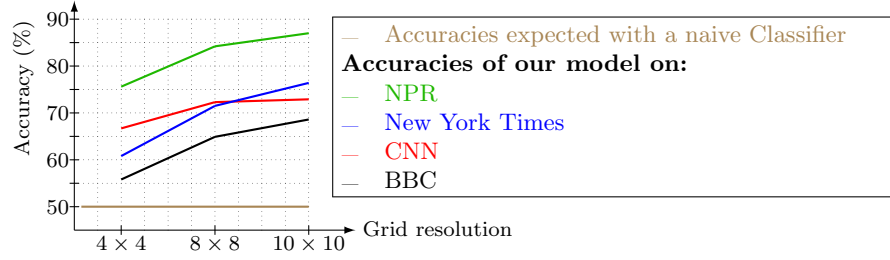


Figure 4.7: Test accuracies in the similarity detection task without human annotations as the grid resolution of the GIST descriptor increases ($k = 25$).

Web Site	Visual Method	Hybrid Visual+Structural Method
NPR	87.0	86.7
NYTimes	76.4	77.0
CNN	72.9	75.0
BBC	68.6	68.6

Table 4.2: Test accuracies (in %) in the fully unsupervised setup using only visual descriptors or combining them with structural metrics. A 10×10 grid resolution is considered ($k = 25$).

resolution of 4×4 , the change detection is already better for all websites than a naive classifier that randomly determines whether a test pair is similar (such a classifier would obtain a performance of 50% accuracy). We reach accuracies up to 87% on NPR with a 10×10 grid resolution. Table 4.2 compares accuracies (using a 10×10 grid resolution) depending on whether visual features are used independently (as in Fig. 4.7) or combined with structural distances. The combination of structural and visual distances improves the accuracy up to 2% on CNN.

All these results illustrate the ability of our model to learn a change detection algorithm without human supervision.

4.4.5 Supervised learning results

The previous experiments were realized without human annotations. We show here that change detection (classification accuracy) can be improved with very little human effort.

Fig 4.8 reports classification accuracies on the different websites as the number of annotated pairs per class ($|\mathcal{S}| = |\mathcal{D}|$) increases³⁷. Using 5 annotated pairs per class improves accuracy of 5%, and using 20 annotated pairs further improves performance of 5.5%. However, we reach a ceiling for $|\mathcal{S}| = |\mathcal{D}| > 20$, around which the accuracy does not improve much. Using a small number of annotated pairs is then sufficient. Moreover, note that the selected pairs in \mathcal{S} and \mathcal{D} are randomly chosen among the $24 \times 5 = 120$ possible pairs. Active strategies can be performed to minimize integrated human supervision.

In Table 4.3, we compare the performance of our learned multimodal distance presented in Section 4.3.3 with a learned multimodal distance that combines the Euclidean distance between GIST regions with structural metrics on hyperlinks and image URLs. The difference between the two methods is that the first one focuses on important page regions to visually compare versions whereas the second one does not. We actually proposed the second method in [Law et al., 2012b]. The margin is 12% in our favour. Moreover, combining structural and visual distances (see Table 4.3) slightly improves recognition over visual distances alone (see Fig 4.8) with a global margin of 1% for all websites. This result shows that structural and visual distances are complementary.

³⁷The accuracies reported with zero annotated pair sample per class correspond to those of Section 4.4.4.2, Fig. 4.7 and Table 4.2.

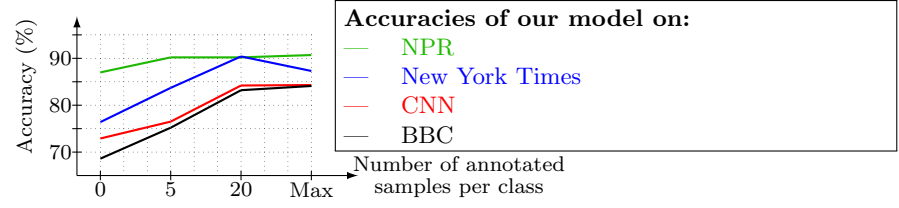


Figure 4.8: Test accuracies in the similarity detection task as the number of annotated samples increases. A 10×10 grid GIST descriptor is used.

	Number of annotated samples per class			
	Law et al. [Law et al., 2012b]		Proposed method	
Web Site	5	20	5	20
NPR	81.4	86.1	90.6	90.6
New York Times	65.3	68.3	83.4	90.2
CNN	70.2	71.6	77.4	85.1
BBC	69.8	72.3	80.0	83.9

Table 4.3: Test accuracies (in %) in the supervised setup of the baseline method described in [Law et al., 2012b] and our method using the same visual and structural descriptors.

4.4.6 Structural segmentation maps

We now study the case where, instead of using a regular grid-based segmentation, we visually segment pages using the segmenter of [Sanoja and Gañarski, 2012] as described in Section 4.3.2.

Fig. 4.9 illustrates the relative importances learned without human supervision for regions obtained using structural segmentation (and using versions crawled during 5 days). The illustrated webpages are the same as the first four pages of Fig. 4.4. The important change regions are well recognized (higher values are darker) and unimportant regions are ignored as expected. However, quantitative results are comparable to those that use a regular grid segmentation. There are many reasons:

- Using the same segmentation structure for all the versions of a webpage is a strong limitation.
- Although the webpage segmentation performed by [Sanoja and Gañarski, 2012] is specific to the analyzed webpage, a regular grid segmentation with high granularity already overlaps well with the different important semantical regions that cover large parts of the page (see Fig. 4.9).
- Learning weights using a regular grid segmentation allows to focus on subregions that are convenient to satisfy the constraints mentioned in Section 4.2. The learned weights are then more specialized than weights that only consider distances on large (segmented) regions.
- Webpage segmentation algorithms [Cai et al., 2003, Sanoja and Gañarski, 2012] rely on heuristics that are not necessarily optimal for a change detection purpose. This is observable in the segmentation performed on the New York Times homepage: the weights learned with a regular grid segmentation (see Fig. 4.4) focus on the top of the main news whereas the segmentation algorithm in [Sanoja and Gañarski, 2012] considers all the news contents (i.e., top and bottom region of the news region, the largest region in this webpage in Fig. 4.9) as the same block (semantical entity). Future work includes further investigating the degree of granularity used by the segmentation algorithm.

Visual segmentation is a difficult task even for real-world images. Moreover, performing a webpage segmentation is computationally expensive (the prototype [Sanoja and Gañarski, 2012] takes from 5 to 8 seconds to segment our pages) and does not improve recognition. In order to be scalable, it is then preferable to use a regular grid segmentation with our framework except if one wants to compute the relative importance of changes in segmented blocks.

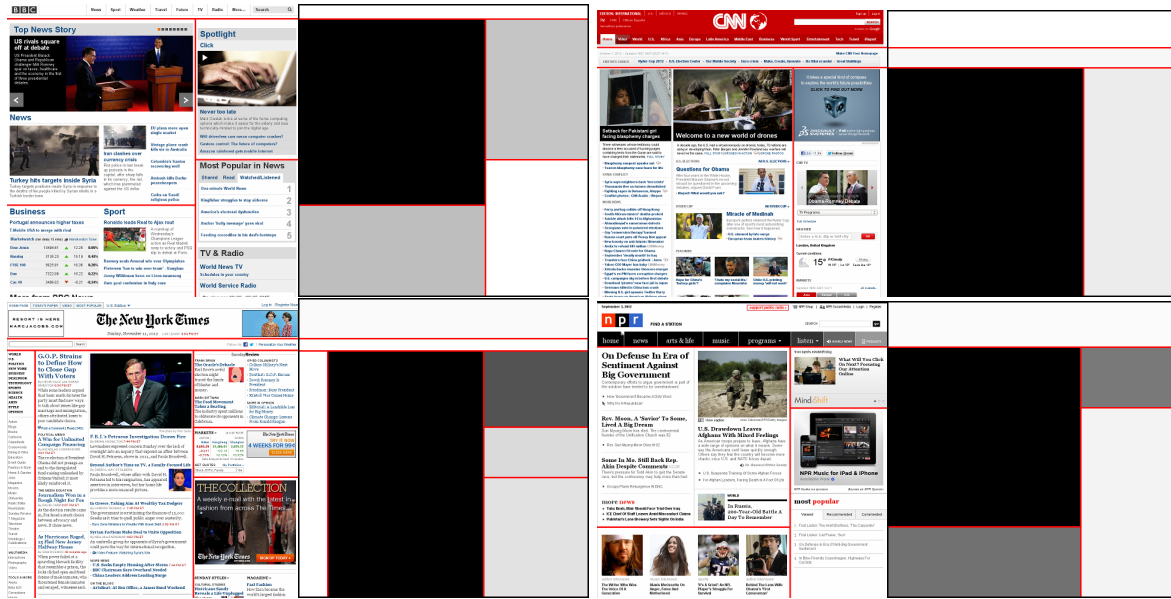


Figure 4.9: Important change maps for BBC, CNN, New York Times and NPR. (left) Webpage screenshot with segmentation blocks (red lines) [Sanoja and Gançarski, 2012]. (right) Spatial weights learned by our method with versions crawled during 5 days and without human supervision (higher values are darker).

4.4.7 Summary

We have shown different interesting results:

- the metric learned with our strategy allows to detect important regions in webpages. The learned metric also implicitly returns small distances for semantically similar pairs of versions and larger values for semantically distant versions.
- our sampling strategy allows to create a lot of significant constraints. This is particularly useful when triplet-wise sampling strategies generate a relatively small number of constraints.
- the metrics learned without human supervision perform very well and their recognition performance can be improved with very little human interaction.
- the learned metric can be extended by combining both visual and structural information metrics.

4.5 Conclusion

We have proposed a novel webpage change detection method that detects important change regions in webpages. Our approach learns a distance metric between versions of a same webpage and exploits temporal relationships between them. The proposed change detection algorithm learned without human supervision obtains good recognition results on different websites. We also showed how a small number of human annotations boost our performances. Since our method mostly relies on visual comparisons on rendered pages, it is generic and robust to the way the analyzed pages are coded. Structural distances, which use the source code of webpages, are easy to integrate in our framework.

The possible applications of our approach are diverse: Web crawling and search engine improvements, navigation in Web archives (e.g., from a given version in a Web archive, find the next one in which a semantical change occurred), improvement of mobile phone applications that load the important content of webpages... Future work includes the implementation of a webpage segmentation method dedicated to change detection by using our algorithm as a preprocessing step. For instance, the adjacent regularly segmented regions with comparable weighs can be merged in a single semantic block. Future work also includes the use of more complex metrics.

Conclusion

In this PhD thesis, we have proposed a supervised distance metric learning framework to deal with rich kind of training information and to efficiently control the complexity of the learned distance model.

Incorporating rich information Most distance metric learning algorithms exploit binary similarity information (e.g., “is similar” or “is dissimilar”) to generate training constraints. A central contribution of this work is the quadruplet-wise distance metric learning framework, presented in Chapter 2, to extend the expressivity of constraints and incorporate rich information. For instance, in the context of relative attributes where degrees of presence of attributes are provided at a class level, relaxing equivalence constraints between pairs of images by exploiting inequality constraints between quadruplets of images seems more natural and intuitive. From this observation, we derived a general distance metric learning framework that exploits constraints which involve quadruplets of images. We demonstrated that the proposed constraints are a generalization of classic pairwise and triplet-wise constraints. In addition, they can also describe relationships between images that are not possible with classic approaches. We experimentally showed in contexts such as relative attributes, hierarchical image classification and webpage analysis that incorporating rich information helps improve recognition.

In the particular context of webpage understanding (see Chapter 4), we proposed a novel framework to automatically discover important change regions by exploiting temporal relationships between successive versions of a webpage. The proposed quadruplet-wise framework allowed us to increase the number of possible constraints and learn a meaningful metric compared to a triplet-wise approach. We experimentally showed that the learned metric can be exploited in the context of webpage change detection. Especially, change detection performance is improved when the learned metric focuses on important regions and ignores irrelevant regions. Moreover, We have successfully extended our metric learning formulation by including manually annotated pairwise constraints. This combination increases performances. We have also proposed to combine visual information with structural information to better describe webpages.

Controlling the complexity of the learned model In Chapter 3, we introduced in Mahalanobis-like distance metric a novel regularization method to explicitly control the rank of the learned distance matrix, and thus avoid overfitting. The key idea is to include a regularization term which minimizes the sum of the smallest singular values of the learned PSD matrix. The regularization term is minimized if and only if the rank of the PSD matrix is smaller than or equal to a target rank. For this purpose, we express the (super-)gradient of the regularization term and propose efficient optimization. We experimentally validated that our regularization framework allows to control the rank of the learned distance matrix. The results obtained were competitive against other distance metric learning approaches on synthetic and real-world computer vision datasets.

In addition to the contributions presented in this dissertation, a number of open questions suggest further investigations:

Dealing with large numbers of constraints and structured predictions In Chapter 2, we have proposed to incorporate rich information by generating “independant” constraints, each of them involving

quadruplets of images. However, if some or many pairs of images are present in a lot of constraints, one can exploit structured predictions, such as rankings over these image pairs, to limit the number of generated constraints. Structural metric learning presents a lot of advantages, one of them is the possibility to exploit efficient optimization techniques such as the 1-slack cutting plane method.

Generalization of the proposed regularization method In Chapter 3, our proposed regularization framework penalizes only the k smallest eigenvalues of the learned PSD matrix and not the other ones. One can imagine a generalization of our regularization term by weighing the penalty depending on the value of eigenvalues. For instance, a penalization such as the one used in [Candès et al., 2008] can be generalized in our framework to PSD matrices. A vast literature exists for cases where the learned model is a vector or any type of matrix. It would be interesting to study the case where the learned model is a symmetric PSD matrix.

Multimodal webpage analysis In Chapter 4, we have proposed a first attempt to combine visual and structural information and compare webpages for change detection. Although recognition is improved by including structural information, the gain is small. Future work includes a further investigation of how structural and visual informations can be combined to improve webpage change detection. A possible direction is the prior structural segmentation dedicated to the change detection task and used to segment webpage screenshots.

List of Publications The material reported in this thesis was the subject of the following publications:

Book chapter

- M. T. Law, N. Thome, M. Cord. “Bag-of-Words Image Representation: Key Ideas and Further Insight” *Fusion in Computer Vision - Understanding Complex Visual Content*, Springer 2014

International conferences

- M. T. Law, N. Thome, M. Cord “Fantope Regularization in Metric Learning” *IEEE Conference on Computer Vision and Pattern Recognition (CVPR)*, 2014
- M. T. Law, N. Thome, M. Cord “Quadruplet-wise Image Similarity Learning” *IEEE International Conference on Computer Vision (ICCV)*, 2013
- M. T. Law, N. Thome, S. Gançarski, M. Cord “Structural and Visual Comparisons for Web Page Archiving” *12th edition of the ACM Symposium on Document Engineering (DocEng)*, 2012

International workshops

- M. T. Law, N. Thome, M. Cord “Hybrid Pooling Fusion in the BoW Pipeline” *ECCV 2012 Workshop on Information fusion in Computer Vision for Concept Recognition (ECCV-IFCVCR 2012)*, 2012
- M. T. Law, C. Sureda Gutierrez, N. Thome, S. Gançarski, M. Cord “Structural and Visual Similarity Learning for Web Page Archiving” *10th workshop on Content-Based Multimedia Indexing (CBMI)* 2012

Appendix A

Positive Semidefinite Cone

A.1 Definitions

We give the basic properties of the set of symmetric positive semidefinite (PSD) matrices \mathbb{S}_+^d that are fundamental for this thesis. The first one is that \mathbb{S}_+^d is a convex set, particularly a proper cone, which allows to use efficient projected algorithms in order to solve convex problems. We first give some definitions related to convex cones.

Definition A.1.1. (*Cone*) In linear algebra, a set \mathcal{X} is called a cone if and only if:

$$\Gamma \in \mathcal{X} \Rightarrow \forall \mu > 0, \mu\Gamma \in \mathcal{X} \quad (\text{A.1})$$

or equivalently

$$\Gamma \in \mathcal{X} \Rightarrow \forall \mu \geq 0, \mu\Gamma \in \bar{\mathcal{X}} \quad (\text{A.2})$$

where $\bar{\mathcal{X}}$ denotes the closure of cone \mathcal{X} . All closed cones³⁸ contain the origin $\mathbf{0}$ and are unbounded, excepting the cone $\{\mathbf{0}\}$.

Definition A.1.2. (*Convex cone*) A set \mathcal{K} is called a convex cone if and only if:

$$\Gamma_1, \Gamma_2 \in \mathcal{K} \Rightarrow \forall \mu_1, \mu_2 \geq 0, \mu_1\Gamma_1 + \mu_2\Gamma_2 \in \bar{\mathcal{K}} \quad (\text{A.3})$$

i.e., any conic combination of elements from \mathcal{K} belongs to its closure. \mathcal{K} is convex since for any particular $\mu_1, \mu_2 \geq 0$, we have:

$$\forall \nu \in [0, 1], \nu\mu_1\Gamma_1 + (1 - \nu)\mu_2\Gamma_2 \in \bar{\mathcal{K}} \quad (\text{A.4})$$

Definition A.1.3. (*Proper cone*) A cone $\mathcal{K} \subseteq \mathbb{R}^n$ is called a proper cone if it satisfies the following:

- \mathcal{K} is convex
- \mathcal{K} is closed
- \mathcal{K} is solid, which means it has nonempty interior
- \mathcal{K} is pointed, which means that it contains no line (i.e., $\Gamma \in \mathcal{K}, -\Gamma \in \mathcal{K} \Rightarrow \Gamma = \mathbf{0}$)

³⁸A set \mathcal{X} is closed iff $\bar{\mathcal{X}} = \mathcal{X}$.

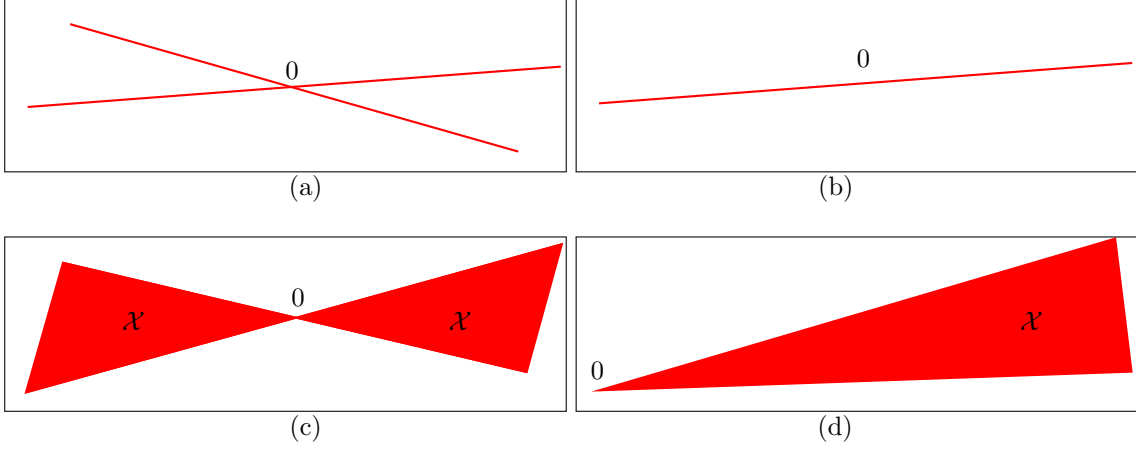


Figure A.1: Examples of truncated cones in \mathbb{R}^2 . (b) and (d) are convex cones, and only (d) is a proper cone.

A proper cone \mathcal{K} can be used to define a *generalized inequality*, which is a partial ordering on \mathbb{R}^n . The partial ordering on \mathbb{R}^n associated with the proper cone \mathcal{K} is defined by

$$\Gamma_1 \preceq_{\mathcal{K}} \Gamma_2 \iff \Gamma_2 \succeq_{\mathcal{K}} \Gamma_1 \iff \Gamma_2 - \Gamma_1 \in \mathcal{K} \quad (\text{A.5})$$

The nonnegative orthant \mathbb{R}_+^n is a proper cone in \mathbb{R}^n and the positive semidefinite cone \mathbb{S}_+^d is a proper cone in \mathbb{S}^d .

Definition A.1.4. The set \mathbb{S}_+^d is the set of $d \times d$ symmetric matrices that have all their eigenvalues non-negative. In other words: $\mathbf{M} \in \mathbb{S}_+^d \iff \mathbf{M} \in \mathbb{S}^d, \lambda(\mathbf{M}) \in \mathbb{R}_+^d$.

This implies the following property:

Property A.1.5. The eigenvalues of a matrix in \mathbb{S}_+^d are also its singular values.

Proof: The singular values of a matrix \mathbf{M} are the square roots of the eigenvalues of $\mathbf{M}^\top \mathbf{M}$. Since for all $\mathbf{M} \in \mathbb{S}_+^d$, we have $\mathbf{M} = \mathbf{M}^\top$ and since every symmetric matrix can be decomposed $\mathbf{M} = \mathbf{V} \text{Diag}(\lambda(\mathbf{M})) \mathbf{V}^\top$ where \mathbf{V} is an orthogonal matrix, we obtain the following eigendecomposition of $\mathbf{M}^\top \mathbf{M}$:

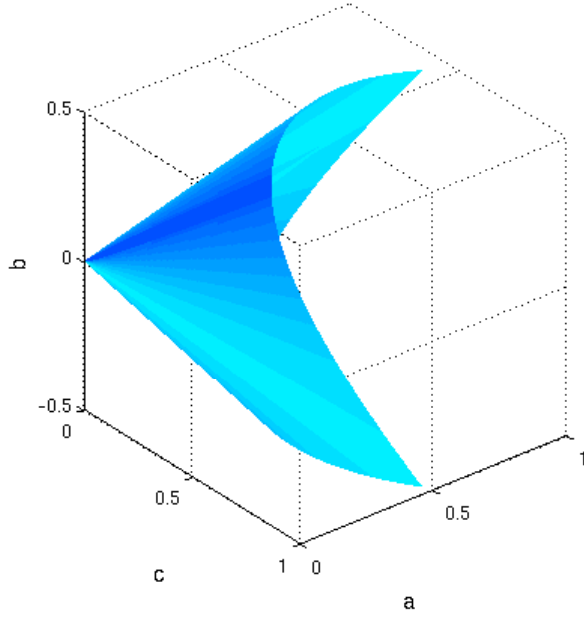
$$\begin{aligned} \mathbf{M}^\top \mathbf{M} &= \mathbf{M} \mathbf{M} = \mathbf{V} \text{Diag}(\lambda(\mathbf{M})) \mathbf{V}^\top \mathbf{V} \text{Diag}(\lambda(\mathbf{M})) \mathbf{V}^\top \\ &= \mathbf{V} \text{Diag}(\lambda(\mathbf{M})) \text{Diag}(\lambda(\mathbf{M})) \mathbf{V}^\top \\ &= \mathbf{V} [\text{Diag}(\lambda(\mathbf{M}))]^2 \mathbf{V}^\top \end{aligned} \quad (\text{A.6})$$

which means that the eigenvalues of $\mathbf{M}^\top \mathbf{M}$ are the squared values of the eigenvalues of \mathbf{M} . Since the eigenvalues of \mathbf{M} are all nonnegative (i.e., $\lambda(\mathbf{M}) \in \mathbb{R}_+^d$), it follows $[\text{Diag}(\lambda(\mathbf{M}))]^2]^{1/2} = \text{Diag}(\lambda(\mathbf{M}))$. The square roots of the eigenvalues of $\mathbf{M}^\top \mathbf{M}$ are then $\lambda(\mathbf{M})$. \square

In the general case where \mathbf{M} is a symmetric matrix, its singular values are the absolute values of its eigenvalues.

Property A.1.5 implies that the nuclear norm of a matrix $\mathbf{M} \in \mathbb{S}_+^d$ (sum of its singular values) is also the trace of \mathbf{M} (sum of its eigenvalues): $\forall \mathbf{M} \in \mathbb{S}_+^d, \|\mathbf{M}\|_* = \text{tr}(\mathbf{M})$.

Moreover, since the rank of a matrix is its number of non-zero singular values, the rank of a matrix in \mathbb{S}_+^d (and in \mathbb{S}^d in general) is also its number of non-zero eigenvalues.



$$\mathbf{X} = \begin{pmatrix} a & b \\ b & c \end{pmatrix} \in \mathbb{S}_+^d \iff a \geq 0, c \geq 0, ac \geq b^2$$

This equivalence is a consequence of the following properties:

- The diagonal entries of a matrix in \mathbb{S}_+^d are real and nonnegative.
- Since the eigenvalues of a matrix in \mathbb{S}_+^d are non-negative, the determinant (product of its eigenvalues) is also nonnegative: we then have $\det(\mathbf{X}) = ac - b^2 \geq 0$.

Figure A.2: Truncated boundary of positive semidefinite cone in \mathbb{S}^2 plotted in \mathbb{R}^3 as (a, b, c) . The boundary of \mathbb{S}_+^2 is the set of parameters (a, b, c) that satisfy $a \geq 0, c \geq 0, ac = b^2$, it represents the set of symmetric PSD matrices that are not full rank. The interior of the cone is the set of positive definite matrices (\mathbb{S}_{++}^2).

A.2 Rank of a Matrix

The rank of a matrix \mathbf{M} is the maximal number of linearly independent rows or columns of \mathbf{M} . If the matrix $\mathbf{M} \in \mathbb{R}^{m \times n}$ is of rank r , then it can be factored

$$\mathbf{M} = \mathbf{C}\mathbf{R} \text{ where } \mathbf{C} \in \mathbb{R}^{m \times r} \text{ and } \mathbf{R} \in \mathbb{R}^{r \times n}. \quad (\text{A.7})$$

This implies that the rank determines the number of independent parameters of \mathbf{M} , i.e., $r \times (m + n)$ in Eq. (A.7). If the matrix $\mathbf{M} \in \mathbb{S}_+^d$ is of rank r , then it can be factored

$$\mathbf{M} = \mathbf{L}^\top \mathbf{L} \text{ where } \mathbf{L} \in \mathbb{R}^{r \times d}. \quad (\text{A.8})$$

which implies that \mathbf{M} has $O(r \times d)$ independent parameters in Eq.(A.8).³⁹

A.3 Projection onto the PSD Cone

We define a projection of a point on a convex set.

Definition A.3.1. The distance of a point $\mathbf{x}_0 \in \mathbb{R}^n$ to a closed set $\mathcal{C} \subseteq \mathbb{R}^n$, in the norm $\|\cdot\|$, is defined as

$$\text{dist}(\mathbf{x}_0, \mathcal{C}) = \inf\{\|\mathbf{x}_0 - \mathbf{x}\| \mid \mathbf{x} \in \mathcal{C}\}$$

The infimum is always achieved in our case. Any point $\mathbf{z} \in \mathcal{C}$ which satisfies $\|\mathbf{z} - \mathbf{x}_0\| = \text{dist}(\mathbf{x}_0, \mathcal{C})$, i.e., which is closest to \mathbf{x}_0 , is called a projection of \mathbf{x}_0 on \mathcal{C} . When \mathcal{C} is closed and convex, and when the norm is strictly convex (e.g., the Euclidean norm), then the projection $\mathbf{z} \in \mathcal{C}$ of \mathbf{x}_0 on \mathcal{C} is unique.

³⁹Actually, when $\text{rank}(\mathbf{M}) = d$, the number of independent parameters is $\sum_{i=1}^d i = \frac{d(d+1)}{2}$ since \mathbf{M} is symmetric.

We note $\Pi_{\mathcal{C}} : \mathbb{R}^n \rightarrow \mathbb{R}^n$ any function for which $\Pi_{\mathcal{C}}(\mathbf{x}_0)$ is a projection of \mathbf{x}_0 on \mathcal{C} :

$$\Pi_{\mathcal{C}}(\mathbf{x}_0) = \underset{\mathbf{x}}{\operatorname{argmin}} \{ \|\mathbf{x} - \mathbf{x}_0\| \mid \mathbf{x} \in \mathcal{C} \} \quad (\text{A.9})$$

Note that when $\mathcal{C} = \mathbb{R}^n$, we have $\Pi_{\mathcal{C}}(\mathbf{x}_0) = \mathbf{x}_0$. In this thesis, we particularly consider two widely used projections that are useful for Mahalanobis distance metric learning:

For $\mathcal{C} = \mathbb{S}_+^d$, and the Euclidean (or Frobenius) norm $\|\cdot\|_F$, we have the following projection $\Pi_{\mathbb{S}_+^d}(\mathbf{X}_0) = \sum_{i=1}^d \max\{0, \lambda_i\} v_i v_i^\top$ where $\mathbf{X}_0 = \sum_{i=1}^d \lambda_i v_i v_i^\top$ is the eigendecomposition of $\mathbf{X}_0 \in \mathbb{S}^d$. The projection on \mathbb{S}_+^d is obtained by forming the eigendecomposition of \mathbf{X}_0 and dropping terms associated with negative eigenvalues.

For $\mathcal{C} = \mathbb{R}_+^d$, we have $\Pi_{\mathcal{C}}(\mathbf{x}_0)_k = \max\{x_{0k}, 0\}$ where $\mathbf{x}_0 = (x_{01}, \dots, x_{0d})$. The Euclidean projection of a vector onto the nonnegative orthant is obtained by replacing negative components of the vector with 0.

Appendix B

Solver for the Vector Optimization Problem

We describe here the optimization process when the goal is to learn a dissimilarity function $\mathcal{D}_{\mathbf{w}}$ parameterized by a vector \mathbf{w} .

B.1 Primal Form of the Optimization Problem

We first rewrite Eq. (2.10) in the primal form in order to use the efficient and scalable primal Newton method [Chapelle and Keerthi, 2010].

The first two constraints of Eq. (2.10) over \mathcal{S} and \mathcal{D} try to satisfy Eq. (2.4) and Eq. (2.5). They are equivalent to $y_{ij}(\mathcal{D}_{\mathbf{w}}(\mathcal{I}_i, \mathcal{I}_j) - b) \geq 1 - \xi_{ij}$ where $y_{ij} = 1 \iff (\mathcal{I}_i, \mathcal{I}_j) \in \mathcal{D}$ and $y_{ij} = -1 \iff (\mathcal{I}_i, \mathcal{I}_j) \in \mathcal{S}$. Eq. (2.10) can then be rewritten equivalently:

$$\begin{aligned} \min_{(\mathbf{w}, b)} & \frac{1}{2}(\|\mathbf{w}\|_2^2 + b^2) + C_P \sum_{(\mathcal{I}_i, \mathcal{I}_j) \in \mathcal{S} \cup \mathcal{D}} L_1(y_{ij}, \mathcal{D}_{\mathbf{w}}(\mathcal{I}_i, \mathcal{I}_j) - b) \\ & + C_Q \sum_{q \in \mathcal{N}} L_{\delta_q}(1, \mathcal{D}_{\mathbf{w}}(\mathcal{I}_k, \mathcal{I}_l) - \mathcal{D}_{\mathbf{w}}(\mathcal{I}_i, \mathcal{I}_j)) \\ \text{s.t. } & \mathbf{w} \in \mathcal{C}^d, b \in \mathcal{C} \end{aligned} \tag{B.1}$$

where L_1 and L_{δ_q} are loss functions and $y_{ij} \in \{-1; 1\}$. In particular, for Eq. (2.10) and Eq. (B.1) to be strictly equivalent, they have to correspond to the classic hinge loss function $L_{\delta}(y, t) = \max(0, \delta - yt)$. We actually use a differentiable approximation of this function to have good convergence properties [Chapelle, 2007, Chapelle and Keerthi, 2010].

For convenience, we rewrite some variables:

- $\boldsymbol{\omega} = [\mathbf{w}^\top, b]^\top$ is the concatenation of \mathbf{w} and b in a single $(d+1)$ -dimensional vector. We note $e = d+1$ and then have $\boldsymbol{\omega} \in \mathbb{R}^e$.
- $\mathbf{c}_{ij} = [(\Psi(\mathcal{I}_i, \mathcal{I}_j))^\top, -1]^\top$ is the concatenation vector of $\Psi(\mathcal{I}_i, \mathcal{I}_j)$ and -1 . We also have $\mathbf{c}_{ij} \in \mathbb{R}^e$.
- $p = (\mathcal{I}_i, \mathcal{I}_j) \iff \mathbf{c}_p = \mathbf{c}_{ij}$ and $y_p = y_{ij}$.
- $q = (\mathcal{I}_i, \mathcal{I}_j, \mathcal{I}_k, \mathcal{I}_l) \iff \mathbf{z}_q = \mathbf{x}_{kl} - \mathbf{x}_{ij}$.

Eq. (B.1) can be rewritten equivalently with these variables:

$$\begin{aligned} \min_{\boldsymbol{\omega} \in \mathcal{C}^e} \quad & \frac{1}{2} \|\boldsymbol{\omega}\|_2^2 + C_P \sum_{p \in \mathcal{S} \cup \mathcal{D}} L_1(y_p, \boldsymbol{\omega}^\top \mathbf{c}_p) \\ & + C_Q \sum_{q \in \mathcal{N}} L_{\delta_q}(1, \boldsymbol{\omega}^\top \mathbf{z}_q) \end{aligned} \quad (\text{B.2})$$

With such a regularization, our scheme may be compared to a RankSVM [Chapelle and Keerthi, 2010], with the exception that the loss function L_{δ_q} works on quadruplets. The complexity of this convex problem w.r.t. $\boldsymbol{\omega}$ is linear in the number of constraints (i.e., the cardinality of $\mathcal{N} \cup \mathcal{D} \cup \mathcal{S}$). It can be solved with a classic or stochastic (sub)gradient descent w.r.t. $\boldsymbol{\omega}$ depending on the number of constraints. The number of parameters to learn is small and grows linearly with the input space dimension, limiting overfitting [Mignon and Jurie, 2012]. It can also be extended to kernels [Chapelle and Keerthi, 2010].

We describe in the following how to apply Newton method [Keerthi and DeCoste, 2005, Chapelle, 2007, Chapelle and Keerthi, 2010] to solve Eq. (B.2) with good convergence properties. The primal Newton method [Chapelle and Keerthi, 2010] is known to be fast for SVM classifier and RankSVM training. As our vector model is an extension of the RankSVM model, the learning is also fast.

B.2 Loss Functions

Let us first describe loss functions that are appropriate for Newton method. Since the hinge loss function is not differentiable, we use differentiable approximations of L_1 and L_{δ_q} inspired by the Huber loss function.

For simplicity, we also constrain the domain of δ_q to be 0 or 1 (i.e., $\delta_q \in \{0, 1\}$). The set \mathcal{N} can then be partitioned as two sets \mathcal{N} and \mathcal{B} such that for all:

- $q \in \mathcal{N}, \delta_q = 1 \iff q \in \mathcal{N}$
- $q \in \mathcal{N}, \delta_q = 0 \iff q \in \mathcal{B}$

In Eq. (B.2), we consider $t_p = \boldsymbol{\omega}^\top \mathbf{c}_p$ or $t_q = \boldsymbol{\omega}^\top \mathbf{z}_q$. Without loss of generality, let us consider t_r with $r \in \beta$ (with $\beta = \mathcal{S}, \mathcal{D}, \mathcal{N}$ or \mathcal{B}) and $y \in \{-1, +1\}$. Our loss functions are written:

$$L_1^h(y, t_r) = \begin{cases} 0 & \text{if } yt_r > 1 + h & \text{set: } \beta_{1,y}^0 \\ \frac{(1+h-yt_r)^2}{4h} & \text{if } |1-yt_r| \leq h & \text{set: } \beta_{1,y}^Q \\ 1-yt_r & \text{if } yt_r < 1-h & \text{set: } \beta_{1,y}^L \end{cases} \quad (\text{B.3})$$

$$L_0^h(y, t_r) = \begin{cases} 0 & \text{if } yt_r > 0 & \text{set: } \beta_{0,y}^0 \\ \frac{t_r^2}{4h} & \text{if } |-h-yt_r| \leq h & \text{set: } \beta_{0,y}^Q \\ -h-yt_r & \text{if } yt_r < -2h & \text{set: } \beta_{0,y}^L \end{cases} \quad (\text{B.4})$$

where $h \in [0.01, 0.5]$. In all our experiments, we set $h = 0.05$. Fig. B.1 illustrates the loss functions L_1^h and L_0^h for the values $h = 0.5$ and $y = 1$.

As described in [Chapelle, 2007], L_1^h is inspired from the Huber loss function, it is a differentiable approximation of the hinge loss ($L_1(y, t) = \max(0, 1 - yt)$) when $h \rightarrow 0$. Similarly, L_0^h is a differentiable approximation when $h \rightarrow 0$ of $L_0(y, t) = \max(0, -yt)$, the adaptation of the hinge loss that considers the absence of security margin. Given set β and $y \in \{-1, +1\}$, we can infer three disjoint sets:

- $\beta_{i,y}^0$ is the subset of elements in β that have zero loss in $L_i^h(y, \cdot)$.
- $\beta_{i,y}^Q$ is the subset of elements in β that are in the quadratic part of $L_i^h(y, \cdot)$.
- $\beta_{i,y}^L$ is the subset of elements in β in the non-zero loss linear part of $L_i^h(y, \cdot)$.

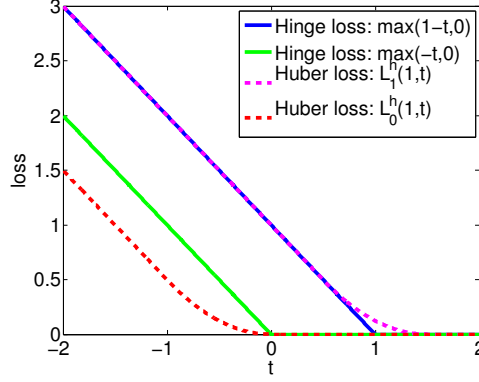


Figure B.1: Illustration of the different loss functions used in this paper for the values $y = 1$ and $h = 0.5$.

Algorithm 4 Projected Newton Step

Require: Sets \mathcal{S} , \mathcal{D} , \mathcal{N} , \mathcal{B} (some of them can be empty)

- 1: Iteration $t = 0$
 - 2: Initialize $\omega_t \in \mathcal{C}^e$ (e.g., $\omega_t = \mathbf{1}$)
 - 3: Initialize the step size $\eta_t > 0$ (e.g., $\eta_t = 1$)
 - 4: **repeat**
 - 5: Compute ∇_t and \mathbf{H}_t (gradient and hessian w.r.t. ω_t)
 - 6: $\omega_{t+1} \leftarrow \Pi_{\mathcal{C}^e}(\omega_t - \eta_t \mathbf{H}_t^{-1} \nabla_t)$
 - 7: $t \leftarrow t + 1$
 - 8: **until** $\|\omega_t - \omega_{t-1}\|_2^2 \leq \epsilon$
 - 9: **Return** ω_t
-

B.3 Gradient and Hessian Matrices

By considering $L_1 = L_1^h$ and $L_0 = L_0^h$ in Eq. (B.2), the gradient $\nabla \in \mathbb{R}^e$ of Eq. (B.2) w.r.t. ω is:

$$\begin{aligned}
\nabla = & \omega + \frac{C_P}{2h} \sum_{p \in (\mathcal{S} \cup \mathcal{D})_{1, y_p}^Q} (\omega^\top \mathbf{c}_p - (1+h)y_p) \mathbf{c}_p \\
& - C_P \sum_{p \in (\mathcal{S} \cup \mathcal{D})_{1, y_p}^L} y_p \mathbf{c}_p + \frac{C_Q}{2h} \sum_{q \in \mathcal{N}_{1,1}^Q} (\omega^\top \mathbf{z}_q - (1+h)) \mathbf{z}_q \\
& + \frac{C_Q}{2h} \sum_{q \in \mathcal{B}_{0,1}^Q} (\omega^\top \mathbf{z}_q) \mathbf{z}_q - C_Q \sum_{q \in (\mathcal{N}_{1,1}^L \cup \mathcal{B}_{0,1}^L)} \mathbf{z}_q
\end{aligned} \tag{B.5}$$

and the Hessian matrix $\mathbf{H} \in \mathbb{R}^{e \times e}$ of Eq. B.2 w.r.t. ω is:

$$\mathbf{H} = \mathbf{I}_e + \frac{C_P}{2h} \sum_{p \in (\mathcal{S} \cup \mathcal{D})_{1, y_p}^Q} \mathbf{c}_p \mathbf{c}_p^\top + \frac{C_Q}{2h} \sum_{q \in (\mathcal{N}_{1,1}^Q \cup \mathcal{B}_{0,1}^Q)} \mathbf{z}_q \mathbf{z}_q^\top \tag{B.6}$$

where $\mathbf{I}_e \in \mathbb{R}^{e \times e}$ is the identity matrix. \mathbf{H} is the sum of a positive definite matrix (\mathbf{I}_e) and of positive semi-definite matrices. \mathbf{H} is then positive definite, and thus invertible (because every positive definite matrix is invertible).

Proof: \mathbf{H} can be written $\mathbf{H} = \mathbf{I}_e + \mathbf{B}$ with $\mathbf{B} \in \mathbb{R}^{e \times e}$ a positive semi-definite matrix. For all vector

$\mathbf{z} \in \mathbb{R}^e$, we have $\mathbf{z}^\top \mathbf{H} \mathbf{z} = \mathbf{z}^\top \mathbf{I}_e \mathbf{z} + \mathbf{z}^\top \mathbf{B} \mathbf{z}$. By definition of positive (semi-)definiteness, we have the following property: for all nonzero $\mathbf{z} \in \mathbb{R}^e$, $\mathbf{z}^\top \mathbf{I}_e \mathbf{z} > 0$ and $\mathbf{z}^\top \mathbf{B} \mathbf{z} \geq 0$. Then for all nonzero $\mathbf{z} \in \mathbb{R}^e$, $\mathbf{z}^\top \mathbf{H} \mathbf{z} > 0$. \mathbf{H} is then a positive definite matrix. \square

The global learning scheme is described in Algorithm 4. The step size $\eta_t > 0$ can be set to 1 and unchanged as in [Chapelle, 2007], or optimized at each iteration through line search (see Section 9.5.2 in [Boyd and Vandenberghe, 2004]). The parameter $\epsilon \geq 0$ determines the stopping criterion by controlling the ℓ_2 -norm of the difference of $\boldsymbol{\omega}$ between iteration t and $t - 1$.

Complexity: Computing the Hessian takes $O(\sigma e^2)$ time (where $\sigma = |(\mathcal{S} \cup \mathcal{D})_{1,y_p}^Q| + |(\mathcal{N}_{1,1}^Q \cup \mathcal{B}_{0,1}^Q)|$) and solving the linear system is $O(e^3)$ because of the inversion of $\mathbf{H}_t \in \mathbb{R}^{e \times e}$. This can be prohibitive if e is large but we restrict $e \leq 1001$ in our experiments; the inversion of \mathbf{H}_t is then very fast. Other optimization methods are proposed in [Chapelle and Keerthi, 2010] (e.g., a truncated Newton method) if e is large.

The projected gradient method requires the projection of the learned vector on the set \mathcal{C}^d at each iteration. The Euclidean projection on \mathbb{R}^d of all vector $\mathbf{a} \in \mathbb{R}^d$ is itself ($\Pi_{\mathbb{R}^d}(\mathbf{a}) = \mathbf{a}$, there is no need of projection in this case) and its projection on \mathbb{R}_+^d is found by replacing each negative component of \mathbf{a} with 0. The latter projection is linear in the size of \mathbf{w} and ensures that the symmetric matrix $\text{Diag}(\mathbf{w}) = \mathbf{M}$ is PSD.

Bibliography

- [Abiteboul, 2002] Abiteboul, S. (2002). Issues in monitoring web data. In *Database and Expert Systems Applications (DEXA)*, pages 51–69. Springer. [66](#)
- [Adar et al., 2009a] Adar, E., Teevan, J., and Dumais, S. (2009a). Resonance on the web: web dynamics and revisitation patterns. In *CHI*. [68](#), [72](#)
- [Adar et al., 2009b] Adar, E., Teevan, J., Dumais, S., and Elsas, J. (2009b). The web changes everything: understanding the dynamics of web content. In *ACM WSDM Conference Series Web Search and Data Mining (WSDM)*. ACM. [67](#), [71](#), [74](#)
- [Agarwal et al., 2007] Agarwal, S., Wills, J., Cayton, L., Lanckriet, G., Kriegman, D. J., and Belongie, S. (2007). Generalized non-metric multidimensional scaling. In *International Conference on Artificial Intelligence and Statistics (AISTATS)*, pages 11–18. [24](#)
- [Akata et al., 2013] Akata, Z., Perronnin, F., Harchaoui, Z., and Schmid, C. (2013). Label-embedding for attribute-based classification. In *IEEE Conference on Computer Vision and Pattern Recognition (CVPR)*, pages 819–826. IEEE. [11](#), [12](#), [15](#)
- [Avila et al., 2013] Avila, S., Thome, N., Cord, M., Valle, E., and de A. Araújo, A. (2013). Pooling in image representation: The visual codeword point of view. *Computer Vision and Image Understanding (CVIU)*, 117(5):453 – 465. [8](#)
- [Bach et al., 2004] Bach, F. R., Lanckriet, G. R., and Jordan, M. I. (2004). Multiple kernel learning, conic duality, and the smo algorithm. In *Proceedings of the twenty-first international conference on Machine learning*, page 6. ACM. [10](#)
- [Bartlett et al., 2006] Bartlett, P. L., Jordan, M. I., and McAuliffe, J. D. (2006). Convexity, classification, and risk bounds. *Journal of the American Statistical Association*, 101(473):138–156. [16](#)
- [Bellet et al., 2013] Bellet, A., Habrard, A., and Sebban, M. (2013). A Survey on Metric Learning for Feature Vectors and Structured Data. *ArXiv e-prints*. [15](#), [17](#)
- [Ben Saad and Gañarski, 2011] Ben Saad, M. and Gañarski, S. (2011). Archiving the Web using Page Changes Pattern: A Case Study. In *JCDL*. [66](#), [67](#), [72](#)
- [Bengio, 2013] Bengio, Y. (2013). Deep learning of representations: Looking forward. In *Proceedings of the First International Conference on Statistical Language and Speech Processing, SLSP’13*, pages 1–37. [10](#)
- [Bengio et al., 2013] Bengio, Y., Courville, A., and Vincent, P. (2013). Representation learning: A review and new perspectives. *Pattern Analysis and Machine Intelligence, IEEE Transactions on*, 35(8):1798–1828. [11](#)
- [Bengio et al., 2007] Bengio, Y., Lamblin, P., Popovici, D., and Larochelle, H. (2007). Greedy layer-wise training of deep networks. *Advances in neural information processing systems (NIPS)*, 19:153. [9](#)

- [Biederman, 1987] Biederman, I. (1987). Recognition-by-components: a theory of human image understanding. *Psychological review*, 94(2):115. [3](#)
- [Borg and Groenen, 2005] Borg, I. and Groenen, P. (2005). Modern multidimensional scaling: Theory and applications. *Springer Series in Statistics*. [2](#), [11](#)
- [Boureau et al., 2010] Boureau, Y.-L., Bach, F., LeCun, Y., and Ponce, J. (2010). Learning mid-level features for recognition. In *IEEE Conference on Computer Vision and Pattern Recognition (CVPR)*, pages 2559–2566. IEEE. [7](#)
- [Boyd et al., 2011] Boyd, S., Parikh, N., Chu, E., Peleato, B., and Eckstein, J. (2011). Distributed optimization and statistical learning via the alternating direction method of multipliers. *Foundations and Trends in Machine Learning*, 3(1):1–122. [62](#)
- [Boyd and Vandenberghe, 2008] Boyd, S. and Vandenberghe, L. (2008). Subgradient. *Notes for EE364b, Stanford University, Winter 2006-07*. [35](#)
- [Boyd and Vandenberghe, 2004] Boyd, S. P. and Vandenberghe, L. (2004). *Convex optimization*. Cambridge university press. [13](#), [90](#)
- [Cai et al., 2003] Cai, D., Yu, S., Wen, J., and Ma, W. (2003). Vips: a vision-based page segmentation algorithm. *Microsoft Technical Report, MSR-TR-2003-79-2003*. [79](#)
- [Candès et al., 2008] Candès, E. J., Wakin, M. B., and Boyd, S. P. (2008). Enhancing sparsity by reweighted l1 minimization. *Journal of Fourier analysis and applications*, 14(5-6):877–905. [62](#), [82](#)
- [Chapelle, 2007] Chapelle, O. (2007). Training a support vector machine in the primal. *Neural Computation*, 19(5):1155–1178. [17](#), [34](#), [87](#), [88](#), [90](#)
- [Chapelle and Keerthi, 2010] Chapelle, O. and Keerthi, S. S. (2010). Efficient algorithms for ranking with svms. *Inf. Retrieval*, 13(3):201–215. [34](#), [36](#), [37](#), [87](#), [88](#), [90](#)
- [Chatfield et al., 2011] Chatfield, K., Lempitsky, V., Vedaldi, A., and Zisserman, A. (2011). The devil is in the details: an evaluation of recent feature encoding methods. *BMVC*. [9](#)
- [Chechik et al., 2009] Chechik, G., Shalit, U., Sharma, V., and Bengio, S. (2009). An online algorithm for large scale image similarity learning. In *Advances in Neural Information Processing Systems (NIPS)*, pages 306–314. [2](#), [15](#)
- [Chechik et al., 2010] Chechik, G., Sharma, V., Shalit, U., and Bengio, S. (2010). Large scale online learning of image similarity through ranking. *JMLR*, 11:1109–1135. [20](#), [23](#)
- [Cho and Garcia-Molina, 2000] Cho, J. and Garcia-Molina, H. (2000). The evolution of the web and implications for an incremental crawler. *Very Large Data Bases (VLDB)*. [66](#), [67](#)
- [Chopra et al., 2005] Chopra, S., Hadsell, R., and LeCun, Y. (2005). Learning a similarity metric discriminatively, with application to face verification. In *IEEE Conference on Computer Vision and Pattern Recognition (CVPR)*, volume 1, pages 539–546. IEEE. [2](#), [3](#)
- [Coates and Ng, 2011] Coates, A. and Ng, A. Y. (2011). The importance of encoding versus training with sparse coding and vector quantization. In *Proceedings of the 28th International Conference on Machine Learning (ICML-11)*, pages 921–928. [7](#)
- [Cortes and Vapnik, 1995] Cortes, C. and Vapnik, V. (1995). Support-vector networks. *Machine learning*, 20(3):273–297. [1](#), [6](#), [10](#), [17](#)
- [Cover and Hart, 1967] Cover, T. and Hart, P. (1967). Nearest neighbor pattern classification. *Information Theory, IEEE Transactions on*, 13(1):21–27. [10](#)

-
- [Crammer and Singer, 2002] Crammer, K. and Singer, Y. (2002). On the algorithmic implementation of multiclass kernel-based vector machines. *The Journal of Machine Learning Research*, 2:265–292. [21](#)
- [Criminisi et al., 2004] Criminisi, A., Pérez, P., and Toyama, K. (2004). Region filling and object removal by exemplar-based image inpainting. *IEEE Transactions on Image Processing*, 13(9):1200–1212. [28](#)
- [Cula and Dana, 2004] Cula, O. G. and Dana, K. J. (2004). 3d texture recognition using bidirectional feature histograms. *International Journal of Computer Vision*, 59(1):33–60. [13](#)
- [Dattorro, 2005] Dattorro, J. (2005). *Convex optimization and Euclidean distance geometry*. Meboo Publishing USA. [14](#), [53](#)
- [Davis et al., 2007] Davis, J. V., Kulis, B., Jain, P., Sra, S., and Dhillon, I. S. (2007). Information-theoretic metric learning. In *International Conference on Machine Learning (ICML)*. [20](#), [23](#), [26](#), [31](#), [50](#), [57](#), [58](#)
- [Deng et al., 2011] Deng, J., Berg, A. C., and Fei-Fei, L. (2011). Hierarchical semantic indexing for large scale image retrieval. In *IEEE Conference on Computer Vision and Pattern Recognition (CVPR)*, pages 785–792. IEEE. [15](#)
- [Deng et al., 2009] Deng, J., Dong, W., Socher, R., Li, L.-J., Li, K., and Fei-Fei, L. (2009). Imagenet: A large-scale hierarchical image database. In *IEEE Conference on Computer Vision and Pattern Recognition (CVPR)*. [45](#)
- [Douglass et al., 1998] Douglass, F., Ball, T., Chen, Y.-F., and Koutsofios, E. (1998). The at&t internet difference engine: Tracking and viewing changes on the web. *World Wide Web*, 1(1):27–44. [66](#)
- [Douze et al., 2009] Douze, M., Jégou, H., Sandhawalia, H., Amsaleg, L., and Schmid, C. (2009). Evaluation of gist descriptors for web-scale image search. In *CIVR*. [71](#)
- [Duchenne et al., 2011] Duchenne, O., Joulin, A., and Ponce, J. (2011). A graph-matching kernel for object categorization. In *Computer Vision (ICCV), 2011 IEEE International Conference on*, pages 1792–1799. IEEE. [9](#)
- [Fan, 1949] Fan, K. (1949). On a theorem of weyl concerning eigenvalues of linear transformations i. *Proceedings of the National Academy of Sciences of the United States of America*, 35(11):652. [53](#)
- [Farhadi et al., 2009] Farhadi, A., Endres, I., Hoiem, D., and Forsyth, D. (2009). Describing objects by their attributes. In *IEEE Conference on Computer Vision and Pattern Recognition (CVPR)*, pages 1778–1785. IEEE. [11](#)
- [Fazel, 2002] Fazel, M. (2002). *Matrix rank minimization with applications*. PhD thesis, Stanford University. [26](#), [50](#)
- [Fei-Fei et al., 2007] Fei-Fei, L., Fergus, R., and Perona, P. (2007). Learning generative visual models from few training examples: An incremental bayesian approach tested on 101 object categories. *Computer Vision and Image Understanding*, 106(1):59–70. [8](#)
- [Fei-Fei and Perona, 2005] Fei-Fei, L. and Perona, P. (2005). A bayesian hierarchical model for learning natural scene categories. In *IEEE Conference on Computer Vision and Pattern Recognition (CVPR)*, volume 2, pages 524–531. IEEE. [6](#)
- [Feng et al., 2011] Feng, J., Ni, B., Tian, Q., and Yan, S. (2011). Geometric lp-norm feature pooling for image classification. In *IEEE Conference on Computer Vision and Pattern Recognition (CVPR)*, pages 2609–2704. IEEE. [8](#), [9](#)
- [Fisher, 1938] Fisher, R. A. (1938). The statistical utilization of multiple measurements. *Annals of Human Genetics*, 8(4):376–386. [11](#)

- [Flesca and Masciari, 2003] Flesca, S. and Masciari, E. (2003). Efficient and effective web change detection. *Data & Knowledge Engineering*, 46(2):203–224. [66](#)
- [Freund and Schapire, 1995] Freund, Y. and Schapire, R. E. (1995). A decision-theoretic generalization of on-line learning and an application to boosting. In *Computational learning theory*, pages 23–37. Springer. [17](#)
- [Friedman et al., 2000] Friedman, J., Hastie, T., Tibshirani, R., et al. (2000). Additive logistic regression: a statistical view of boosting (with discussion and a rejoinder by the authors). *The annals of statistics*, 28(2):337–407. [17](#)
- [Frome et al., 2007] Frome, A., Singer, Y., Sha, F., and Malik, J. (2007). Learning globally-consistent local distance functions for shape-based image retrieval and classification. In *IEEE International Conference on Computer Vision (ICCV)*. [2](#), [23](#)
- [Galton, 1889] Galton, F. (1889). *Natural inheritance*, volume 42. Macmillan. [11](#)
- [Geman et al., 1992] Geman, S., Bienenstock, E., and Doursat, R. (1992). Neural networks and the bias/variance dilemma. *Neural computation*, 4(1):1–58. [27](#)
- [Globerson and Roweis, 2006] Globerson, A. and Roweis, S. (2006). Metric learning by collapsing classes. *Advances in neural information processing systems (NIPS)*. [14](#)
- [Globerson and Roweis, 2007] Globerson, A. and Roweis, S. T. (2007). Visualizing pairwise similarity via semidefinite programming. In *International Conference on Artificial Intelligence and Statistics*, pages 139–146. [13](#)
- [Goh et al., 2012] Goh, H., Thome, N., Cord, M., and Lim, J.-H. (2012). Unsupervised and supervised visual codes with restricted boltzmann machines. In *Computer Vision–ECCV 2012*, pages 298–311. Springer. [7](#), [9](#)
- [Goldberger et al., 2004] Goldberger, J., Roweis, S., Hinton, G., and Salakhutdinov, R. (2004). Neighbourhood components analysis. *Advances in neural information processing systems (NIPS)*. [2](#), [3](#), [18](#), [23](#)
- [Goodrum, 2000] Goodrum, A. A. (2000). Image information retrieval: An overview of current research. *Informing Science*, 3(2):63–66. [10](#)
- [Grauman and Darrell, 2005] Grauman, K. and Darrell, T. (2005). The pyramid match kernel: Discriminative classification with sets of image features. In *Computer Vision, 2005. ICCV 2005. Tenth IEEE International Conference on*, volume 2, pages 1458–1465. IEEE. [9](#)
- [Guillaumin et al., 2009] Guillaumin, M., Verbeek, J., and Schmid, C. (2009). Is that you? metric learning approaches for face identification. In *IEEE International Conference on Computer Vision (ICCV)*. [2](#), [3](#), [20](#), [23](#), [57](#), [58](#), [59](#)
- [Harris and Stephens, 1988] Harris, C. and Stephens, M. (1988). A combined corner and edge detector. In *Alvey vision conference*, volume 15, page 50. Manchester, UK. [6](#)
- [Hinton et al., 2006] Hinton, G., Osindero, S., and Teh, Y.-W. (2006). A fast learning algorithm for deep belief nets. *Neural computation*, 18(7):1527–1554. [9](#)
- [Hotelling, 1933] Hotelling, H. (1933). Analysis of a complex of statistical variables into principal components. *Journal of educational psychology*, 24(6):417. [11](#)
- [Hu et al., 2013] Hu, Y., Zhang, D., Ye, J., Li, X., and He, X. (2013). Fast and accurate matrix completion via truncated nuclear norm regularization. *IEEE PAMI*, 35(9):2117–2130. [28](#), [50](#), [62](#)

-
- [Huang et al., 2007] Huang, G. B., Ramesh, M., Berg, T., and Learned-Miller, E. (2007). Labeled faces in the wild: A database for studying face recognition in unconstrained environments. Technical Report 07-49, University of Massachusetts, Amherst. [57](#)
- [Hunter and Lange, 2004] Hunter, D. R. and Lange, K. (2004). A tutorial on mm algorithms. *The American Statistician*, 58(1):30–37. [62](#)
- [Hwang et al., 2011] Hwang, S. J., Grauman, K., and Sha, F. (2011). Learning a tree of metrics with disjoint visual features. In *Advances in neural information processing systems (NIPS)*. [23](#)
- [Hwang et al., 2013] Hwang, S. J., Grauman, K., and Sha, F. (2013). Analogy-preserving semantic embedding for visual object categorization. In *International Conference on Machine Learning (ICML)*. [24](#)
- [Jacob et al., 2004] Jacob, J., Sanka, A., Pandrangi, N., and Chakravarthy, S. (2004). Web-vigil: an approach to just-in-time information propagation in large network-centric environments. *Web dynamics. Springer*. [66](#)
- [Jatowt et al., 2007] Jatowt, A., Kawai, Y., and Tanaka, K. (2007). Detecting age of page content. In *Proceedings of the 9th annual ACM international workshop on Web information and data management*, pages 137–144. ACM. [67](#)
- [Jégou et al., 2010] Jégou, H., Douze, M., Schmid, C., and Pérez, P. (2010). Aggregating local descriptors into a compact image representation. In *IEEE Conference on Computer Vision and Pattern Recognition (CVPR)*, pages 3304–3311. IEEE. [7](#)
- [Joachims, 2002] Joachims, T. (2002). Optimizing search engines using clickthrough data. In *Proceedings of the eighth ACM SIGKDD international conference on Knowledge discovery and data mining*, pages 133–142. ACM. [18](#), [32](#), [36](#)
- [Joachims, 2005] Joachims, T. (2005). A support vector method for multivariate performance measures. In *Proceedings of the 22nd international conference on Machine learning*, pages 377–384. ACM. [22](#)
- [Joachims et al., 2009] Joachims, T., Finley, T., and Yu, C.-N. J. (2009). Cutting-plane training of structural svms. *Machine Learning*, 77(1):27–59. [22](#)
- [Keerthi and DeCoste, 2005] Keerthi, S. S. and DeCoste, D. (2005). A modified finite newton method for fast solution of large scale linear svms. *Journal of Machine Learning Research*, 6(1):341. [35](#), [88](#)
- [Kohlschütter et al., 2010] Kohlschütter, C., Fankhauser, P., and Nejd, W. (2010). Boilerplate detection using shallow text features. In *ACM WSDM Conference Series Web Search and Data Mining (WSDM)*. ACM. [67](#)
- [Kovashka et al., 2012] Kovashka, A., Parikh, D., and Grauman, K. (2012). Whittlesearch: Image search with relative attribute feedback. In *IEEE Conference on Computer Vision and Pattern Recognition (CVPR)*. [12](#)
- [Krizhevsky et al., 2012] Krizhevsky, A., Sutskever, I., and Hinton, G. E. (2012). Imagenet classification with deep convolutional neural networks. In *Advances in neural information processing systems*, pages 1097–1105. [2](#), [5](#), [9](#)
- [Kruskal, 1964] Kruskal, J. B. (1964). Nonmetric multidimensional scaling: a numerical method. *Psychometrika*, 29(2):115–129. [24](#)
- [Kulis, 2012] Kulis, B. (2012). Metric learning: a survey. *Found. and Trends in Machine Learning*, 5(4):287–364. [17](#), [18](#), [62](#)
- [Kumar et al., 2009] Kumar, N., Berg, A., Belhumeur, P., and Nayar, S. (2009). Attribute and simile classifiers for face verification. In *IEEE International Conference on Computer Vision (ICCV)*. [11](#), [40](#), [60](#)

- [Lajugie et al., 2014] Lajugie, R., Bach, F., and Arlot, S. (2014). Large margin metric learning for constrained partitioning problems. In *Proc. International Conference on Machine Learning*. 22
- [Lampert et al., 2009] Lampert, C. H., Nickisch, H., and Harmeling, S. (2009). Learning to detect unseen object classes by between-class attribute transfer. In *IEEE Conference on Computer Vision and Pattern Recognition (CVPR)*, pages 951–958. IEEE. 2, 11, 38
- [Law et al., 2012a] Law, M., Thome, N., and Cord, M. (2012a). Hybrid pooling fusion in the bow pipeline. In *Proceedings of the 12th international conference on Computer Vision - Volume Part III, ECCV’12*, pages 355–364, Berlin, Heidelberg. Springer-Verlag. 8
- [Law et al., 2013] Law, M. T., Thome, N., and Cord, M. (2013). Quadruplet-wise image similarity learning. In *IEEE International Conference on Computer Vision (ICCV)*. 29, 65
- [Law et al., 2014a] Law, M. T., Thome, N., and Cord, M. (2014a). Bag-of-words image representation: Key ideas and further insight. In *Fusion in Computer Vision*, pages 29–52. Springer. 8
- [Law et al., 2014b] Law, M. T., Thome, N., and Cord, M. (2014b). Fantope regularization in metric learning. In *IEEE Conference on Computer Vision and Pattern Recognition (CVPR)*. 49
- [Law et al., 2012b] Law, M. T., Thome, N., Gañarski, S., and Cord, M. (2012b). Structural and visual comparisons for web page archiving. In *ACM Symposium on Document Engineering (DocEng)*. 65, 71, 78, 79
- [Lazebnik et al., 2006] Lazebnik, S., Schmid, C., and Ponce, J. (2006). Beyond bags of features: Spatial pyramid matching for recognizing natural scene categories. In *IEEE Conference on Computer Vision and Pattern Recognition (CVPR)*. 5, 8, 9
- [LeCun et al., 1989] LeCun, Y., Boser, B., Denker, J. S., Henderson, D., Howard, R. E., Hubbard, W., and Jackel, L. D. (1989). Backpropagation applied to handwritten zip code recognition. *Neural computation*, 1(4):541–551. 9
- [Lim et al., 2013] Lim, D., McFee, B., and Lanckriet, G. (2013). Robust structural metric learning. In *International Conference on Machine Learning (ICML)*. 4, 21, 50
- [Lim and Ng, 2001] Lim, S.-J. and Ng, Y.-K. (2001). An automated change-detection algorithm for html documents based on semantic hierarchies. In *IEEE International Conference in Data Engineering (ICDE)*. 66
- [Liu et al., 2000] Liu, L., Pu, C., and Tang, W. (2000). Webcq-detecting and delivering information changes on the web. In *CIKM*. ACM. 66
- [Liu et al., 2011] Liu, L., Wang, L., and Liu, X. (2011). In defense of soft-assignment coding. In *Computer Vision (ICCV), 2011 IEEE International Conference on*, pages 2486–2493. IEEE. 5, 7, 8, 9
- [Lowe, 2004] Lowe, D. (2004). Distinctive image features from scale-invariant keypoints. *IJCV*, 60(2):91–110. 6, 57
- [Luo et al., 2009] Luo, P., Fan, J., Liu, S., Lin, F., Xiong, Y., and Liu, J. (2009). Web article extraction for web printing: a dom+ visual based approach. In *ACM Symposium on Document Engineering (DocEng)*. ACM. 67
- [Ma and Manjunath, 1997] Ma, W. and Manjunath, B. (1997). Netra: A toolbox for navigating large image databases. In *ICIP*. 1, 5, 6
- [MacQueen et al., 1967] MacQueen, J. et al. (1967). Some methods for classification and analysis of multivariate observations. In *Proceedings of the fifth Berkeley symposium on mathematical statistics and probability*, volume 1, pages 281–297. California, USA. 10

-
- [Mahalanobis, 1936] Mahalanobis, P. C. (1936). On the generalized distance in statistics. *Proceedings of the National Institute of Sciences (Calcutta)*, 2:49–55. [14](#)
- [Mahdavi, 2014] Mahdavi, M. (2014). Exploiting smoothness in statistical learning, sequential prediction, and stochastic optimization. *arXiv preprint arXiv:1407.5908*. [17](#)
- [McFee and Lanckriet, 2009] McFee, B. and Lanckriet, G. (2009). Partial order embedding with multiple kernels. In *International Conference on Machine Learning (ICML)*, pages 721–728. ACM. [24](#)
- [McFee and Lanckriet, 2010] McFee, B. and Lanckriet, G. (2010). Metric learning to rank. In *International Conference on Machine Learning (ICML)*. [4](#), [21](#), [22](#), [23](#), [50](#), [63](#)
- [Mensink et al., 2013] Mensink, T., Verbeek, J., Perronnin, F., and Csurka, G. (2013). Distance-based image classification: Generalizing to new classes at near-zero cost. *IEEE Transactions on Pattern Analysis and Machine Intelligence*, 35(11):2624–2637. [2](#), [3](#), [10](#), [12](#), [27](#), [50](#), [55](#)
- [Mignon and Jurie, 2012] Mignon, A. and Jurie, F. (2012). Pcca: A new approach for distance learning from sparse pairwise constraints. In *IEEE Conference on Computer Vision and Pattern Recognition (CVPR)*. [3](#), [14](#), [17](#), [21](#), [23](#), [27](#), [31](#), [50](#), [55](#), [57](#), [58](#), [59](#), [88](#)
- [Mikolajczyk and Schmid, 2004] Mikolajczyk, K. and Schmid, C. (2004). Scale & affine invariant interest point detectors. *International journal of computer vision*, 60(1):63–86. [6](#)
- [Mood, 1950] Mood, A. M. (1950). Introduction to the theory of statistics. [13](#)
- [Natarajan, 1995] Natarajan, B. K. (1995). Sparse approximate solutions to linear systems. *SIAM journal on computing*, 24(2):227–234. [26](#), [49](#)
- [Ntoulas et al., 2004] Ntoulas, A., Cho, J., and Olston, C. (2004). What’s new on the web?: the evolution of the web from a search engine perspective. In *World Wide Web Conference (WWW)*. ACM. [67](#)
- [Oliva and Torralba, 2001] Oliva, A. and Torralba, A. (2001). Modeling the shape of the scene: A holistic representation of the spatial envelope. *IJCV*, 42(3):145–175. [40](#), [60](#), [70](#), [71](#), [72](#), [75](#)
- [Oquab et al., 2014] Oquab, M., Bottou, L., Laptev, I., Sivic, J., et al. (2014). Learning and transferring mid-level image representations using convolutional neural networks. In *IEEE Conference on Computer Vision and Pattern Recognition (CVPR)*. [10](#)
- [Overton and Womersley, 1992] Overton, M. L. and Womersley, R. S. (1992). On the sum of the largest eigenvalues of a symmetric matrix. *SIAM Journal on Matrix Analysis and Applications*, 13(1):41–45. [53](#)
- [Overton and Womersley, 1993] Overton, M. L. and Womersley, R. S. (1993). Optimality conditions and duality theory for minimizing sums of the largest eigenvalues of symmetric matrices. *Mathematical Programming*, 62(1-3):321–357. [53](#), [54](#)
- [Parikh and Grauman, 2011] Parikh, D. and Grauman, K. (2011). Relative attributes. In *IEEE International Conference on Computer Vision (ICCV)*. [2](#), [12](#), [17](#), [23](#), [30](#), [31](#), [38](#), [39](#), [40](#), [41](#), [42](#), [43](#), [57](#), [60](#), [61](#)
- [Parkash and Parikh, 2012] Parkash, A. and Parikh, D. (2012). Attributes for classifier feedback. In *ECCV*. [42](#)
- [Pearson, 1901] Pearson, K. (1901). Liii. on lines and planes of closest fit to systems of points in space. *The London, Edinburgh, and Dublin Philosophical Magazine and Journal of Science*, 2(11):559–572. [11](#)
- [Pehlivan et al., 2010] Pehlivan, Z., Ben-Saad, M., and Gançarski, S. (2010). Vi-diff: understanding web pages changes. In *Conference on Database and expert systems applications: Part I*. Springer-Verlag. [66](#), [67](#)

- [Perronnin and Dance, 2007] Perronnin, F. and Dance, C. (2007). Fisher kernels on visual vocabularies for image categorization. In *IEEE Conference on Computer Vision and Pattern Recognition (CVPR)*, pages 1–8. IEEE. [7](#)
- [Perronnin et al., 2010] Perronnin, F., Sánchez, J., and Mensink, T. (2010). Improving the fisher kernel for large-scale image classification. In *Computer Vision–ECCV 2010*, pages 143–156. Springer. [7](#), [8](#), [9](#)
- [Prechelt, 1998] Prechelt, L. (1998). Early stopping-but when? In *Neural Networks: Tricks of the trade*, pages 55–69. Springer. [27](#)
- [Rakotomamonjy et al., 2008] Rakotomamonjy, A., Bach, F., Canu, S., Grandvalet, Y., et al. (2008). Simplemkl. *Journal of Machine Learning Research*, 9:2491–2521. [10](#)
- [Rakotomamonjy et al., 2011] Rakotomamonjy, A., Flamary, R., Gasso, G., and Canu, S. (2011). Penalty for sparse linear and sparse multiple kernel multitask learning. *Neural Networks, IEEE Transactions on*, 22(8):1307–1320. [62](#)
- [Rosasco et al., 2004] Rosasco, L., Vito, E., Caponnetto, A., Piana, M., and Verri, A. (2004). Are loss functions all the same? *Neural Computation*, 16(5):1063–1076. [17](#)
- [Rubner et al., 2000] Rubner, Y., Tomasi, C., and Guibas, L. J. (2000). The earth mover’s distance as a metric for image retrieval. *International Journal of Computer Vision*, 40(2):99–121. [13](#)
- [Salton, 1975] Salton, G. (1975). *A theory of indexing*, volume 18. SIAM. [10](#)
- [Sanoja and Gançarski, 2012] Sanoja, A. and Gançarski, S. (2012). Yet another hybrid segmentation tool. In *International Conference on Preservation of Digital Objects*. [71](#), [79](#), [80](#)
- [Schölkopf et al., 2001] Schölkopf, B., Herbrich, R., and Smola, A. J. (2001). A generalized representer theorem. In *Computational learning theory (COLT)*, pages 416–426. Springer. [15](#)
- [Scholkopf and Smola, 2001] Scholkopf, B. and Smola, A. J. (2001). *Learning with kernels: support vector machines, regularization, optimization, and beyond*. MIT press. [10](#)
- [Schultz and Joachims, 2004] Schultz, M. and Joachims, T. (2004). Learning a distance metric from relative comparisons. *Advances in neural information processing systems (NIPS)*, page 41. [18](#), [25](#)
- [Serre et al., 2007] Serre, T., Wolf, L., Bileschi, S., Riesenhuber, M., and Poggio, T. (2007). Robust object recognition with cortex-like mechanisms. *IEEE Transactions on Pattern Analysis and Machine Intelligence*, 29(3):411–426. [5](#)
- [Shalev-Shwartz et al., 2004] Shalev-Shwartz, S., Singer, Y., and Ng, A. Y. (2004). Online and batch learning of pseudo-metrics. In *Proceedings of the twenty-first international conference on Machine learning*, page 94. ACM. [14](#)
- [Shaw et al., 2011] Shaw, B., Huang, B. C., and Jebara, T. (2011). Learning a distance metric from a network. In *Advances in Neural Information Processing Systems (NIPS)*, pages 1899–1907. [23](#)
- [Shen et al., 2009] Shen, C., Kim, J., Wang, L., and van den Hengel, A. (2009). Positive semidefinite metric learning with boosting. In *Advances in neural information processing systems (NIPS)*. [4](#), [50](#)
- [Shepard, 1962a] Shepard, R. N. (1962a). The analysis of proximities: Multidimensional scaling with an unknown distance function. i. *Psychometrika*, 27(2):125–140. [24](#)
- [Shepard, 1962b] Shepard, R. N. (1962b). The analysis of proximities: Multidimensional scaling with an unknown distance function. ii. *Psychometrika*, 27(3):219–246. [24](#)
- [Simonyan and Zisserman, 2014] Simonyan, K. and Zisserman, A. (2014). Very deep convolutional networks for large-scale image recognition. *arXiv preprint arXiv:1409.1556*. [10](#)

-
- [Sivic and Zisserman, 2003] Sivic, J. and Zisserman, A. (2003). Video Google: A text retrieval approach to object matching in videos. In *IEEE International Conference on Computer Vision (ICCV)*. [1](#), [5](#), [45](#)
- [Smeulders et al., 2000] Smeulders, A. W., Worring, M., Santini, S., Gupta, A., and Jain, R. (2000). Content-based image retrieval at the end of the early years. *IEEE Transactions on Pattern Analysis and Machine Intelligence*, 22(12):1349–1380. [1](#)
- [Smith and Chang, 1997] Smith, J. R. and Chang, S.-F. (1997). Visualeek: a fully automated content-based image query system. In *Proceedings of the fourth ACM international conference on Multimedia*, pages 87–98. ACM. [7](#)
- [Song et al., 2004] Song, R., Liu, H., Wen, J., and Ma, W. (2004). Learning block importance models for web pages. In *WWW*. [67](#), [70](#)
- [Spengler and Gallinari, 2010] Spengler, A. and Gallinari, P. (2010). Document structure meets page layout: Loopy random fields for web news content extraction. In *ACM Symposium on Document Engineering (DocEng)*. [67](#)
- [Steinhaus, 1956] Steinhaus, H. (1956). Sur la division des corp materiels en parties. *Bull. Acad. Polon. Sci*, 1:801–804. [10](#)
- [Stricker and Orengo, 1995] Stricker, M. A. and Orengo, M. (1995). Similarity of color images. In *IS&T/SPIE’s Symposium on Electronic Imaging: Science & Technology*, pages 381–392. International Society for Optics and Photonics. [13](#)
- [Szegedy et al., 2013] Szegedy, C., Toshev, A., and Erhan, D. (2013). Deep neural networks for object detection. In *Advances in Neural Information Processing Systems (NIPS)*, pages 2553–2561. [9](#)
- [Tenenbaum et al., 2000] Tenenbaum, J., De Silva, V., and Langford, J. (2000). A global geometric framework for nonlinear dimensionality reduction. *Science*, 290(5500):2319–2323. [2](#), [11](#)
- [Tewari and Bartlett, 2007] Tewari, A. and Bartlett, P. L. (2007). On the consistency of multiclass classification methods. *The Journal of Machine Learning Research*, 8:1007–1025. [16](#)
- [Theriault et al., 2013] Theriault, C., Thome, N., and Cord, M. (2013). Dynamic scene classification: Learning motion descriptors with slow features analysis. In *IEEE Conference on Computer Vision and Pattern Recognition (CVPR)*. [5](#)
- [Tsochantaridis et al., 2005] Tsochantaridis, I., Joachims, T., Hofmann, T., and Altun, Y. (2005). Large margin methods for structured and interdependent output variables. In *Journal of Machine Learning Research*, pages 1453–1484. [21](#)
- [Tuytelaars and Mikolajczyk, 2008] Tuytelaars, T. and Mikolajczyk, K. (2008). Local invariant feature detectors: a survey. *Foundations and Trends® in Computer Graphics and Vision*, 3(3):177–280. [13](#)
- [Varma and Zisserman, 2009] Varma, M. and Zisserman, A. (2009). A statistical approach to material classification using image patch exemplars. *Pattern Analysis and Machine Intelligence, IEEE Transactions on*, 31(11):2032–2047. [13](#)
- [Verma et al., 2012] Verma, N., Mahajan, D., Sellamanickam, S., and Nair, V. (2012). Learning hierarchical similarity metrics. In *IEEE Conference on Computer Vision and Pattern Recognition (CVPR)*. [4](#), [23](#), [24](#), [44](#), [45](#), [47](#)
- [Wang et al., 2010] Wang, J., Yang, J., Yu, K., Lv, F., Huang, T., and Gong, Y. (2010). Locality-constrained linear coding for image classification. In *IEEE Conference on Computer Vision and Pattern Recognition (CVPR)*, pages 3360–3367. IEEE. [9](#)
- [Weinberger and Chapelle, 2008] Weinberger, K. and Chapelle, O. (2008). Large margin taxonomy embedding with an application to document categorization. In *Advances in neural information processing systems (NIPS)*. [4](#), [23](#), [24](#), [45](#)

- [Weinberger and Saul, 2009] Weinberger, K. and Saul, L. (2009). Distance metric learning for large margin nearest neighbor classification. *JMLR*, 10:207–244. [2](#), [19](#), [23](#), [25](#), [33](#), [35](#), [36](#), [37](#), [43](#), [44](#), [46](#), [50](#), [60](#)
- [Weinberger et al., 2005] Weinberger, K. Q., Blitzer, J., and Saul, L. K. (2005). Distance metric learning for large margin nearest neighbor classification. In *Advances in neural information processing systems (NIPS)*, pages 1473–1480. [3](#), [19](#)
- [Xing et al., 2002] Xing, E., Ng, A., Jordan, M., and Russell, S. (2002). Distance metric learning, with application to clustering with side-information. In *Advances in neural information processing systems (NIPS)*. [2](#), [18](#), [19](#), [23](#), [25](#), [36](#)
- [Yang et al., 2009] Yang, J., Yu, K., Gong, Y., and Huang, T. (2009). Linear spatial pyramid matching using sparse coding for image classification. In *IEEE Conference on Computer Vision and Pattern Recognition (CVPR)*. [5](#), [8](#), [9](#)
- [Yu et al., 2013] Yu, F. X., Cao, L., Feris, R. S., Smith, J. R., and Chang, S.-F. (2013). Designing category-level attributes for discriminative visual recognition. In *IEEE Conference on Computer Vision and Pattern Recognition (CVPR)*, pages 771–778. IEEE. [12](#)
- [Yue et al., 2007] Yue, Y., Finley, T., Radlinski, F., and Joachims, T. (2007). A support vector method for optimizing average precision. In *Proceedings of the 30th annual international ACM SIGIR conference on Research and development in information retrieval*, pages 271–278. ACM. [22](#)
- [Zhang et al., 2006] Zhang, H., Berg, A. C., Maire, M., and Malik, J. (2006). Svm-knn: Discriminative nearest neighbor classification for visual category recognition. In *IEEE Conference on Computer Vision and Pattern Recognition (CVPR)*, volume 2, pages 2126–2136. IEEE. [9](#)